

Applied Particle Technology Proceedings 2005

Prof. Dr. Dr. h.c.* Herbert Eichele (Editor)
* Staatsuniversität Tomsk Russland (TUSUR)

Georg-Simon-Ohm-Fachhochschule Nürnberg
Keßlerplatz 12
90489 Nürnberg

Prof. Dr. U. Teipel, Dr. A. Gromov

International Seminar at Tomsk Polytechnical
University - Sept. 22, 2005 -

Tomsk Polytechnical University TPU, Russia

Georg-Simon-Ohm-University of Applied Sciences
Nuremberg, Germany



Preface

Georg-Simon-Ohm-University of Applied Sciences Nuremberg/Germany (GSO-FHN) has lively relations with the Tomsk Science Region for more than a decade. Exchange of many students and professors took and still takes place. Joint research programs and curriculum development programs in the Bologna Process context have been executed especially with Tomsk State University of Control Engineering and Radio Electronics TUSUR.

The International Seminar of Applied Particle Technology which took place at Tomsk Polytechnical University TPU is another step extending international cooperation and scientific progress between Germany and Russia.

I optimistically look forward to more upcoming joint actions in science, teaching, research and development especially between GSO-FHN and TPU.

Prof. Dr. rer.nat. Dr. h.c.* Herbert Eichele

Rector Georg-Simon-Ohm-University of Applied Sciences Nuremberg/Germany

*TUSUR

Preface

A lot of pre- and end products which are offered by many different industrial suppliers are particulate materials or contain finely dispersed particles in the range from a few nanometers up to several hundred micrometers. These particles and disperse systems must meet customer-specific and application-oriented requirements in order to place such products on the market successfully with respect to the increasing globalisation and severe competition. In recent years, the research and development on nanoparticles has become more and more important. Nanotechnology offers a lot of innovative possibilities for the international market.

The international seminar "Applied Particle Technology" which was held at the Tomsk Polytechnical University in September 2005 was focused on this subject. This seminar is based on the collaboration between the Tomsk Polytechnical University (TPU), the University of Applied Sciences Nuremberg and the Fraunhofer Institute for Chemical Technology (ICT) in Pfinztal. The aim was the discussion of modern achievements in the field of fabrication, properties and application. The articles printed in this book are based on the lectures of the seminar.

Special thanks go to all the people who participated in form and content in the preparation and realisation of the seminar and who aided in making this book. We would like to thank the authors for supplying the manuscripts. For their excellent assistance, we would like to express our special thanks to the Vice-Rector of the Tomsk Polytechnical University Professor Alexander Chuchalin, the Dean of the Chemical Technology Department of the Tomsk Polytechnical University Professor Valery Pogrebenkov, the PhD students of the TPU Ms. Olga Neuvonen, Ms. Katya Kulinich and Ms. Sveta Antipina, Dipl.-Ing. Ulrich Förter-Barth from the Fraunhofer ICT, the Rector of the University of Applied Sciences Nuremberg Professor Herbert Eichele and Ms. Sigrid Lindstadt from the University of Applied Sciences in Nuremberg.

Nuremberg and Tomsk, January 2006

Prof. Dr.-Ing. Ulrich Teipel

Dr. Aleksandr A. Gromov

Content	Seite
Ceramic Nanopowder Dry Compacting for Manufacturing of Nanostructured Ceramics O.L Khasanov	9
Product Design of Particles of Energetic Materials U. Teipel, U. Förter-Barth	17
Progress in Metal Nanoparticle Technology for Industrial Application A. A. Gromov	31
Fabrication, Properties and Application of Electroexplosive Aluminum Nanopowders in Highly Energetic Materials V. V. An, V. A. Arkhipov, A. P. Ilyin, Y.-S. Kwon, A.G. Korotkikh, D.V. Tkhonov	39
Study of Ultrafine Powders Produced by the Exploding Wire Method V. S. Sedoi, Yu. F. Ivanov, M. N. Osmonoliev	47
Material Properties of Gel Propellants U. Teipel, U. Förter-Barth	59
Ignition and Combustion of Propellants containing Aluminum Nanoparticles V. A. Arkhipov, A. G. Korotkikh, V. T. Kuznetsov, A. B. Vorozhtsov	69

Ceramic Nanopowder Dry Compacting for Manufacturing of Nanostructured Ceramics

O.L Khasanov

Tomsk Polytechnical University, Russia

R&D Center of Advanced Technologies

Abstract

The method of cold uniaxial compaction of dry powders under powerful ultrasonic action (PUA) was applied to shape the zirconia nanopowder. The influence of the PUA on powder compaction on the density, microhardness, fracture toughness and lattice parameters of sintered zirconia ceramics have been investigated. It was found the correlative behaviour mentioned characteristics for ceramics with parameters of PUA for powders.

Introduction

The important problems of manufacturing bulk nanostructured ceramics are the following:

- shaping of dust-like nanopowder into the required shape with uniform density, without gradients of internal stresses;
- high friction forces at particle-particle and particle-die interaction due to the high specific area of the nanopowder;
- preventing of grain growth and warping, distortions during green compact sintering to achieve nanoscale structure;
- providing the required purity and density of the product;
- economy.

It was shown the efficiency of dry uniaxial pressing of nanostructured powders under powerful ultrasound action (PUA) for manufacturing structural and functional nanoceramics [1-3].

At optimum conditions of nanopowder compaction, the method ensures a uniform density distribution in products having a complex shape owing to even packaging particles when their vibration displacement is comparable to a particle or agglomerate size. Also interparticle and die-wall friction forces decrease under PUA which promotes the fracture of agglomerates and nanostructure formation at sintering green compacts due to effects of mechanoactivation of particles [4].

The method eliminates the application of plasticizers and binders as potential sources of impurities. The method of compaction under PU-action can be combined with another developed method of dry powder compaction - the collector method, which uses the special design of the die, where the active and passive shaping surfaces are combined in the one shaping member of the mold according to the principle of minimisation of the particle-die friction forces and the certain rules of mutual moving of such shaping members [5].

The work aim was the investigation of the PUA influence during dry nanopowder compacting on physical properties, microstructure and lattice parameters of sintered ceramics.

Experiments

The $\text{ZrO}_2\text{-}5\text{wt}\%\text{Y}_2\text{O}_3$ powder, produced by the Siberian Chemical Industrial Complex (Russia) using plasma-chemical synthesis, had an average particle and agglomerate size of 500 nm.

Cold uniaxial compaction of the dry powder was carried out in the steel cylindrical moulds being acoustic waveguides up to $p = 600$ MPa at simultaneous PU-action by the technique described in [3]. The frequency of the ultrasonic generator was $f = 21$ kHz. The generator output voltage of $U = 25\text{...}150$ V corresponded to the amplitude of the die wall vibration $A = 2\text{...}20$ μm . The PUA duration, τ , for the different samples was 2, 10 and 40 minutes.

Compacted pellets with a diameter of 10 mm and a thickness of 3 mm were sintered in vacuum (0.1 mPa at 1700 °C, 1 hour).

After sintering the grain and pore size distributions was studied by SEM (JSM-820 JEOL), optical microscopy (Neofot-21) and calculated by the ImageJ1.28 software (<http://isb.info.nih.gov>).

The lattice parameters of sintered zirconia ceramics were determined by XRD using D/Max-B, Rigaku ($2\theta = 15^\circ\text{...}80^\circ$, step 0.05°), and calculated by the Powder Cell 2.23 software [6].

The density was determined by the measurement of the mass and volume of the samples. Microhardness and fracture toughness were measured by the indentation of Vickers pyramid using Micromet, PMT-3, TP-78-1 devices.

Results and Discussion

It was found the similar behaviour of the relative density of the green compacts (a), sintered ceramics (b), microhardness (c) and fracture toughness (d) of sintered samples vs U and τ . There is the optimum of PUA intensity at 50 V ($A = 5 \mu\text{m}$) – Fig. 1.

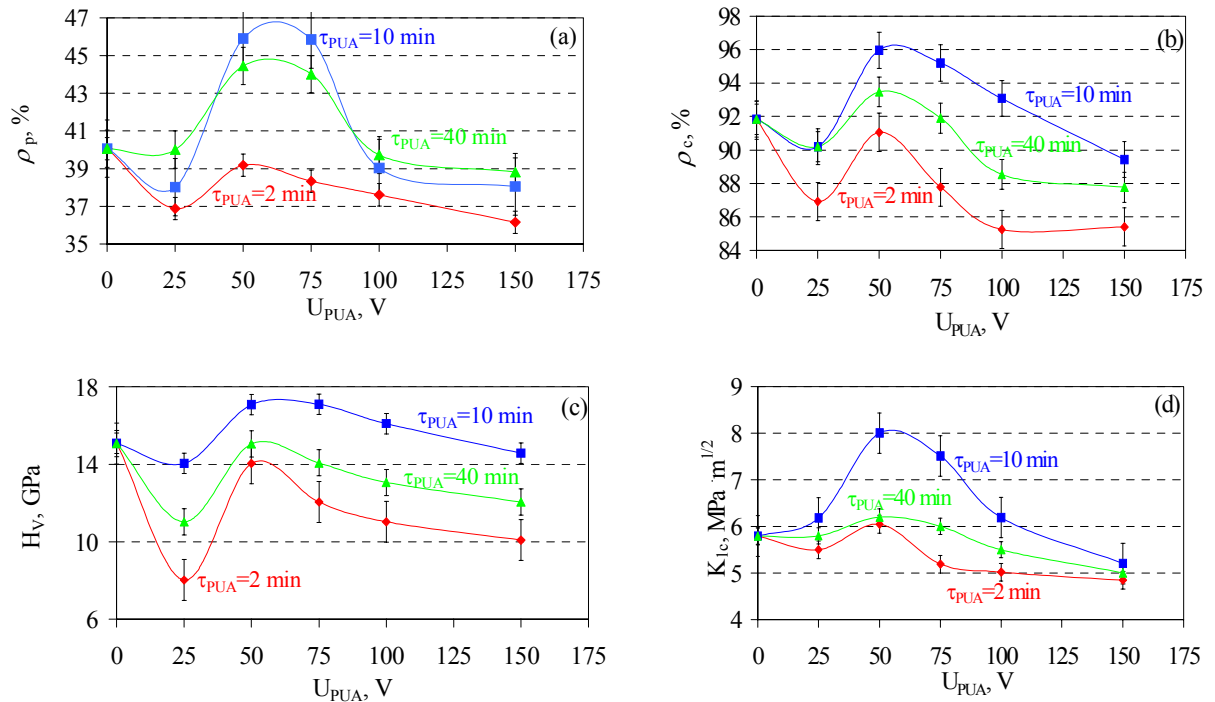


Figure 1: Relative density of the green compacts (a), sintered ceramics (b), microhardness (c) and fracture toughness (d) of sintered samples vs U and τ

The SEM micrographs of ceramics sintered after usual pressing of the powder ($U = 0$ V) and after compaction under PU-action show the smaller grain size for the sonicated samples (Fig. 2).

The grain size distributions in sintered zirconia ceramics are more narrow for sonicated samples (Fig. 3) that indicates the grain growth inhibition due to nanoparticle activation by the PU-action at powder compaction.

The pore size distributions in sintered zirconia ceramics also demonstrate their narrowing for the samples sonicated during powder compacting (Fig. 4).

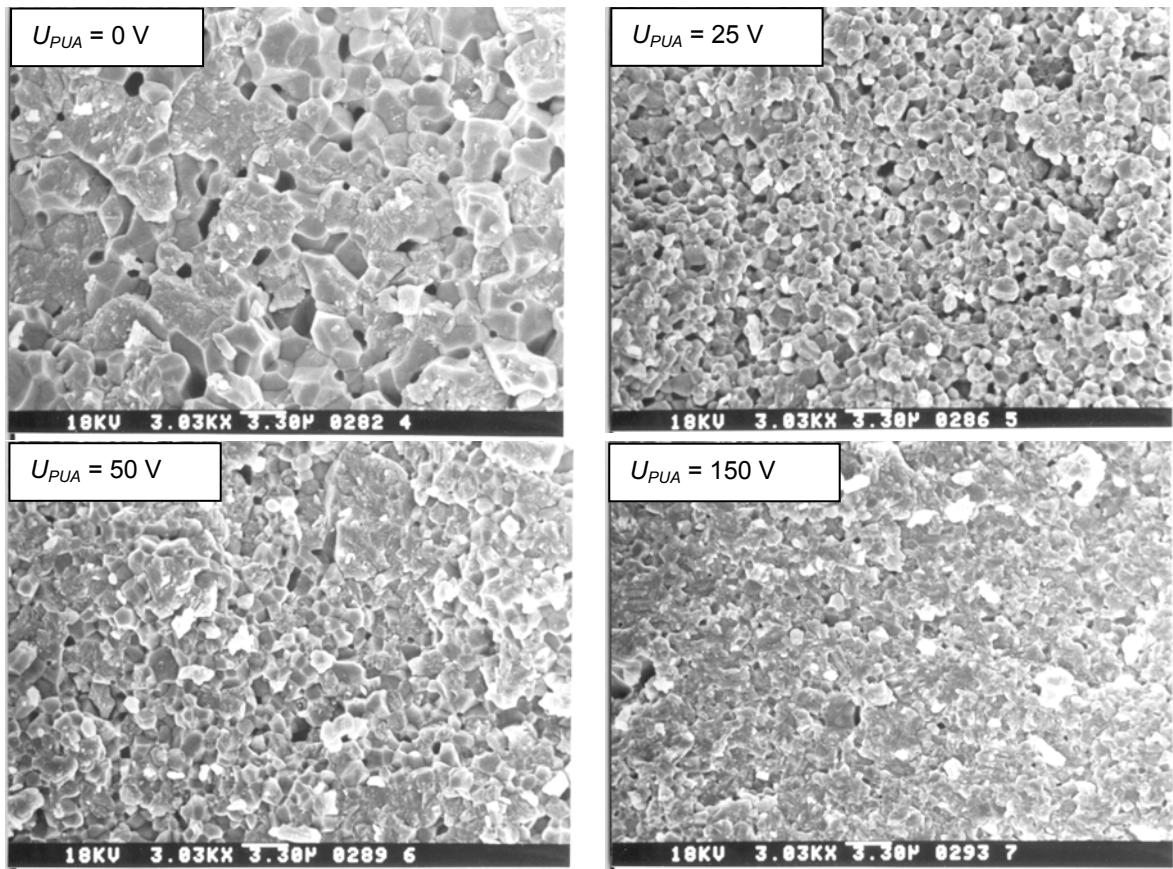


Figure 2: The SEM micrographs of ceramics sintered after usual pressing of the powder ($U = 0\text{ V}$) and after compaction under PUA at 25 V, 50 V and 150 V

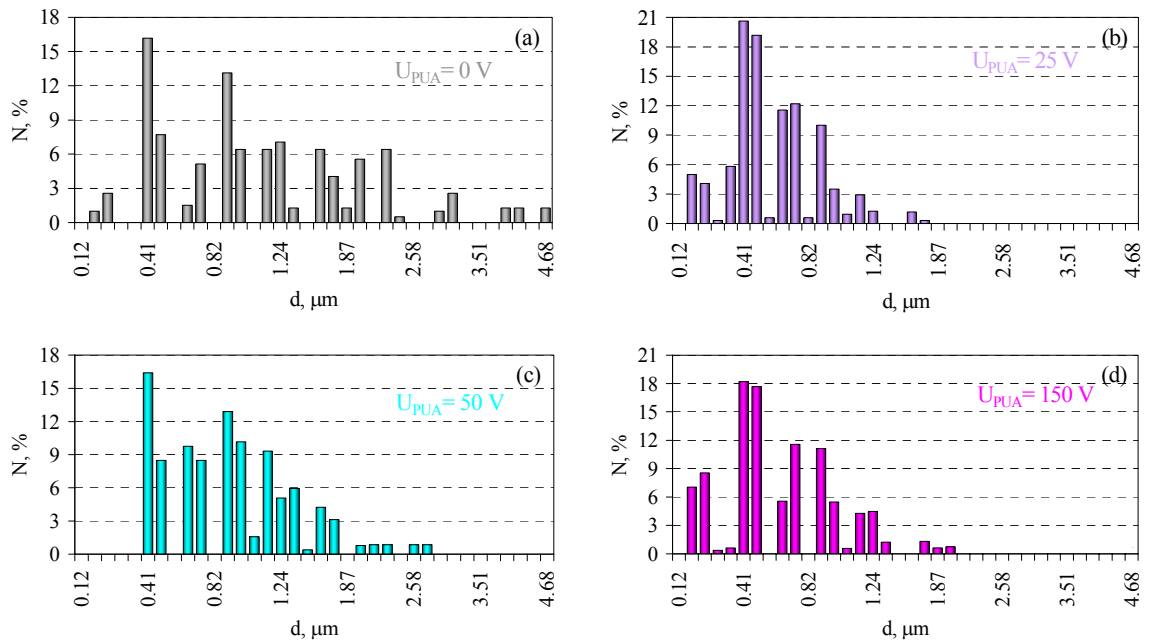


Figure 3: The grain size distributions in sintered zirconia ceramics after usual pressing of the powder (a) and after compaction under PU-action (b, c, d)

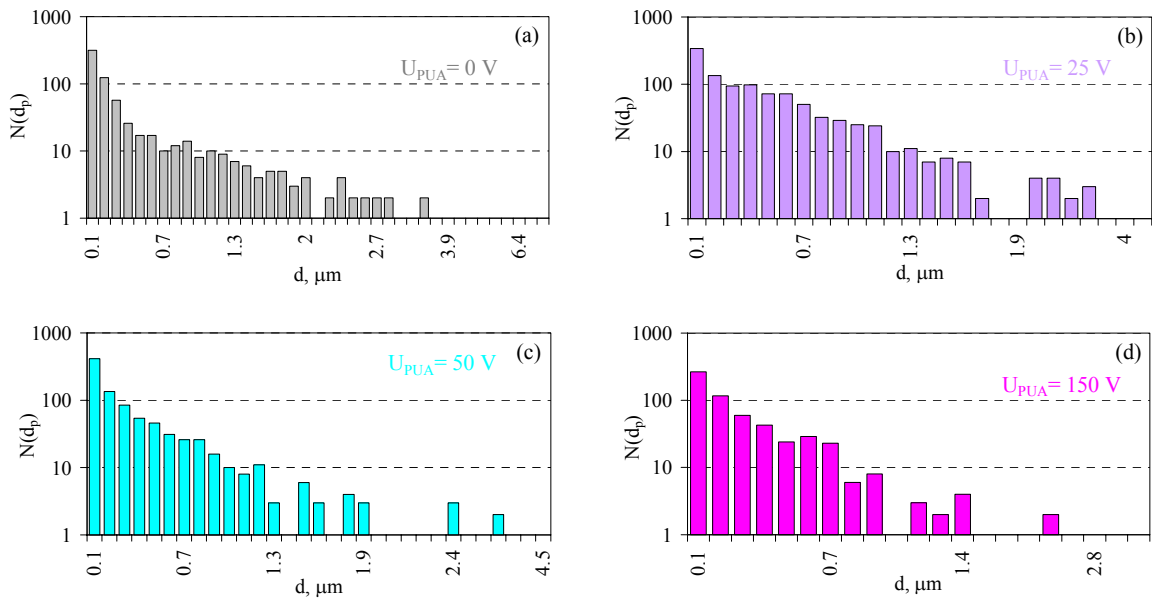


Figure 4: The pore size distributions in sintered zirconia ceramics after usual pressing of the powder (a) and after compaction under PU-action (b, c, d)

Calculations of the mean sizes of the grains d_g and pores d_p in sintered zirconia ceramics vs compaction conditions of the nanopowder showed that d_g depends on U similar to the dependencies of ρ_p , ρ_c , H_V , K_{1c} . The largest pores and grains are in the non-sonicated samples; minimum sizes are in the samples sonicated at the maximum amplitude of PU-action (Fig. 5).

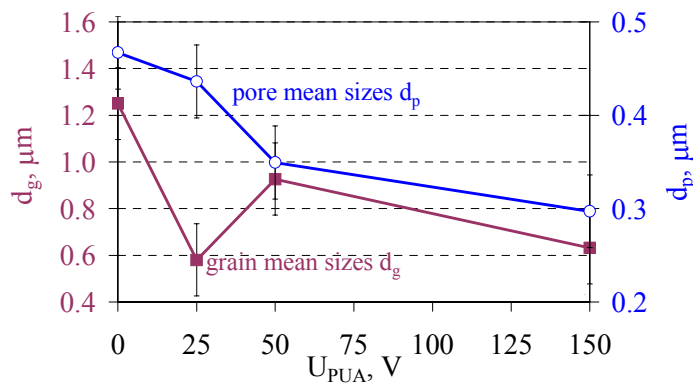


Figure 5: The mean sizes of the grains d_g and pores d_p in sintered zirconia ceramics vs compaction conditions of the nanopowder

It was found the interesting fact: the lattice parameter of the *cubic* phase a and the lattice angle β_m of the *monoclinic* phase in sintered zirconia ceramics vs nanopowder compaction conditions have correlative behaviour between them as well as with the behaviour of ρ_p , ρ_c , H_V , K_{1c} , d_g (Fig. 6).

Moreover, the lattice parameter a of the cubic phase and the combination parameter β_m/a of the monoclinic and cubic phases in sintered zirconia ceramics show monotonic dependencies vs lattice angle β_m for the investigated ceramic samples (Fig. 7a,b). Taking into account the absence of monotonic dependence between apparent microstrains and the crystallite size of zirconia m- and c- phases with β_m , the linear dependence β_m/a

$=f(\beta_m)$ (Fig. 7b) points to the correlative behaviour of the monoclinic and cubic structures in a separate crystallite without involvement of the crystallite boundary, similar to the observed co-existence of the zirconia tetragonal and monoclinic phases in separate nanoparticles [7, 8].

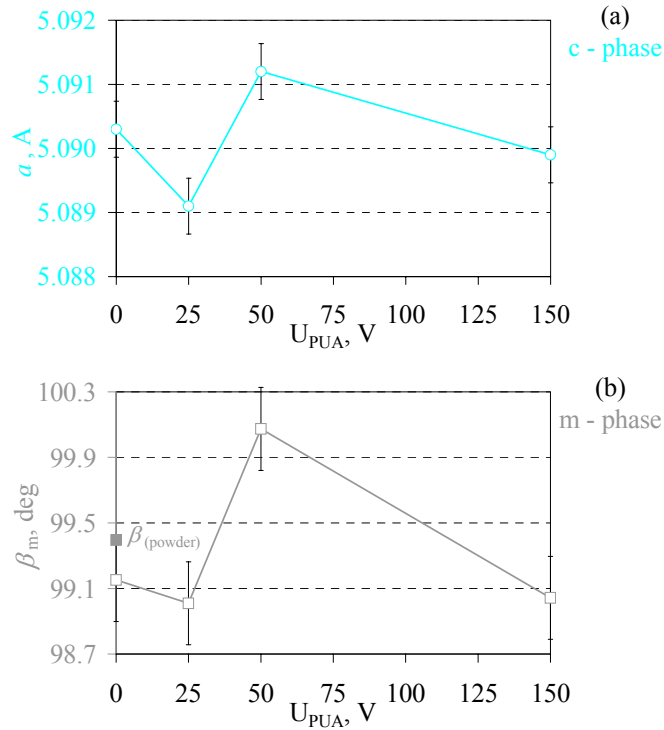


Figure 6: The lattice parameter of the *cubic* phase a and the lattice angle β_m of the *monoclinic* phase in sintered zirconia ceramics vs nanopowder compaction conditions

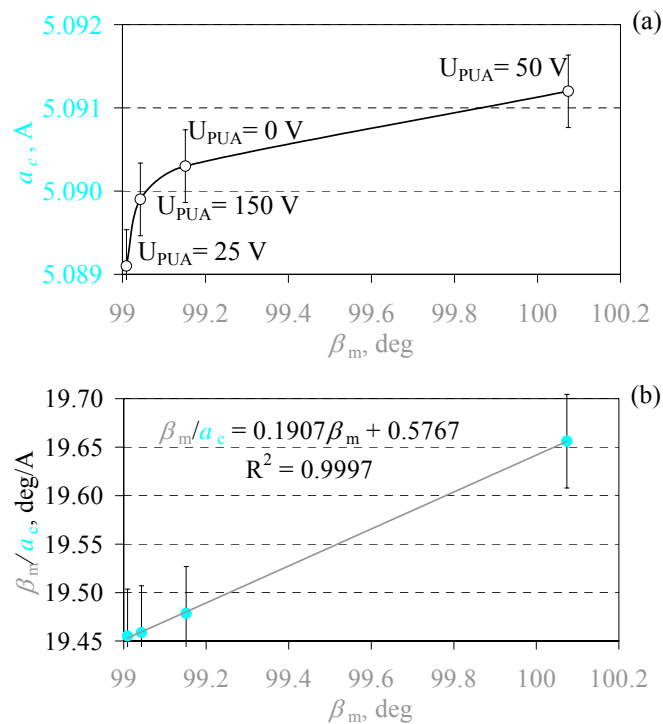


Figure 7: The correlative behavior of the lattice parameters of cubic and monoclinic phases in sintered zirconia ceramics

Conclusion

- The powerful ultrasonic action during zirconia nanopowder compaction influences the density, grain and pore sizes, mechanical properties and the lattice parameters in sintered ceramics.
- There is the optimal PU-intensity to achieve the best properties: $U \approx 50 \text{ V}$ ($A \approx 5 \text{ }\mu\text{m}$).
- The correlative behaviour of the lattice angle β_m of the zirconia monoclinic phase and the lattice parameter a of the cubic phase points to the possible co-existence of monoclinic and cubic structures in a nanocrystallite with lack of inter-crystallite boundaries and inter-crystallite microstresses.

References

- 1) O. L. Khasanov, Yu. P. Pokholkov, V. M. Sokolov, E. S. Dvilis, Z. G. Bikbaeva, V. V. Polisadova: *Particularities of Powerful Ultrasound Action on Nanostructured Powders*, Proc. MRS Symposium - Nanostructured Powders and Their Industrial Applications, 520, p.77-82, 1998
- 2) O. L. Khasanov, Yu. P. Pokholkov, Yu. F. Ivanov, L. L. Ljubimova, A. A. Makeev: *Effect of ultrasonic compaction of nanopowder on structure and fracture character of zirconia nanoceramics*, In: Fracture Mechanics of Ceramics, 13, Kluwer Academic/Plenum Publishers, New York, p. 503–512, 2002
- 3) O. L. Khasanov, E. S. Dvilis, V. M. Sokolov, Yu. P. Pokholkov: *Ceramic powders dry compaction under powerful ultrasound action*, Key Eng. Mat., 264-268, p.73-76, 2004
- 4) O. L. Khasanov, O. V. Karban, E. S. Dvilis: Investigation of structural hierarchy of nanoceramics compacted by dry pressing under powerful ultrasound action, Key Eng. Mat., 264-268, p.2327–2330, 2004
- 5) RF Patent 2225280 (03/12/2004), Eurasian Patent 005325 (02/24/2005), US Patent 6919041 B2 (19/07/2005), Europatent Application 02805039.1 (17/03/2004), publication 1459823 in European Patent Bulletin 2004/39, 22.09.2004.
- 6) W. Kraus, G. Nolze: POWDER CELL – A Program for the Representation and Manipulation of Crystal Structures and Calculation of the Resulting X-ray Powder Patterns, Journal of Applied Crystallography, 29, p. 301 – 303, 1996
- 7) V. Ya. Shevchenko, O. L. Khasanov, G. S. Yur'ev, Yu. F. Ivanov: *Coexistence of Cubic and Tetragonal Structures in Yttria-Stabilized Zirconia Nanoparticles*, Inorganic Materials, 37 (9), p. 950 – 952, 2001
- 8) V. Ya. Shevchenko, O. L. Khasanov, A. E. Madison, J. Y. Lee: *Investigation of the Structure Zirconia Nanoparticles by HRTEM*, Glass Physics and Chemistry, 28(5), p.322-325, 2002

Product Design of Particles of Energetic Materials

Ulrich Teipel*, **
Ulrich Förter-Barth**

* Georg-Simon-Ohm Fachhochschule Nürnberg
Fachbereich Verfahrenstechnik
Mechanische Verfahrenstechnik
Partikeltechnologie und Fluidmechanik

** Fraunhofer Institut für Chemische Technologie
(ICT) Dept. Energetische Materialien

Abstract

The crystal quality and the internal microstructure of crystals have a great influence on the sensitivity of energetic materials. Besides, the particle size and the particle size distribution are of great importance to the processing technology of energetic materials. Particle properties can especially be influenced by applying different crystallization techniques, such as cooling crystallization, membrane crystallization, emulsion crystallization and others.

The goal of the investigations was to determine the interrelationship between the properties of the gained crystals and the process parameters. Special attention was directed to the qualitative and quantitative examination of crystal defects and their dependence on the experimental conditions. Besides, the morphology and structure of crystals were calculated by molecular modelling. The effect of crystal defects on the sensitivity of the material was tested on different collectives of particles having varying amount of crystal defects.

Introduction

Particulate energetic materials and systems produced with such particulates, such as solid propellants, propellant powders and explosives, have assumed an ever more important role in industry. Important material properties of these materials, including burn rate behavior and sensitivity, are decisively affected by particulate properties such as particle morphology, size and size distribution.

Particles are generally manufactured using well-known solids formation techniques such as crystallization, precipitation, size-reduction, spray drying or deagglomeration [1]. Although a large amount of information exists on these different processing techniques, there are still gaps in our understanding of how to completely control the particle formation process or reliably predict processing phenomena and the properties of the particulate products.

A number of subjects related to particle technology and the design of particulate products require further investigation, including the characterization and experimental determination of various particle properties, the simulation and modeling of process operations involving dispersed products and, in particular, the relationship between product properties and the properties of dispersed systems and particles.

Product Design of Particles

The goal of product design is to develop end products with a defined set of properties that can be economically commercialized in an environmentally acceptable manner [2, 3]. The design of particulate products and dispersed systems is complex because obtaining the desired end product properties requires achieving an optimal combination of the chemical and physical properties of each component of the system. An essential problem in product design is to selectively and reproducibly achieve the desired material characteristics that meet the demands required of the particulate product or dispersed system under development. Such characteristics may include:

- insensitivity
- defect free particles
- absence of gas or fluid inclusions
- high density
- high purity
- surface and adhesion properties
- wettability, particle-binder interactions
- high packing density
- high performance
- rheological properties
- storage stability
- low propensity to form fine dusts
- filterability
- low tendency to agglomerate

Many of these product material properties are currently optimized empirically based on process and product requirements. The product properties are strongly dependent on the physical properties of the incorporated powder and on the dispersity characteristics of the system. The functional relationship between the product

properties and the dispersity characteristics for chemically identical products can be described via the property function:

$$\xi_i = f(\kappa_j)$$

The dependence of the product properties ξ_i on the dispersity characteristics κ_j is expressed via this equation.

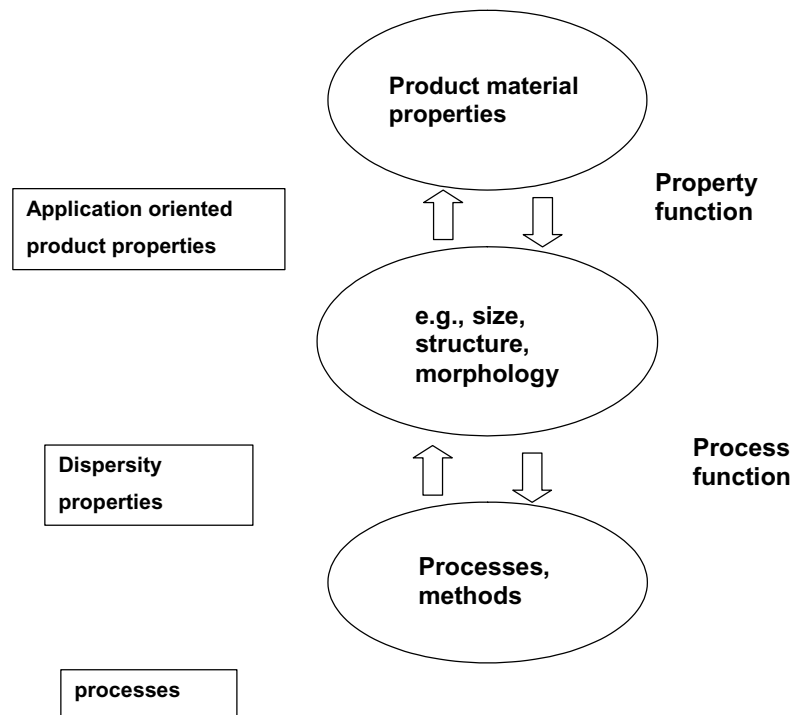


Figure 1: Product design in particulate technology

Important dispersity properties for particulate materials include:

- particle size
- particle size distribution
- morphology
- polymorphism
- crystallinity
- inner structure, porosity
- particle density, bulk density

One of the main challenges in the field of particle technology is attaining a better understanding of the relationship between the product properties ξ_i and the dispersity properties for different types of products and product applications.

By considering the process function, particles with defined dispersity properties can be manufactured using a variety of processing technologies, including methods such as crystallization or spray drying.

The dispersity properties of particulate products represent, through the property and process functions, a connection between the feedstock, the chosen processing method and the required application oriented product properties of the end product (see Fig. 1). Besides appropriate chemical design of the feedstock, when designing particulate products one or more suitable processing methods with appropriate process parameters must be selected and the required dispersity properties must be set to create an end product with the required material properties.

Crystal Defects and Flaws

In addition to “hot spots“ in the binder [4,5] and interactions between particles and binder, another property that significantly influences the sensitivity of energetic systems is the crystal quality of the particulates. When describing the product quality of particulate materials, one distinguishes between flaws within the crystal [6-10] and the crystal’s surface properties. Inner flaws that can significantly impair the crystal quality include point defects (Schottky or Frenkel defects), screw and edge dislocations, two dimensional defects (e.g., twin formation) and three dimensional defects (e.g., fluid or gas inclusions).

Defects are essentially a deviation in the perfect periodicity of a crystal. In an ideal crystal all the atoms assume a configuration corresponding to the global energy minimum. However, a real crystal does not exhibit a global energy minimum, but instead adopts configurations corresponding to numerous local energy minima. Because crystal defects have a significant effect on the physical properties of a crystal (e.g., the internal stress distribution), they also have a significant influence on the sensitivity of energetic materials. Figure 2 shows an example defect in the FOX 7 crystal.

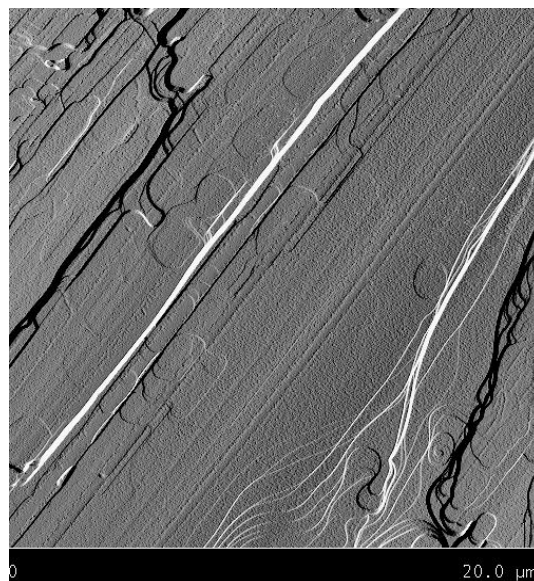


Figure 2: Defect in a FOX 7 crystal

Because crystal defects are related to the crystal’s formation history, optimizing the crystallization method offers the possibility to minimize crystal defects. Figures 3 and 4 show FOX 7 crystal surfaces; surface defects are clearly visible in the crystal depicted in Fig. 3. In contrast, Fig. 4 shows crystal growth layers of FOX 7 produced using optimized crystallization conditions.

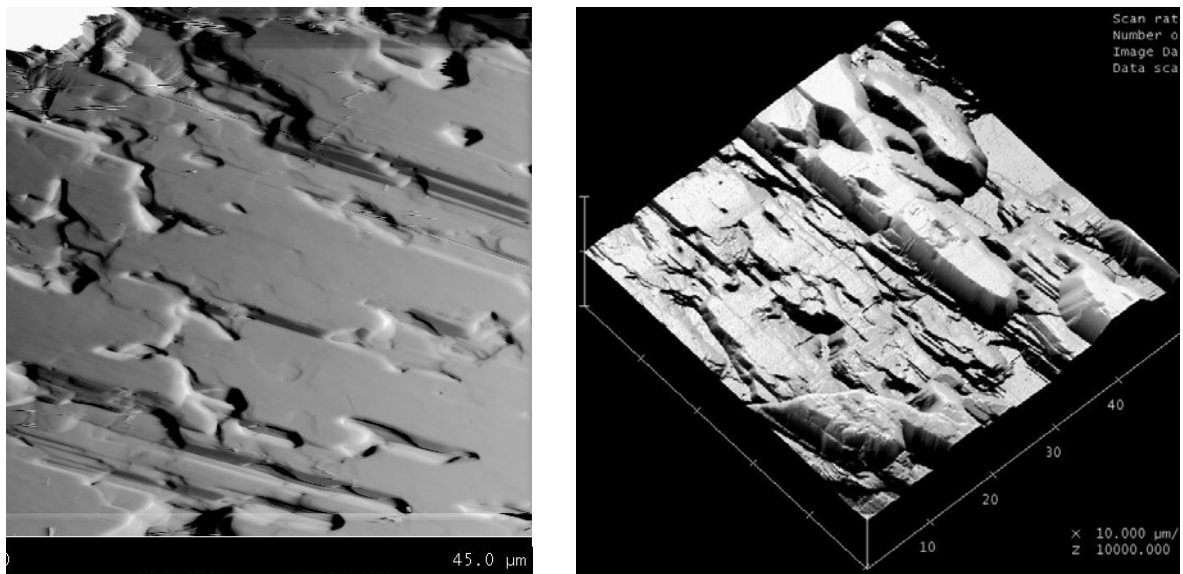


Figure 3: Surfaces of FOX 7 crystals

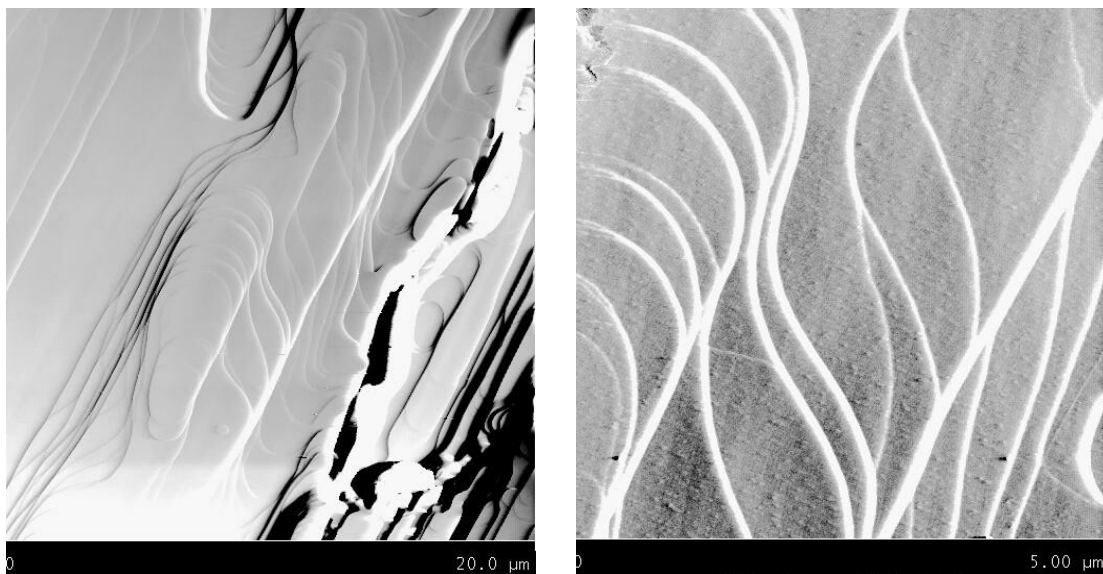


Figure 4: Crystal growth layers (FOX 7)

At high suspension concentrations and local regions of high supersaturation, nucleation may occur in liquid bridges. After crystallization, this causes the transition to solid bridges (see Fig. 5) and the agglomeration of particles.

Subjecting the agglomerated crystals to mechanical energy (e.g., through processing) leads to their deagglomeration and can also produce crystals with sharp edges (as also occurs in particle grinding), a condition which leads to a clear increase in the material's sensitivity.

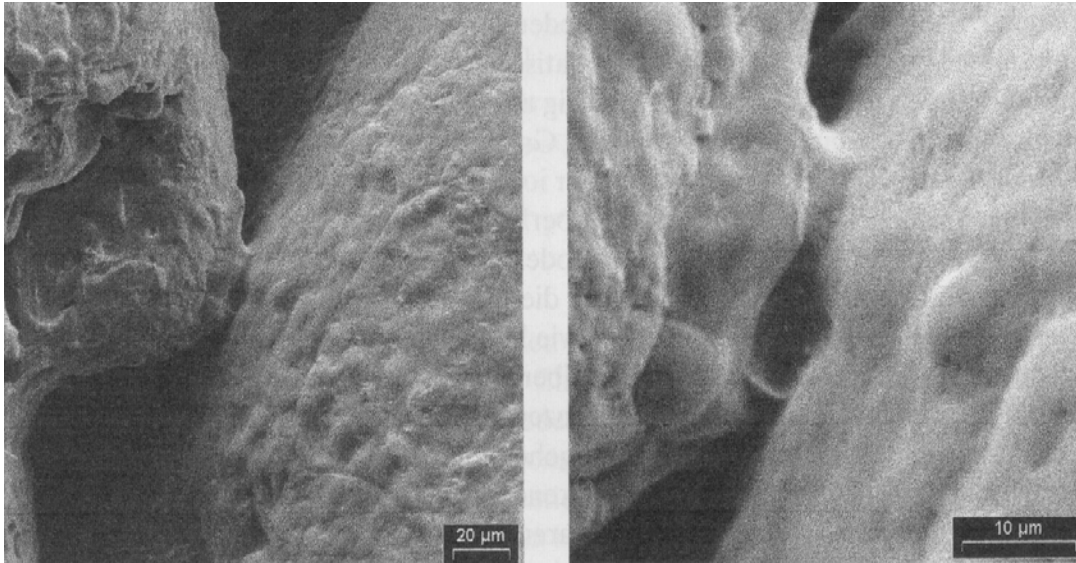


Figure 5: Solid bridges

Product Design via Crystallisation

The starting point for many particle formation processes is a fluid phase sufficiently oversaturated with an active component. Transport processes, chemical reactions and other processes cause nucleation, which then leads to the formation of clusters. Typically, nucleation is categorized either as primary (both homogeneous and heterogeneous) or secondary. During suspension crystallization, nucleation is followed by crystal growth of the dispersed phase in the oversaturated solution. Besides the decisive particle growth stage, critical steps in the product design process include: homogenization/stabilization of the dispersed system, or suppressing aggregation of the dispersed phase, depending on the specific application requirements of the end product.

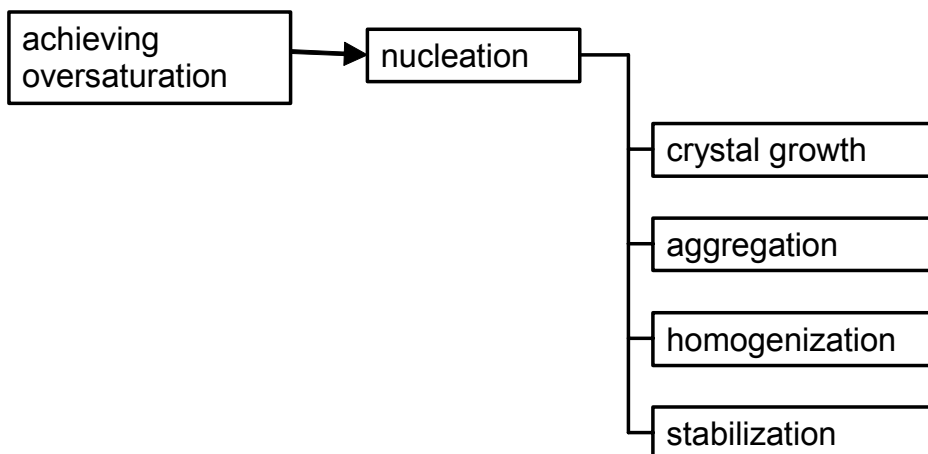


Figure 6: Product design via crystallization

Particle design via molecular modelling

Besides particle size and particle size distribution, other important dispersity properties include morphology, polymorphism and crystal structure. The morphology and structure of crystals are largely determined by the type of interactions that occur between the crystal surface and the surrounding fluid [11]. In the last few years, computation programs have been developed and become commercially available that allow the morphology of various crystalline materials to be calculated. The inner crystalline structure and distance and symmetry positions of the elementary cells are known exactly for many energetic materials. There are various theories for describing the relationship between the inner crystalline structure and outer crystal form, such as the Bravais-Friedel-Donnay-Harker model [12], which allows the crystal structure to be pre-calculated based on pure geometry, and the Hartman-Perdok method [13], which, besides geometrical parameters, includes the effect of energetic interactions. Another method of modelling the crystal structure is the "Attachment Energy" method [14, 15, 16]. The surface deposition energy E_{An} is the energy released when a layer deposits onto the crystal surface.

$$\Delta E_{An} = E_{Kri} - E_{Sch}$$

Here, E_{Kri} is the lattice energy and E_{Sch} is the energy of a layer of infinite thickness. The growth rate of the crystal surface is directly proportional to the surface deposition energy E_{An} , so that surfaces with low deposition energy grow more slowly and therefore have the greatest influence on the crystalline morphology.

The environment in which crystallization takes place (i.e., the solvent) has a decisive influence on the crystal habit. Use of different solvents leads to formation of various morphologies of a material. This influence on the crystal growth process is still not fully understood or amenable to modelling. A well-known method from the literature describes the incorporation of solvent into the crystal lattice structure (Build-up method; see Fig. 8).

One newly developed method, instead of simulating the substitution of molecules at the crystal lattice points, describes the accumulation of solvent on the crystalline surface and calculates the crystal habit on the basis of interactions between the crystal surface and solvent (see Fig. 7).

$$\Delta E = -(E_{Krist} + E_{Lösungsm.} - E_{Krist+Lösungsm.})$$

This method allows one to more realistically simulate the growth of the crystal habit and its dependence on the solvent. Figure 8 shows an example of the solvent nMP's influence on FOX 7 crystals.

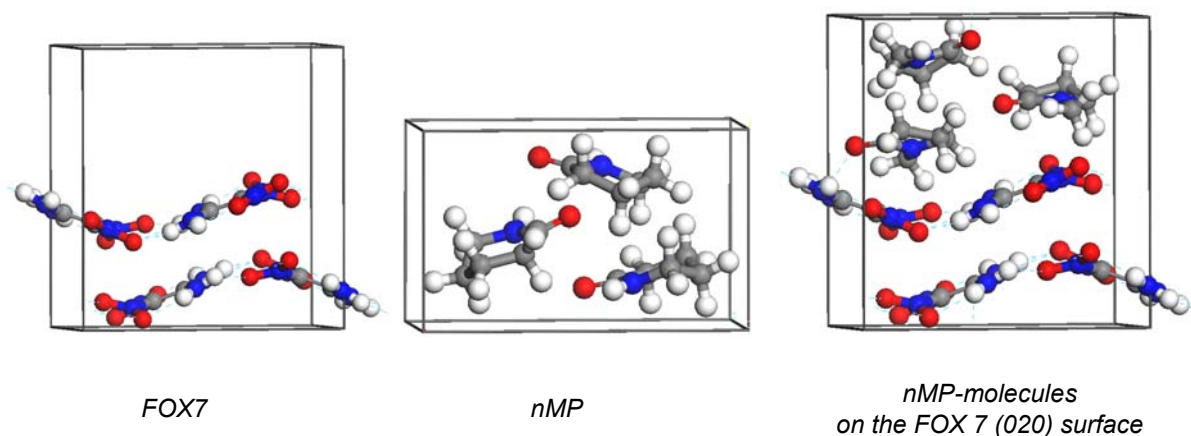


Figure 7: Accumulation method



Figure 8: Solvent influences; Fox7/nMP

Crystallization of 1,1 diamino-2,2-dinitroethylene (FOX 7)

Cooling crystallization was used to recrystallize FOX 7. Example results using nMP as the solvent are presented here. It is clear from Fig. 9 that due to its various surfaces, FOX 7 crystallizes at a range of different crystallization rates and surface defects form on those crystal surfaces in which the growth process is hindered.

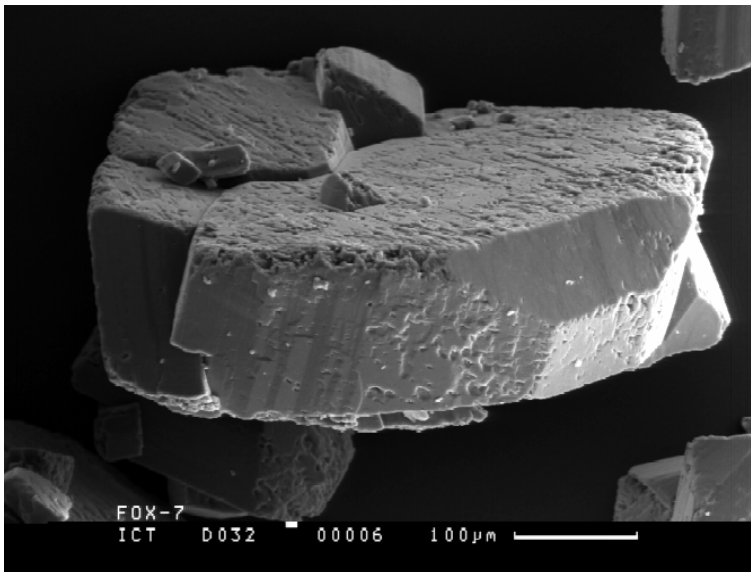
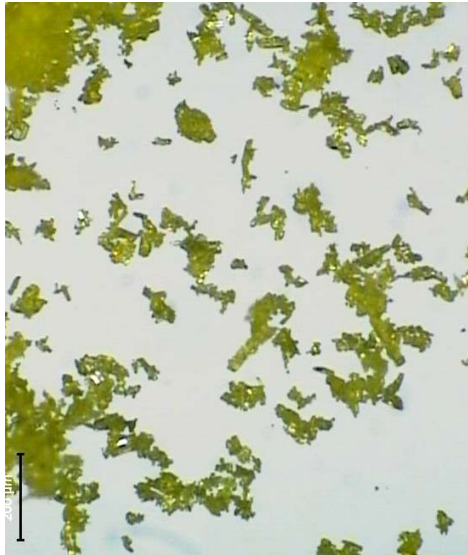
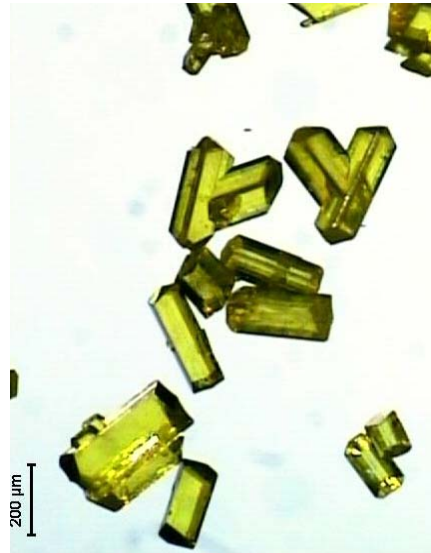


Figure 9: FOX 7 crystal

All of the following experiments were conducted using a cooling gradient dT/dt of 10 K/h. Pure nMP and an nMP/water mixture were employed as solvents. It was found that using pure solvent and a certain portion of water as antisolvent yielded crystals ranging in size $x_{50.3}$ from 40 to 50 μm . Using solvent mixtures, particles with sizes ranging from $100 \mu\text{m} \leq x_{50.3} \leq 400 \mu\text{m}$ can be produced via cooling crystallization.



$x_{50.3} = 55 \mu\text{m}$



$x_{50.3} = 306 \mu\text{m}$

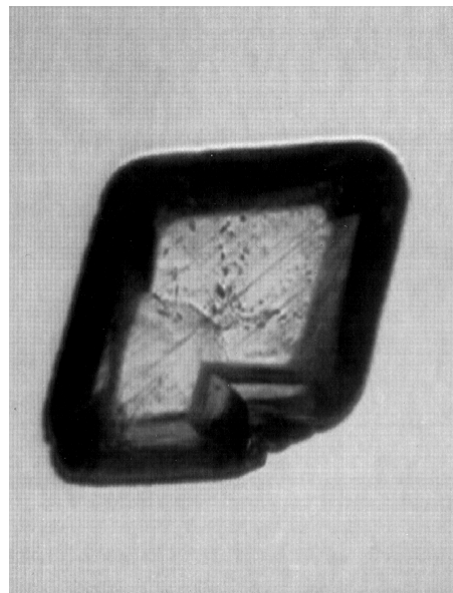
Figure 10: FOX 7 crystals

Crystallization of insensitive HMX

Using a modified cooling crystallization process, insensitive HMX (ICT-i-HMX) was produced at the Fraunhofer Institute-ICT. Figure 11 shows the original HMX and ICT-i-HMX.



HMX



ICT-i-HMX

Figure 11: HMX crystals

Using this special crystallization process, HMX with a significantly higher particle density was produced. The higher density is directly attributable to the reduced number of inner crystal defects in the molecules. Model PBX test slabs were produced using this HMX and subjected to gap tests. The ICT-i-HMX exhibits an insensitivity nearly a factor of two better than conventional HMX based on the shock wave loading test (Fig. 12).

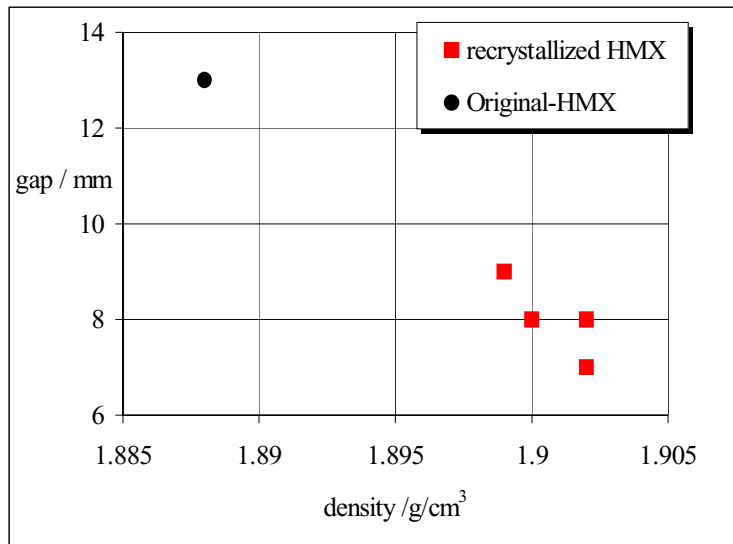


Figure 12: Gap test results, HMX and ICT-i-HMX

Product improvement using ultrasound to initiate nucleation

The use of ultrasound to initiate precipitation leads to a significant improvement in the quality of the end product and a narrower particle size distribution [17, 18]. Primary homogeneous nucleation is a process that occurs under thermodynamically unstable conditions. For many materials, a solid phase forms only under conditions of supersaturation. The point at which nucleation begins depends on the concentration of foreign material, the type of secondary material and the amount of mechanical energy applied to the system. When ultrasound is used during the cooling crystallization process, the onset temperature for nucleation is nearly independent of the temperature gradient and significantly higher than in the absence of ultrasound. In addition, the particle size distribution is significantly narrower when nucleation is initiated via ultrasound. The particle size distribution can be described in terms of the distribution coefficient λ_i :

$$\xi_i = \frac{x_{84,3} - x_{16,3}}{2 \cdot x_{50,3}}$$

where $x_{i,3}$ is the particle size for a volume sum distribution of $i\%$.

Particle manufacture via the membrane crystallization process

Membrane crystallization is a new crystallization process that offers an interesting alternative to cooling or steam crystallization, especially for energetic materials [19, 20, 21]. This method is especially interesting for use with thermolabile products, because the process can be carried out at low temperatures. In addition, the energy balance for membrane crystallization is considerably more favorable compared to cooling or steam processes. Like other processes, membrane crystallization occurs in an oversaturated solution, in which the

solvent is transported through a semi-permeable membrane, thereby becoming more concentrated at a nearly constant process temperature. The membrane must be chosen so that it provides a selective barrier to the active ingredient while allowing the solvent to penetrate the membrane (see Fig. 13). Membrane processes are typically pressure driven methods, such as reverse osmosis or micro or nano-filtration [22]. After transport of the solvent through the membrane to form a highly concentrated fluid phase, nucleation begins and is followed by the desired crystal growth stage.

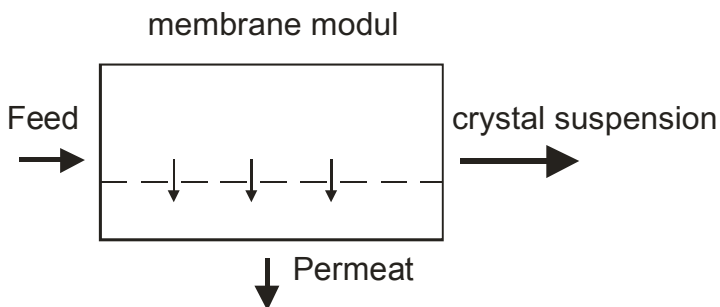
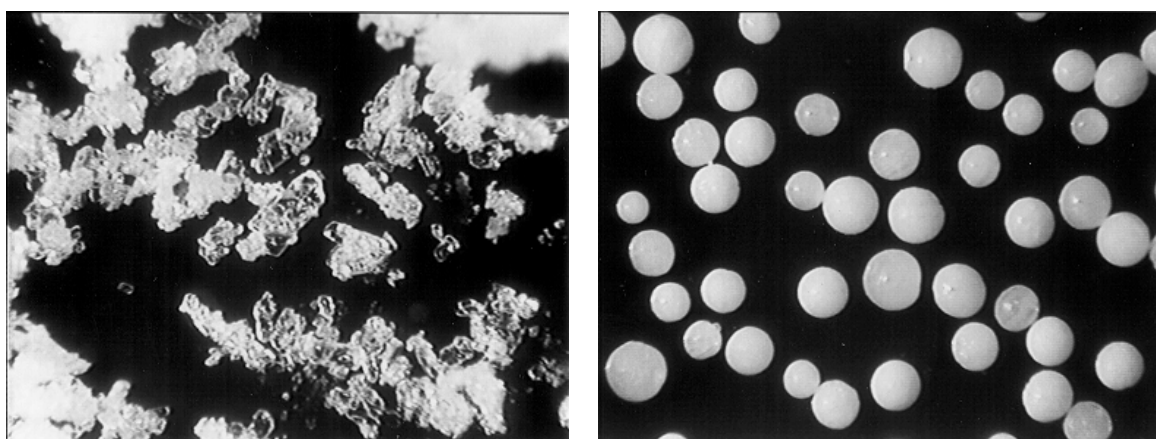


Figure 13: Membrane crystallization

Product design of spherical ammonium dinitramide (ADN)

Emulsion crystallization is particularly suitable for producing spherical particles of materials that melt at temperatures accessible with conventional processing technologies. The emulsion crystallization process consists of two linked process steps. The first step is production of an emulsion consisting of molten material dispersed in an inert continuous phase. The droplet size of an emulsion can be controlled by choosing the appropriate emulsification method and equipment. Various dispersion and size reduction processes exist, using equipment such as rotor-stator mixers (gear rim dispersers and colloid mills) or static mixers.

The second step in emulsion crystallization, which is decisive to the process, is the transition of the fluid dispersed phase into solid particles. For materials with particularly sluggish nucleation behavior, in addition to application of a sharp temperature gradient, some combination of mechanical energy input, particle-particle and/or particle-wall interactions or addition of seed crystals is necessary to initiate the nucleation process. The possibility of producing ammonium dinitramide (ADN) via the emulsion crystallization process is demonstrated in Fig. 14.



a. Synthetic product

b. Emulsion crystallization product

Figure 14: Crystallization of ammonium dinitramide

Figure 14a shows the product after synthesis and 14b depicts the spherical ammonium dinitramide after the emulsion crystallization process [23]. Afterwards, the continuous and dispersed phase of the suspension are separated and the product is dried.

A process newly developed at the Fraunhofer ICT offers the possibility of designing stabilized ADN particles. During crystallization of molten ADN, stabilator particles are incorporated into the ADN. Figure 15 shows the weight loss as a function of time for ADN immediately after synthesis and for conventional ADN particles and ADN particles stabilized via the ICT process. It is clearly evident that ADN particles produced using the new process exhibit significantly less weight loss in these experiments.

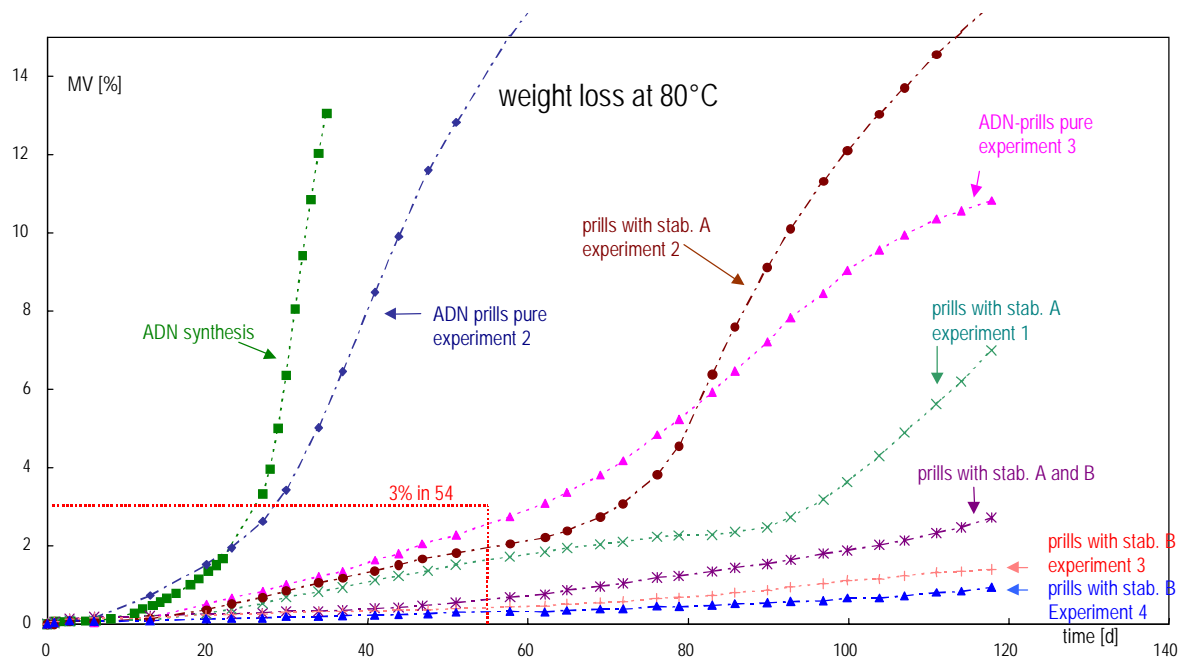


Figure 15: Weight loss function of ADN

References

- 1) U. Teipel: *Production of Particles of Explosives*, Propellants Explosives and Pyrotechnics, 24, p.134 – 139, 1999
- 2) U. Teipel: *Produktgestaltung in der Partikeltechnologie*, Fraunhofer-IRB-Verlag, Stuttgart, 2002
- 3) E. Favre, L. Marchal-Heusler, M. Kind: *Chemical Product Engineering: Research and Educational Challenges*, Trans IChemE, 80, p. 65 – 74, 2002
- 4) R. W. Armstrong, H. L. Ammon, W. L. Elban, D. H. Tsai: *Investigation of hot spot characteristics in energetic crystals*, Thermochemica Acta, 384, p. 303 – 313, 2002
- 5) R. W. Armstrong, C. S. Coffey, V. F. De Vost, W. L. Elban: *Crystal size dependence for impact initiation of cyclotrimethylenetrinitramine explosive*, Journal of Applied Phys., 68, p. 979 – 983, 1990
- 6) K. A. Gross: *Liquid Inclusions in RDX Crystals*, Journal of Crystal Growth, 6, p. 210 – 212, 1970
- 7) L. Borne, J.-C. Patedoye: *Quantitative Characterization of Internal Defects in RDX Crystals*, Propellants Explosives and Pyrotechnics, 24, p. 255 – 259, 1999
- 8) R. Janssen- van Rosmalen, P. Bennema: *The role of hydrodynamics and supersaturation in the formation of liquid inclusions in KDP*, Journal of Crystal Growth, 42, p. 224 – 227, 1977

- 9) E. D. M. van der Heijden, W. Duvalois, C. J. M. van der Wulp: *Micro-inclusions in HMX Crystals*, Proc. 30th Int. Annual Conference of ICT, Karlsruhe, p. 41/1 – 41/10, 1999
- 10) H. H. Cady: *Growth and Defects of Explosives Crystals*, Proc. Material Research Society Symposium, 296, Pittsburgh, p. 243 – 254, 1993
- 11) Fuhr, H. Kröber, U. Teipel: *Molecular Modelling: Produktgestaltung in der Kristallisation (Produktgestaltung in der Partikeltechnologie, U. Teipel)*, Fraunhofer IRB-Verlag, Stuttgart, p. 275 – 285, 2002
- 12) J. D. H. Donnay, D. Harker: *A New Law for Crystal Morphology Extending the Law of Bravais*, Am. Mineral., 22, p. 446 – 467, 1937
- 13) P. Hartman, W. G. Perdok: *On the relation between structure and morphology of crystals*, Acta Cryst., 8, p. 49 -52, 1955
- 14) P. Hartman, P. Bennema: *The Attachment Energy as a Habit Controlling Factor, 1. Theoretical Considerations*, J. Crystal Growth, 49, p. 145 – 156, 1980
- 15) Z. Berkovitch-Yellin: *Toward an ab initio derivation of crystal morphology*, J. Am. Chem. Soc., 107, p. 8239 – 8253, 1985
- 16) R. Docherty, G. Clydesdale, K. J. Roberts, P. Bennema: *Application of Bravais-Friedel-Donnay-Harker, Attachment-Energy and Ising Models to Prediction and Understanding the Morphology of Molecular Crystals*, J. Phys. D: Appl. Phys., 24, p. 88 – 99, 1991
- 17) U. Teipel, I. Mikonsaari, H. Krause, J. Ulrich: *Influence of ultrasound on potassium alum crystallization*, Proc. 4th World Congress on Particle Technology, Sydney, 2002
- 18) Mikonsaari, U. Teipel, J. Ulrich: *Kristallisation unter Anwendung von Ultraschall, (Produktgestaltung in der Partikeltechnologie, U. Teipel)*, Fraunhofer IRB-Verlag, Stuttgart p. 255 – 261, 2002
- 19) U. Teipel, U. Förter-Barth: *Verfahren zur Kristallisation aus Lösungen*, EP 1 140 313 B1
- 20) U. Teipel, U. Förter-Barth: *Method for producing crystals from solutions*, US 6.616.847 B1
- 21) E. Curcio, A. Criscuoli, E. Orioli: *Membrane Crystallizers*, Ind. Eng. Chem. Res., 40, p. 2679 – 2684, 2001
- 22) R. Rautenbach: *Membranverfahren: Grundlagen der Modul- und Anlagenauslegung*, Springer Verlag, Berlin, 1996
- 23) U. Teipel, T. Heintz, H. Krause: *Crystallization of Spherical Ammonium Dinitramide (ADN) Particles*, Propellants Explosives and Pyrotechnics, 25, p. 81 – 85, 2000

Progress in Metal Nanoparticle Technology for Industrial Application

Aleksandr A. Gromov

Tomsk Polytechnical University, Russia

Abstract

Properties of aluminum nanoparticles, passivated by non-inert compounds, have been studied. The most important advantage of non-inert coated aluminum nanoparticles is their expected higher combustion enthalpy compared to Al_2O_3 -passivated Al nanoparticles. The drawback of non-oxide coatings is the decreasing of the specific metal content in the powders. For all particles, coated by organic compounds, the organic layer is transparent for oxygen and results in the formation of an internal oxide layer on the particles.

Introduction

Metal nanoparticles have been recently studied for the application in a wide variety of materials, e.g. ceramics as promoters for sintering processes of oxides [1], lubricants for micro-cracking recovering and tear decreasing [2], energetic materials as burning rate accelerators and hydrogen sources [3] and in catalysis for hydrocarbon conversion [4]. The behaviour of metallic nanopowders in different media is mainly defined by their reactivity with air and water [5], because traces of these substances are present almost everywhere: during the period after production and before application, the powders often come into contact with such oxidizing media. Hence, a lot of studies, devoted to this problem, were published [6], but the problem of the protection of the surface of the metal nanoparticles seems to be one of the most important for the development of applications for industrial metallic nanopowders [7].

This work is mainly focused on the protection of aluminum nanoparticles used in energetic materials. Recently, aluminum nanopowders (ANPs), produced by the electrical explosion of wires (EEW) method, are mostly propagated in the world market [8]. This method has a lot of advantages compared to others [9]: high productivity (100-200 g of ANPs/hour for each machine) and low cost of the powders because only electrical energy is consumed for the metal wire destruction (no additional plasma sources, no vacuum and cooling system). After the production, the reactivity of the surface of EEW-ANPs is extremely high: powder storage in an inert gas media results in self-sintering, thus particles should be passivated before the further treatment because non-passivated ANPs immediately self-ignite if exposed to air. The majority of commercially available ANPs are passivated by inert oxide layers consisting of amorphous or crystalline Al_2O_3 [10]. The mechanism of the stabilization of oxide layers on metal particles is widely studied [11]. In fact, the process of oxide layer formation on the surface of nanoparticles upon slow oxidation in air should be called "passivation-up-to-self-saturation" (the structure of such self-saturated oxide layers on Al nanoparticles produced by EEW was studied in [11]). But experimental approaches for the maximal metal storage in Al particles and comprehensive analysis of the processes, occurring during the particle passivation by different substances, should be developed.

Materials and Methods

In the present work, powders were prepared by the EEW method and passivated by different substances: nickel, fluoropolymer, boron, stearic and oleic acid, suspended in kerosene and ethanol. This technique of coating particles by non-inert substances before they come into contact with air was selected because, when the oxide layer was already built up on particles (usually 10-20 wt. % of Al_2O_3), it cannot be removed or substituted under any kind of after-passivation treatment. The properties of the produced powders were comprehensively studied by several chemical analyses. Experimental data of the passivation and oxidation of EEW-ANPs in air and in water were accumulated and analyzed.

ANPs were produced in argon atmosphere by using the EEW facilities developed by the High Voltage Institute at Tomsk Polytechnic University, Tomsk, Russia [9]. The initial Al wire, used for the production of the ANPs, was 0.27 mm in diameter and of 99.8 % purity. The rate of wire feeding was about 50 mm/s and the explosions were repeated with a frequency of ~ 1.1 Hz. The optimal electric parameters, preliminary found, were $e/e_s = 1.4$, $U = 26$ kV, $L = 0.6$ μH for the EEW machine UDP-4G. After producing 1-2 kg of powder, the collector with the powder was removed, and the working cycle was repeated. While the EEW machine was stopped, the collector with the powder was placed into a separate pressure tight passivation chamber. The list of samples, studied within this work, and their specific surface area (S_{sp}), determined by BET method, as well as the metal aluminum content (C_{Al}) after passivation, measured by volumetric analysis, and the volume mean particle diameter (a_v) are shown in table 1. The "Zetasizer 3000" by Malvern Instruments, UK, was used for the determination of the particle size distribution and the volume mean particle diameter (a_v).

Sample 1 (commercial powder ALEX) with widely studied characteristics [12] has been taken for comparison. Samples 2 and 3 were obtained from the composite wires Al-Ni and Al-B, respectively [13]. Air-passivation (samples 1-3) was carried out at $\vartheta=30\pm 2$ °C and $p=1.1$ atm. in argon having an air content of about 0.1 vol. %. The ANP samples 1-3, table 1, were completely passivated for 72 hours. At higher concentration of air in the passivation gas mixture, self-heating and powder self-sintering occur.

Samples 4-7 were passivated by organic substances in solvents before they came into contact with air:

- wt. % stearic acid ($C_{18}H_{36}O_2$) solution in ethanol (C_2H_6O);
- wt. % stearic acid solution in kerosene;
- wt. % oleic acid ($C_{18}H_{34}O_2$) solution in ethanol;
- wt. % fluoropolymer solution.

The solution for passivation was added to the fresh powder immediately after production and the powder solution was mechanically stirred for ~2 hours. The temperature was maintained at 30 ± 5 °C in order to avoid self-heating of the powder. The residual solvent was evaporated from the ANPs by vacuum treatment at room temperature.

The morphology and the compositions of the particles (table 2) were tested by TEM-EDS (Philips CM 200 FEG), SEM (Jeol 6500 F) and XRD (Rigaku "MAX-B" diffractometer) with $CuK\alpha$ radiation. Two types of ANP-tests were used: reactivity in air (table 3), and in 10 wt. % NaOH water solution (Fig. 2). DTA-DSC-TG (Universal 2.4 F TA Instruments) was used for testing the non-isothermal oxidation.

Results

The specific surface area was at the same level (11-14 m^2/g , table 1) for all samples except sample 2 (40.7 m^2/g) and 5 (7.3 m^2/g). The reduction of C_{Al} is maximal for ANP passivated by oleic acid – down to 45 wt. %. One of the possible reasons is the interaction of oleic acid with NaOH, resulting in a formation of a non-soluble sodium oleate layer which protects the fresh metal from further oxidation in static solution. Hence, the coating of particles by organic reagents leads to a considerable reduction of the specific metal content because the particles hold a lot of organic substances on their surface (table 1). In the case of boron this effect is not so obvious. The term "specific metal content" (table 1, last column) characterizes the content of metal in the powder, but not in the particle (table 2). ALEX has a relatively high metal content and S_{sp} is comparable to sample 3 (boron coated).

№	Sample code	Initial wire composition	Gas media in explosive chamber	Passivation condition	S_{sp} (BET), m^2/g	a_v , nm	C_{Al} , wt. %
1.	ALEX	Al	Ar	Air	11.3	484	86
2.	Al (Ni)	Al (Ni)			40.7	237	53
3.	Al (B)	Al (B)			12.0	610	84
4.	Al (St Ac) ethanol	Al		Stearic acid in ethanol	12.1	255	74
5.	Al (St Ac) kerosene	Al		Stearic acid in kerosene	7.3	410	79
6.	Al (Ol Ac)	Al		Oleic acid in ethanol	14.3	393	45
7.	Al (F)	Al		Teflon	11.6	284	81

Table 1: Properties of aluminum nanopowders studied

According to TEM, the concentration of Al inside the particles increases when applying organic coatings (Fig. 1), while the specific metal content is lower for powders passivated by organic substances (table 1). The content of metal in the particles, passivated by oleic acid, is higher than for ANP passivated by air. According to TEM data, the particles, passivated by air, are covered by oxide films (thickness of 4-8 nm), while the particles, passivated by oleic acid (Fig. 1 b), do not have any visible oxide layer. Analyzing the image in Fig. 1 a, we can observe the beginning of oxide film crystallization, i.e. the critical thickness for the amorphous oxide film is 4-5 nm after which crystallization begins. Thus, under selected air-passivation conditions, at a thickness of the oxide layer of 4-5 nm, the oxidation of the particle's surface stops and crystallization of the oxide layer occurs.

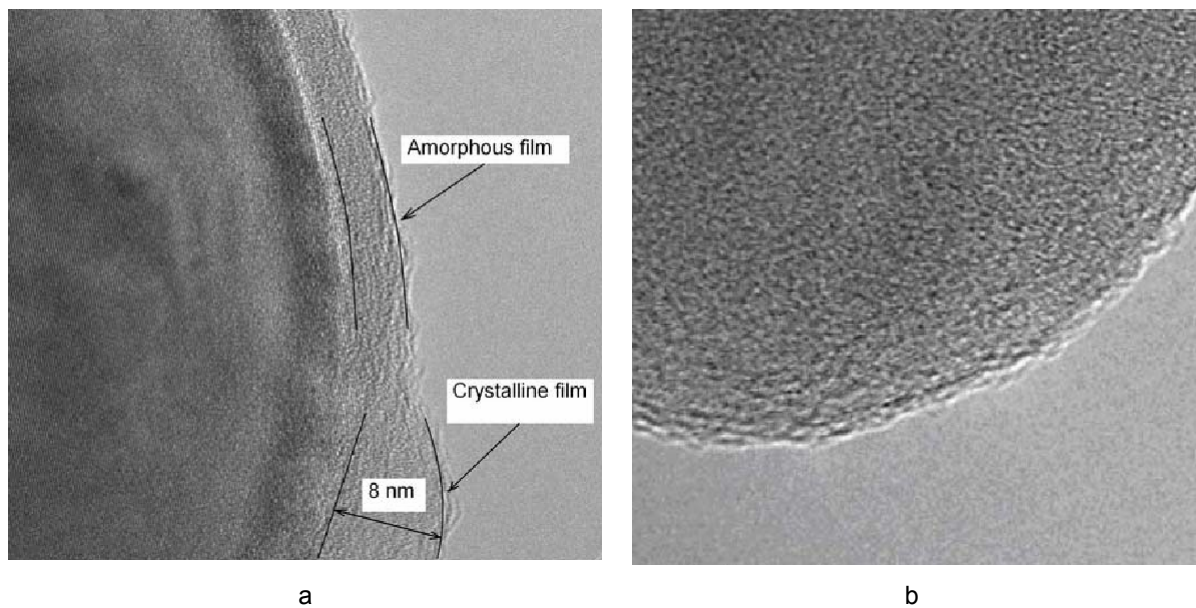


Figure 1: TEM images of ANPs passivated by air (a, sample 1) and oleic acid (b, sample 4)

BET and a_v data from table 1 do not correlate, that probably also means the presence of a small amount of very fine particles in the samples, but even a small quantity of very fine particles determine the high value of S_{sp} . The diameter of the largest particles found was not more than 1-2 μm (by TEM, SEM and size distribution analyses) for all samples.

The results of EDX and XRD study are presented in table 2. All powders contain more than 10 wt. % of oxygen (as oxides) on the particle surface. Traces of aluminum carbide were found by XRD for the samples 4-6, but carbon was not determined by EDX because carbon films were used as object slides for the samples. Boron in sample 3 was not found, probably because of its low molecular weight and, hence, EDX method has low sensitivity for this element.

№	Sample code	Wt. content of elements, % (EDX)			Phase composition (XRD)
		O	Al	Ni	
1.	ALEX	10	90	-	Al
2.	Al (Ni)	22	74	4	
3.	Al (B)	11	89	-	
4.	Al (St Ac) ethanol	15	85	-	Al, traces of Al_4C_3
5.	Al (St Ac) kerosene	15	85	-	
6.	Al (Ol Ac)	18	82	-	
7.	Al (F)	12	88	-	Al

Table 2: Elemental and phase composition of aluminum nanopowders

The beginning of intensive ANP oxidation in air was below the melting point of aluminum (660 °C). The results of the DSC - TG analysis of the ANP samples, passivated in air, are represented in table 3. The non-isothermal heating of the samples was executed with a rate of heating 10 of K/min. The maximum temperature of the oxidation onset (T_{ox} onset) is characteristic for sample 2. Probably, this is caused by the presence of refractory nickel (see table 2) in the composition of the passivating layer on the surface of the particles. The T_{ox} onset of the samples, passivated by air, changes in the range of 556-565 °C and does not correlate with the dimensional characteristics of the powders and the type of the passivating coating. For sample 8, the oxidation begins at 486 °C (much lower than the melting point of aluminum). The adsorbed gas weight for the samples of "dry" ANP (samples 1-3) does not exceed 2 % with exception of the nickel-containing sample. The mass of organic coatings (samples 4-7) is 3-4 times higher than for the "dry" samples 1-3. The degree of conversion (α) to

1400 °C (last column, table 3) is relatively high for all samples.

№	Sample code	T _{ox onset} , °C	Weight of coating (gases), %	+Δ m (up to 660°C), %	+Δ m (up to 1400°C), %	Δ H _{ox} Al, J/g	α* (500÷1400°C), %
1.	ALEX	558	2	26	68	5465	89
2.	Al (Ni)	565	9	13	43	-	88
3.	Al (B)	556	2	24	63	6232	84
4.	Al (St Ac) ethanol	549	5	23	58	5997	88
5.	Al (St Ac) kerosene	557	6	27	74	6282	105
6.	Al (Ol Ac)	486	10	15	38	4875	95
7.	Al (F)	538	6	21	68	5184	94

Table 3: Reactivity parameters of aluminum nanopowders (m=7.5 mg) under non-isothermal heating in air

$$\alpha(Al \rightarrow Al_2O_3) = \frac{+\Delta m}{C_{Al} \cdot 0,89} \cdot 100 \quad \%$$

C_{Al}, % - metal content in the samples (table 1)

The kinetics of the interaction of the powders with water was investigated using a 10 wt. % NaOH solution at 20 °C (Fig. 2). The kinetic curves for all powders have the same character, but ALEX does practically not have an induction period. The coated ANP samples show a good stability in the NaOH solution. Thus, practically each of the organic coating protects the particle surface against oxidation in water better than the oxide ones.

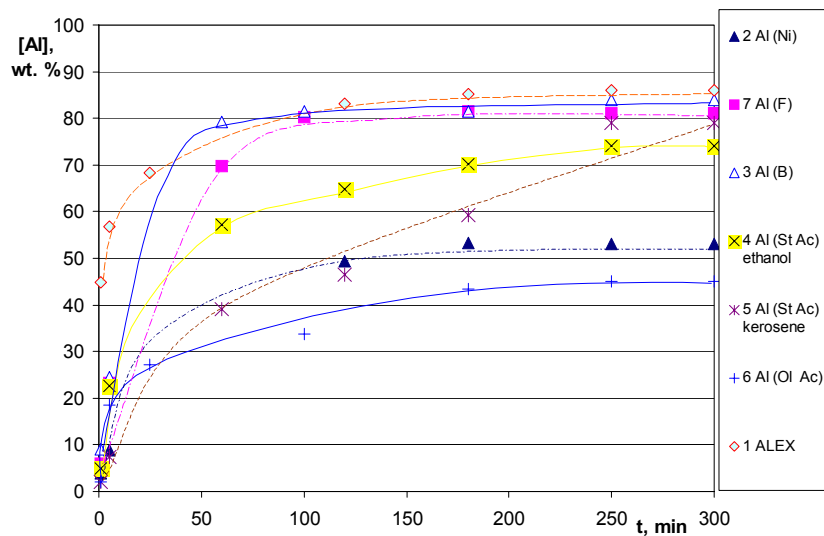


Figure 2: Kinetic curves for aluminum nanopowders with different coatings, interaction with 10 wt.% NaOH water solution. Numbers of samples in table 1

The specific metal content for ALEX is the highest compared to the other powders. The reaction of the “dry” powders with water has no induction period (Fig. 2). Hence, the oxide film has low protective properties in water.

According to TEM, the sample Al (Ni) consists of two types of particles: a very fine fraction and large particles. 4 wt. % of Ni (table 2), according to EDX, does not cover the surface of the large Al particles, but are separately distributed in a small oxidized fraction. The particle surfaces of this sample are not smooth. Thus, the explosion of Al-Ni composite wires results in the formation of smaller particles (table 1) than for Al without coating, but the size of such small particles is less than the border of stability – about 30 nm for Al [7]. The residual non-oxidized Al particles react with air completely at $T < 1000$ °C (table 3): Ni does not increase the stability of fine Al particles towards oxidation in air.

The aluminum content and S_{sp} for the sample Al (B) was nearly the same as for sample 1 (ALEX, table 1), and the degree of conversion up to 1400 °C is high enough (table 3). Boron-coated powder has also a high value of ΔH_{ox} in air. Boron-coated particles react with water having a very short induction period (few seconds, Fig. 2). Ni-coated particles have a low Al metal content under reaction with water. It can be caused by the presence of a lot of NiO and a big fraction of very fine oxidized particles.

Stearic acid and oleic acid mostly interact chemically with the aluminum particle surface during passivation. In the case of oleic acid, interaction with metal was more intensive. C_{Al} decreased to 45 wt. % in sample 8 (table 1). It is noticeable that the interaction of Al with stearic acid and oleic acid results in the carbidization of the particles surfaces (see table 2). For the majority of the organic coated particles, we did not observe strong organic layers which could completely protect Al particles from further oxidation. In the case of Al (OI Ac), the particles hold more oxygen than other samples (table 2). Moreover, according to TEM, organic coated metal particles have two layers: an organic layer and an internal oxide layer (Fig. 3).

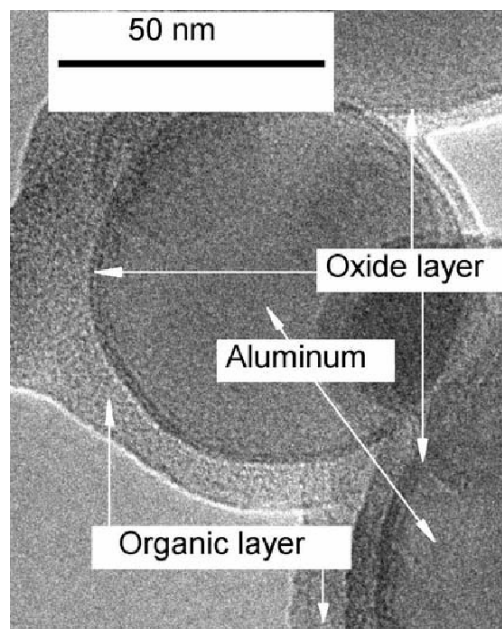


Figure 3: Two-layer coating of organically passivated Al particles

Conclusion

The most important advantage of non-inert coated aluminum nanoparticles is their expected higher combustion enthalpy compared to Al_2O_3 -passivated Al particles. The drawback of non-oxide coatings is the decreasing of the specific metal content in the powders. For all organic-coated particles, the organic layer is transparent for oxygen and results in an internal oxide layer formation (Fig. 3). Aluminum particles, produced from composite Al (B) and Al (Ni) wires, show approximately the same characteristics as oxide coated ones.

Acknowledgments

This work has been supported by INTAS grant YSF 55-03-671.

References

- 1) T. A. Khabas, *Glass and Ceramics*, 59, 2002
- 2) Y.S. Kwon, A.P. Ilyin, D.V. Tikhonov, S.V. Richert, G.V. Yablunovskii, *Proc. KORUS-2004, 8th Kor.-Rus. Int. Symp. on Sci. and Tech.*, Tomsk, Russia, June 2004.
- 3) U. Teipel (Ed.), *Energetic Materials*, Wiley, 2004.
- 4) M. Bowker, D. James, P. Stone, R. Bennett, N. Perkins, L. Millard, J. Greaves, A. Dickinson, *Journ. Catal.*, 217, 2003
- 5) V.G. Ivanov, M.N. Safronov, O.V. Gavriluk, *Comb. Expl. Shock Waves*, 37, 2001
- 6) N. Eisenreich, H. Fietzek, M.M. Juez-Lorenzo, V. Kolarik, A. Koleczko, V. Weiser, *Prop., Explos., Pyrot.*, 29, 2004
- 7) K.J. Klabunde (Ed.), *Nanoscale Materials in Chemistry*, Wiley, 2001
- 8) Y.F. Ivanov, M.N. Osmonoliev, V.S. Sedoi, V.A. Arkhipov, S.S. Bondarchuk, A.B. Vorozhtsov, A.G. Korotkikh, V.T. Kuznetsov, *Prop., Explos., Pyrot.*, 28, 2003
- 9) Y.S. Kwon, Y.H. Jung, N.A. Yavorovsky, A.P. Ilyin, J.S. Kim, *Scripta mater.*, 44, 2001
- 10) J. C. Sánchez-López, A. Fernández, C. F. Conde, A. Conde, C. Morant, J. M. Sanz, *Nanostruct. Mater.*, 7, 1996
- 11) J.C. Sanchez-Lopez, T.C. Rojas, J.P. Espinos, A. Fernandez, *Scripta mater.*, 44, 2001
- 12) M.M. Mench, K.K. Kuo, C.L. Yeh, Y.C. Lu, *Comb. Sci. Tech.*, 135, 1998
- 13) A. P. Ilyin, Yu. A. Krasnyatov, D. V. Tikhonov, Russian Federation Patent 2139776

Fabrication, Properties and Application of Electroexplosive Aluminum Nanopowders in Highly Energetic Materials

V.V. An*
V.A. Arkhipov**
A.P. Ilyin*
Y.-S. Kwon***
A.G. Korotkikh**
D.V. Tkhonov*

* Tomsk Polytechnical University, Russia
High Voltage Research Institute

** Tomsk State University, Russia
Research Institute of Applied Mechanics and
Mathematics

*** University of Ulsan, Republic of Korea

Abstract

A study of fabrication, properties and application of electroexplosive aluminum nanopowders in highly energetic materials was carried out. In order to study the influence of nanopowders on the burning rate of highly energetic materials (HEM) based on ammonium perchlorate and a combustible binder, butyl rubber BKL was used. It was shown that the increase in the burning rate of the HEMs containing metal nanopowders is caused by the increase of the heat flow from the combustion surface to the heating zone.

Introduction

Wire electrical explosion (WEE) is a promising fabrication method for a number of materials with unusual physicochemical properties [1]. The WEE process is characterized by a high current density ($j > 10^{10} \text{ A/m}^2$), fast heating ($> 10^7 \text{ K/s}$) of metal up to high temperatures ($T > 10^4 \text{ K}$) and extremely high power density ($\sim 10^{14} \text{ W/m}^3$). A “fast” regime of electrical explosion is optimal for the fabrication of nanopowders. In this case, instabilities do not have a noticeable impact on the destruction of the conductor, and the character of the WEE process depends on the rate of energy release in it [2, 3]. The increase of energy input into the wire leads to the increase of the part of metal passed into the vapor. However, the obtaining of a merely vapor phase is considered to be impossible. The particles of powder are formed both due to the condensation of the vapor phase and the dispersion of liquid metal [3].

The dispersivity of aluminum powders is described by the empirical dependence:

$$\bar{a}_\sigma = 0,3 \cdot 10^{-6} (W / W_c)^{-3} \quad (1)$$

provided $0.7 \leq W/W_c \leq 2.1$, where W is the energy input into the wire, and W_c is the energy of sublimation of the exploded conductor. When $W/W_c > 2.1$, the dispersivity is approximated by the following expression:

$$\bar{a}_s = 0,5 \cdot 10^{-7} (W / W_c)^{-0,5} \quad (2)$$

The refractoriness of initial materials and the big difference in their melting temperatures are not an obstacle for the WEE technology. The use of the wire electrical explosion technology allows fabrication of alloys and intermetallic compounds in the ultra-dispersed state that is the advantage of this method [5].

Materials and Methods

The 0.35 mm diameter wire with aluminum content of 99,5 wt% was used as exploded conductors. Explosions were conducted in the argon atmosphere at the pressure of $1.5 \cdot 10^5 \text{ Pa}$ in the experimental setup of which the scheme is shown in Fig. 1. Before filling the setup with inert gas, it was vacuumized down to 100-200 Pa. The energy input into the wire was calculated using current oscillograms and circuit electrical parameters according to the known method [6]. In a series of experiments, the energy input into the wire was adjusted by changing the charging voltage of the capacity storage. The powder phase composition was measured using an X-ray diffractometer DRON-3.0. The surface-average diameter of particles was calculated on the basis of the low-temperature nitrogen adsorption data (BET method).

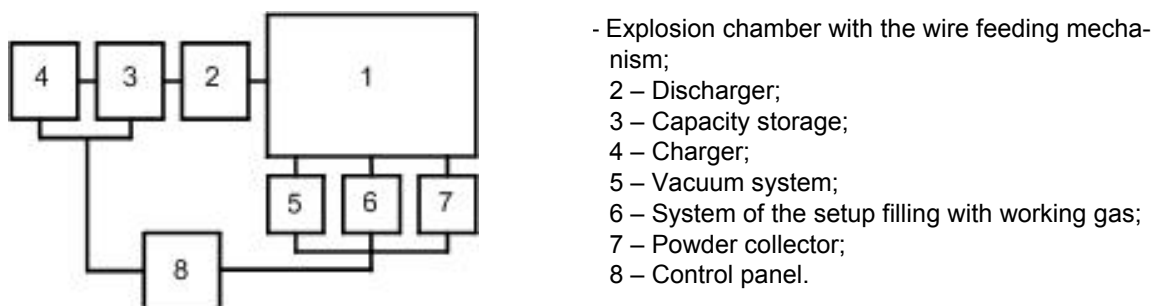


Figure 1: Structural scheme of the experimental setup

Results and Discussion

Characteristics of the powders are given in tab. 1. The particle size distribution is close to the normal-logarithmic one. When increasing the energy input into the wire, W/W_c , the dispersivity of the powder rises, whereas the metal aluminum content decreases. After WEE, the particles spontaneously precipitate in the powders collector (position 7, Fig. 1). At the same time, their fast sintering was not observed. Taking into consideration that the explosion process occurs at overpressure and nanopowders possess a very low apparent density ($\sim 0.1 \text{ g/cm}^3$), the presence of a gas shell of argon adsorbed at the surface of particles was assumed. At first after the manufacturing, the gas shell does not allow the particles to contact and preserves them from sintering. Subsequently, the collector with powder was placed to a hermetic box filled with argon at atmospheric pressure. The oxygen content in argon did not exceed 0.1 vol. %.

Nr.	Energy input into the wire, W/W_c	Metal content, wt%	Specific surface area (S_{sp}), m^2/g	Surface-average diameter of particles (\bar{a}_s), nm	Oxide content (calculated), wt. %	Oxide layer thickness, nm
1	1,82	88,0±1,4	10,8±0,3	210	19,0	4,96
2	1,71	87,9±0,3	9,9±0,3	220	19,1	5,44
3	1,62	88,1±1,1	9,9±0,9	220	18,9	5,37
4	1,45	88,5±0,9	9,3±0,3	240	18,4	5,56
5	1,30	90,9±0,8	8,8±0,25	250	16,1	4,91
6	1,13	90,0±0,6	6,7±0,2	330	17,0	6,92
7	0,92	91,0±0,7	7,7±0,25	290	16,0	5,56

Table 1: Characteristics of aluminum powders obtained in argon atmosphere

Recently, it was shown [7] that the dispersivity of the products of explosion of copper and aluminum wires in argon increases with the increase of the energy input into the wire, whereas the particle size distribution narrows. Experiments have shown that both the size of the particles and the coherent scattering areas (d_{SCA}) decrease when increasing W (Fig. 2). It can be assumed that primary products of wire dispersion during their spreading and interaction transform into bigger particles with the crystal structure reflecting the sizes of the primary products. Indeed, an increase in the sizes, d_{SCA} , is observed when the dispersivity of final WEE products increases. According to obtained results, the increase of the input energy more than $0,8 \div 1,6 W/W_c$ (W_c is the sublimation energy of the exploded wire) leads to a drastic rise of the dispersivity of the final products (Fig. 2). During subsequent increase in W/W_c , the dispersivity rises significantly slower. The calculations show that the increase in the specific surface area to the increase of energy inputs ($\Delta S/\Delta W$) in the first region is $\sim 1 \text{ m}^2/\text{kJ}$ and $1.5 \text{ m}^2/\text{kJ}$ ($W/W_c = 1.8 - 2.0$) for the second region.

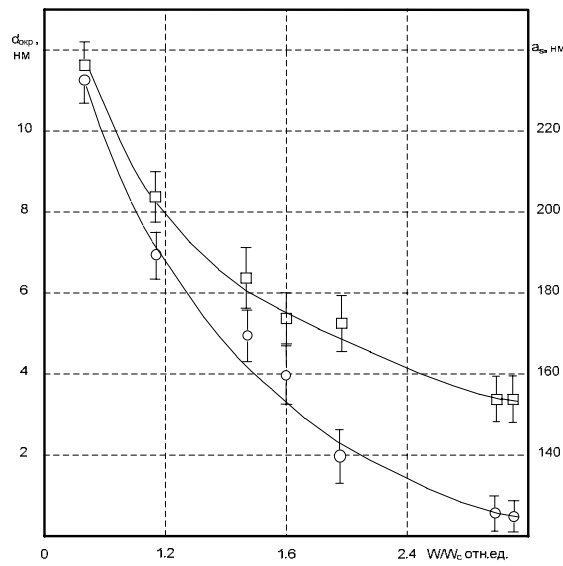


Figure 2: Dependencies of the average diameter of the particles, a_s , and the coherent scattering areas, d_{SCA} , on the energy input into the wire during the electrical explosion of aluminum wires in argon atmosphere

In order to study the influence of nanopowders on the burning rate of highly energetic materials (HEM) based on ammonium perchlorate and combustible-binder, butyl rubber BKL was used. HEM samples of 10 mm diameter and 30 mm height were prepared by through pressing with subsequent hardening in a drying chamber at 343 K for 3 days [8]. For comparison, industrial aluminum powder ASD-1 and ASD-4 were used as metal fuels. Their surface-average diameters of particles were 80 and 10 μm , respectively. In order to study the burning rate, aluminum nanopowders produced by WEE in argon were used. Their content in HEMs varied from 5 to 20 wt%. In this work nanopowders of copper, iron and nickel were employed as combustion catalysts. They were also fabricated by WEE in argon atmosphere. Their content in HEMs was 1 to 4 wt%. The determination of the HEMs burning rate was conducted in a constant pressure bomb at an increased argon pressure (1.0-8.0 MPa). Samples were armored at the side surface. The samples were ignited out with a nichrome spiral. The average burning rate was determined by the time of the combustion wave passing through a certain charge site by applying the following formula:

$$u = l / t_u \tag{3}$$

where l is the distance passed by the combustion wave front, mm; t_u is the time of sample combustion, s.

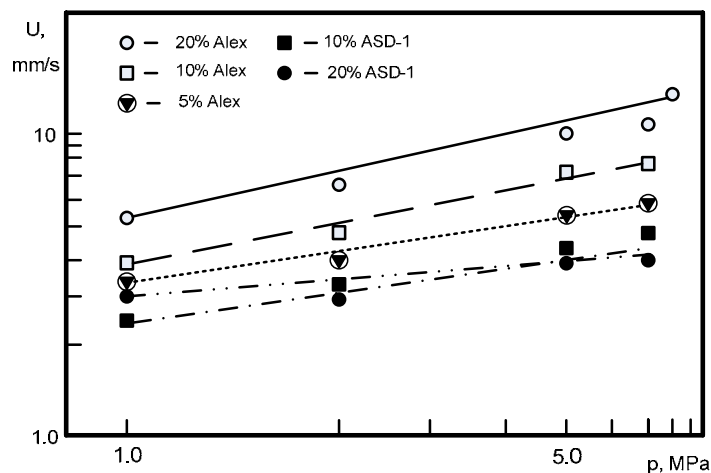


Figure 3: Burning rate of HEMs samples depending on the surrounding pressure

Dependencies on the pressure of the burning rate of the HEMs samples based on the mixture of ammonium perchlorate and butyl rubber are presented in Fig.3 . These mixtures contain 5 to 20 wt% of different powders. The coefficient of oxidizer excess is $\alpha=0.4$.

According to the obtained results, the HEMs burning rate increases with the increase of the surrounding pressure in the range of 1.0 to 6.3 MPa. For the HEM containing 5 wt% of aluminum nanopowder (composition No. 5), the rate varies from 3.4 to 6.6 mm/s (increased by a factor of 1.9). For the HEM containing 10 wt% of aluminum nanopowder (composition No. 3), the rate is 3.8 to 9.5 mm/s (increased by a factor of 2.9). If the aluminum nanopowder content is of 20 wt%, the rate increases from 6 to 21.5 mm/s (by a factor of 3.6) in the range of pressures from 1.0 to 8.0 MPa. According to the experimental data, the burning rate of HEMs samples increases at the same surrounding pressure with the increase of aluminum nanopowder content in the HEM composition. For the HEM samples containing 10 and 20 wt% (composition No. 4 and No. 2) of aluminum powder ASD-1, the burning rate increases from 2.8 to 5.6 mm/s and from 3 to 4.9 m/s, respectively. The decrease in the burning rate for the HEM containing 20 wt% of aluminum powder ASD-1 is most probably due to the heat rejection from the combustion zone and to the undercombustion of metal. The same effect is observed to a lesser degree for the ASD-1 powder content equal or higher 10 wt%.

K	Catalyst content in the HEM				
	1 wt% of Fe nanopowder	1 wt% of Cu nanopowder	1 wt% of Ni nanopowder	1% of Fe nanopowder	4% Fe nanopowder
	1.15	1.47	1.10	1.24	1.11

Table 2: Combustion efficiency of HEMs based on APC and BKL containing 10 wt% of ASD-4

The influence of metal nanopowder additives as catalysts during the HEM combustion was estimated using a combustion efficiency coefficient K. The latter is equal to the ratio of the burning rate of a metallized composition with catalyst to that of the composition without catalyst upon other equal conditions (tab. 2). The studies were carried out in the air at atmospheric pressure.

The HEM containing 10 wt% of ASD-4 powder as a metal fuel was used to study the catalytic activity of nanopowders. According to the experiments, when injecting additives of metal nanopowders, the burning rate of blend compositions increases by a factor of 1.10-1.47. The highest increase of the burning rate was observed for the sample containing 1 wt% of copper nanopowder (tab. 2).

Conclusion

The cause of the increase in the burning rate of the HEMs containing metal nanopowders is the increase of the heat flow from the combustion surface to the heating zone. As a result, the chemical reactivity of metal nanopowders and their oxidation in the gas phase increase. The low mass of metal nanoparticles and, accordingly, their low thermal capacity lead to an increase of the ignition delay time several times higher in comparison to the industrial powders ASD. The observed mass burning rate of metal nanoparticles is therefore higher than that for particles of regular aluminum powders.

The action of metal nanopowders as catalysts is obviously related to their participation in destruction of oxide shells on aluminum nanoparticles and in oxidation of aluminum vapors and intermediate products at high temperatures. It is necessary to note that thermal effects of the copper oxidation are lower than those of aluminum.

References

- 1) W. Chace, H. Moore (Eds.): *Exploding Wires*, Plenum, 1, New York, p. 373, 1959
- 2) N. N. Stolovich: *Electroexplosive energy converters*, Nauka i tekhnika, Minsk, p. 152, 1983
- 3) V. A. Burtsev, N. V. Kalinin, A. V. Luchinsky: *Electrical explosion of wires and its application in electrophysical plants*, Energoatomizdat, Moscow, p. 289, 1990
- 4) N. A. Yavorovsky: *Electrical explosion of wires as a method of powder producing*, Thesis of Candidate of Technical Sciences, Tomsk, p. 118, 1981
- 5) E. I. Azarkevich, A. P. Ilyin, D. V. Tikhonov, G. V. Yablunovski: *Electroexplosive synthesis of ultra-dispersed powders of alloys and intermetallic compounds*, *Fizika i khimia obrabotki materialov* (in Russian), 4, p. 85-88, 1997
- 6) I. F. Kvarsthava, V. V. Bondarenko, A. A. Plutto: *Oscillographic determination of the energy of wire electrical explosion*, *Zhurnal tekhnicheskoi fiziki* (in Russian), 31, 5(II), p. 745-751, 1956
- 7) Yu. A. Kotov, N. A. Yavorovsky: *Study of particles formed during wire electrical explosion*, *Fizika i khimia obrabotki materialov* (in Russian), 4, p. 24-29, 1978
- 8) A. G. Korotkikh: *Study of process of ignition and combustion of highly energetic materials containing ultra-dispersed aluminum powder*, Thesis of Candidate of Physical and Mathematical Sciences. Tomsk, p. 138, 2004

Study of Ultrafine Powders Produced by the Exploding Wire Method

V.S. Sedoi
Yu.F. Ivanov
M.N. Osmonoliev

Institute of High Current Electronics RAS
Tomsk, Russia

Abstract

Fine and ultra-fine powders are actively used in pyrotechnics, explosives and propellants. The important questions are how to produce a powder with specified characteristics and how to use the powder produced.

Previous studies have shown that the essential factor is the size distribution of the particles. It is important to point out that the powder activity depends on the surface state of the particles. This paper presents a new approach to produce powders by the exploding wire method. The influence of the initial conditions on the properties of the powders is discussed.

The data produced shed new light on particle formation under the fast Joule heating: the particle size depends on the initial size of crystallites of a metal. From beginning, the power of Joule dissipation is higher on the boundaries of these crystallites. As a result, "a gas of drops" is formed instead of "a gas of atoms". Initial conditions of explosion regulate size and morphology of the particles, phase compositions, and thermal properties of the powders. During expansion, particles contact with surrounding gas and it is possible to produce particles with different state of a surface. Investigations performed have shown that the electrical explosion allows synthesizing the powders passivated by a thick surface layer of oxide or nitride.

The phase constitution of the produced powder can be varied from pure aluminum to pure alumina and from pure aluminum to nitride. Nitrogen is a perspective gas since it has a lower mass density than those of inert gases and this allows increasing the powder fineness. A thin layer of nitride prevents particles from agglomeration and the metal powders produced in nitrogen exhibit a rather high activity in oxidation. With that, the activity of powders produced in the low-pressure nitrogen remains high and stable during long time of storage. Nitride reacts with water vapor contained in the air and according to the reaction $2\text{AlN} + 3\text{H}_2\text{O} = 2\text{NH}_3 + \text{Al}_2\text{O}_3$ a thin layer of oxide arises.

To determine activities of the powder samples in the combustion reactions, the Differential Thermal Analysis (DTA) and Thermogravimetry (TG) were conducted. In conclusion it may be said that the exploding wire method is a very promising method of ultra-fine powder production. It is possible to produce ultra-fine powders of a pure metal and compounds with controlled phase compositions. Real future success requires the coordinated joint efforts of a wide circle of researchers and technologists, producers and users.

Introduction

Nowadays, nanophase materials formed of ultra-fine particles or crystallites attract a building up attention by possibilities to develop new technologies and to produce materials with new properties. This area opens a wide range of commercial applications. The perspective route is the exploitation of ultra-fine powders as a component of energetic materials. Recent investigations [1-3] show that the use of nanopowders allows modifying the burning rate, increasing the specific impulse, and preventing the agglomeration. It is natural that size, size distribution, morphology, and nanostructure of particles are very important characteristics.

The purpose of the present paper is to highlight the possibilities of the exploding wire method for the production of ultra-fine powders, to comment its merits and demerits, and to describe some of the features of the powder produced. The description rests on the evidence obtained experimentally.

The structure of the paper is as follows: the second section describes the exploding wire method, it has been shown that the method is energy saving and the size of the particles depends on the initial size of crystallites of a metal. Sections 3 and 4 dwell on such powder properties like size and morphology, phase composition of Al-based powders and thermal properties. The final section summarizes the production and characterization of ultra-fine powders produced by the exploding wire method.

Exploding Wire Method of Powder Production

The exploding wire (EW) method is based on the Joule heating of a thin wire. Compared to other methods of vaporization, the electrical explosion has the advantage of the direct conversion of electrical energy into heat. The specific energy released in a wire is given by the equation:

$$w = \int j^2 \rho \, dt / \gamma \approx j^2 \bar{\rho} t / \gamma \quad (1)$$

Here j is the current density in the wire, ρ is the specific resistance, γ is the density, and t is the time. The effectiveness of conversion of electrical energy w_0 into heat w is described by the empirical formula [4].

$$w/w_0 = (h/h_0)^{0,5} \quad (2)$$

$$h = \int j^2 dt \quad (3)$$

$$h_0 = j_0^2 \sqrt{LC} / 2, \quad h \leq h_0 \quad (4)$$

In the matched explosion regime ($h = h_0$) practically all energy stored in the circuit is released in the wire resistance during the first pulse of current. The EW technology is energy saving.

It is clear that the mean particle size d and the function of the particle size distribution will vary with increasing input energy density. The current conception supposes [5] that due to the level of Joule heating, the state of a metal changes from solid to vapor-plasma. When the input energy density is of the order of the sublimation energy w_s , and more, the ion condensation of the metal vapor occurs. The condensation centers are ions, and the size of particles depends on the ionicity and the expansion velocity. This idealized model leaves out of account the heterogeneity of heating and the fluctuation of mass density in an expanding metal. It should be expected most precise that, if the input energy density $w/w_s \geq 1 \div 2$, the condensation centers appear in the beginning of the metal expansion, in the so-called phase of "expanded metal".

It is known that the metal structure is not uniform. Boundaries of grains, defects, impurities, and dislocations determine the resistivity and may cause the heterogeneity of Ohmic heating. This point requires examination, and one of the principal objectives of this study is to investigate the influence of the initial microstructure of a metal on the particle size. The certification of powders is also an important question and another goal of the paper presented. This line is urgent both from the phenomenological and technological viewpoints.

Method of investigation

A choice of conditions to compare correctly various metals is a grave aspect. Major properties of the produced powders, for instance, the medium size, are considered at least in a five-dimensional space of initial conditions. The introduced energy density w , the current density j , the diameter of a wire d , the density and reactivity of the environment are important factors [5, 6]. Characteristics of the exploded metal must be added to that, namely, the energy of sublimation w_s and the minimum current density j_m at which magnetohydrodynamic instabilities have no time to develop [4]. The shape of the current pulse is also important.

- On this basis, a comparison of various metals has been performed under the following conditions:
- The introduced energy density is close to the sublimation energy of a metal.
- The current density in a wire is close to j_m for the given metal resulting in the fast explosion mode.
- The explosion is carried out in a mode close to the matched one, when $h=h_0$ and according to (2) actually
- the whole energy initially stored in the capacitor is released in the wire during the first half-period of the discharge current.
- In all cases the low-pressure nitrogen has been used as a surrounding gas. The low-pressure nitrogen allows producing pure metal particles and metal particles coated with nitride [6].

For comparison, the medium-surface particle sizes d_s of the powder and the medium sizes of the crystallites d_{rcs} were confronted. The size d_s has been evaluated from the specific surface area S (BET): $d_s = 6/\gamma S$. The size of the crystallites has been determined by the X-ray diffraction method as the size of the region of coherent scattering (RCS). For completeness, the electron-microscopic measurements of a count-medium size D of the particles and empirical standard deviation σ of sizes were performed as well.

Investigations of the particle size and morphology have been accomplished by the 125 kV transmission electron microscope. In preparation, the powder - industrial alcohol suspension was applied on a slide and dried. Then a carbon layer was sputtered on the powder-slide using the vacuum post VUP-2K. The resulted carbon replica was isolated by the use of a water solution of gelatin, gelatin was dissolved, and the carbon replica with the sputtered powder was placed on a copper mesh. The mesh with the powder was used as the subject for electron-microscopic investigations. Medium sizes of the particles and their size distribution were analyzed with microphotographs with X250 -...-300x10³ magnification. The results are given in the figures. The number of measured particles averaged 300-500 depending on the size uniformity of powder. The algebraic number of particles with the size of a given interval were plotted on histograms. It is necessary to have in view that this procedure is limited to a particle size of not more than 5-8 micrometer, because such particles may be lost. So, the results will be distorted and the size of particles determined by TEM will be lower than one determined by BET.

Investigation results

The following table shows the initial conditions and gives observations.

Sample	w/w_s	j/j_m	$S, m^2/g$	d_s, nm	d_{rcs}, nm	D, nm	σ, nm
Al (93)	1.0	1.0	17.5	127	50	40.2	16.4
Al (94)	1.0	1.0	11.0	200	77	48.3	30.5
In	1.0	1.3	5.2	160	71	-	-
Cu	0.9	1.1	6.1	110	64	-	-
Fe	1.0	1.0	8.0	95	67	-	-
Ti	0.8	1.0	29.6	45	25	14.2	8.1
W	0.8	1.0	2.4	130	-	13.6	14

Table 1: Initial conditions and results

The data produced shed new light on the particle formation under the fast Joule heating: the size of particles depends on the initial size of crystallites of a metal. From beginning, the power of Joule dissipation is higher on the boundaries of these fluctuations. As a result, “a gas of drops” is formed instead of “a gas of atoms”. Besides such known factors as the density and uniformity of the introduced energy, the density and reactivity of surroundings, the wire diameter and the current density there is a new major factor to control the process. This is the microstructure of the exploded metal.

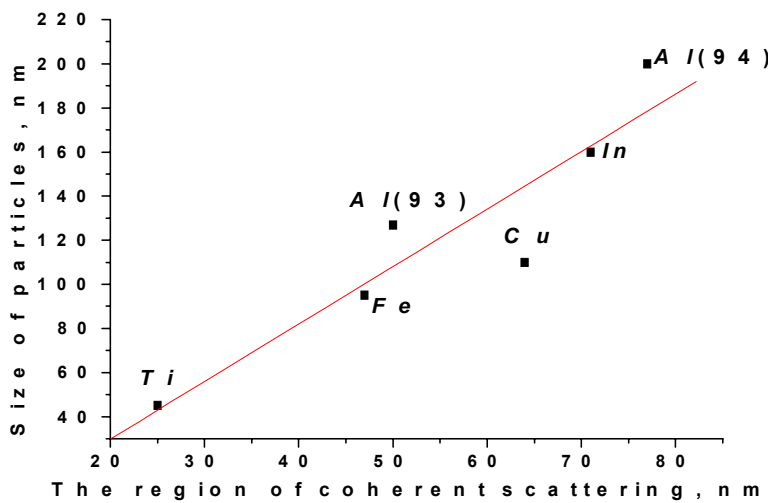


Figure 1: Dependence of the particle size on the initial crystallite size

Properties of Powders

The initial conditions of the explosion regulate the size and morphology of particles, phase compositions, and thermal properties of powders. It is very important to know this connection.

Size and morphology

Investigations of particle size and morphology have been accomplished with a 125-kV transmission electron microscope. The specific surface area S also has been determined because common measurements by TEM and BET methods are more informative.

Titanium powder

The particles of the titanium powder have an intricate spatial form with cross sections in a plane as a square, rectangle, triangle, and in some cases, hexagon shape (Fig. 2). The medium size of the particles is $D = 14.24$ nm and the root-mean-square deviation $\sigma = 8.11$ nm. The particle size distribution is monomodal and logarithmic-normal (Fig. 3).

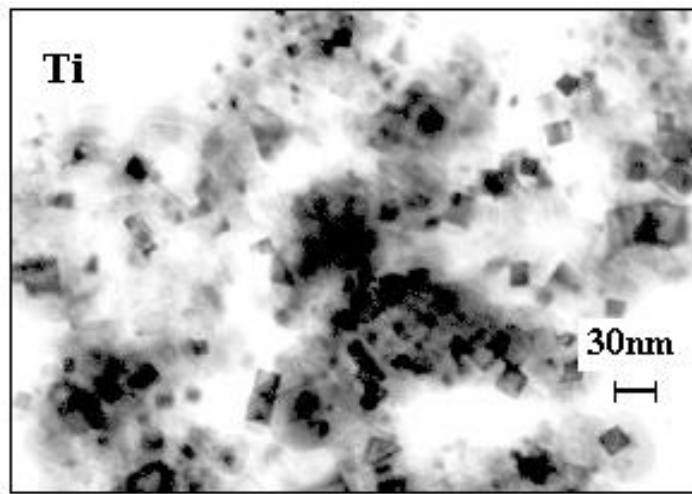


Figure 2: TEM photo of the titanium powder

The specific surface area S of the titanium powder is 30 m²/g (see Table 1).

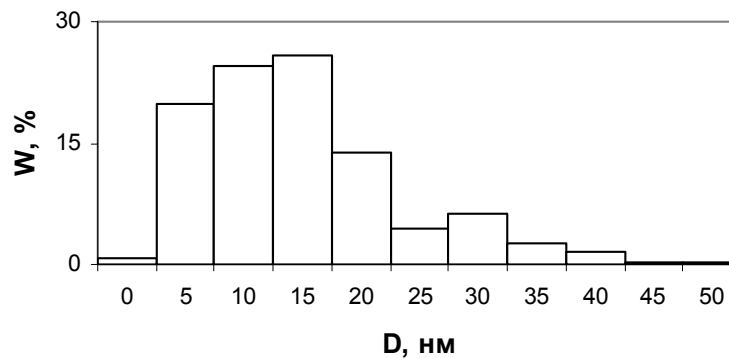


Figure 3: The size distribution of Ti particles

Tungsten powder

The particles of the tungsten powder are of spherical form. The medium size of the particles, D , is 13.6 nm and the root-mean-square deviation, q , is 14.0 nm. The scattering of the powder size (Fig.4) results in the low value of the specific surface area: $S = 2,4 \text{ m}^2/\text{g}$, $d_s = 130 \text{ nm}$.

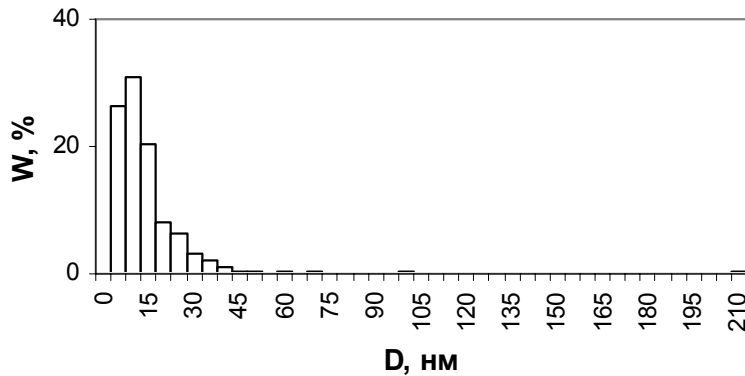


Figure 4: The size distribution of W particles

Aluminum powder

Observations indicate that the analyzed powder is morphologically single-component and presented by spherical particles. The medium size of the particles of the Al powder varies from 30 to 50 nm, that is, the particles are slightly of coarser sizes than the alumina powder ones. In analyses for the size histograms a distinction between the powders of aluminum and alumina is noticeably revealed.

As evident from the results presented in the Table 2, the sizes of the particles of the Al powder vary in a wider value range than those of the aluminum oxide powder. The spread for powder particles produced by an exploding wire with previously annealed coarse grains is maximum (Table 1, Sample AI94).

Phase compositions

The prevention from spontaneous combustion and agglomeration of particles is an important question and requires being clear. Investigations performed have shown that the electrical explosion allows synthesizing the powders passivated with a thick surface layer of oxide or nitride. With that, the activity of powders produced in the low-pressure gas containing oxygen or nitrogen remains high.

Synthesis of Al-Al₂O₃ compositions with controlled phase ratio

Table 2 gives the conditions for the electrical explosion of aluminum in the low-pressure oxygen containing gas.

Sample	w/w_s	p , mm Hg	O ₂ , %	S, m ² /g	Al ₂ O ₃ (γ), %
N5	1.0	150	0	29	0
N9	0.6	150	5	31	5 (100)
N59	0.6	350	5	34	15-20 (90)
A30	0.6	150	22	39	80-85
A13	0.6	250	25	49	100 (70)
A11	0.9	250	25	38	98 (70)
A12	0.25	250	25	45	95 (80)

Table 2: Synthesis of powders in oxygen-containing gas

There are the ratio w/w_s , gas pressure p , and oxygen content (O₂, %) in the table. The following properties of produced powders are represented: percentage of Al oxide (the high-temperature γ-phase is in the brackets) and the specific surface area S of the powders. X-ray diffraction analyses indicate that there is a constitution of oxide phases in the powder: the γ-phase prevails and a quantity of the α- and other phases is also presented. From the Table 2 it is seen that the oxygen content within the explosion chamber is an essential factor in the synthesis of oxides, and the phase constitution of the produced powder can be varied from pure aluminum to oxide. This is demonstrated with Fig. 5 where the experimental data of the aluminum oxide yield versus the oxygen pressure within the chamber are presented. Proceeding to an oxygen-containing gas, the powder fineness is elevated and the particle size decreases. Logically, two effects can explain this result: 1) exoergic reaction of combustion adds fineness and 2) the layer of oxide prevents particles from coagulation.

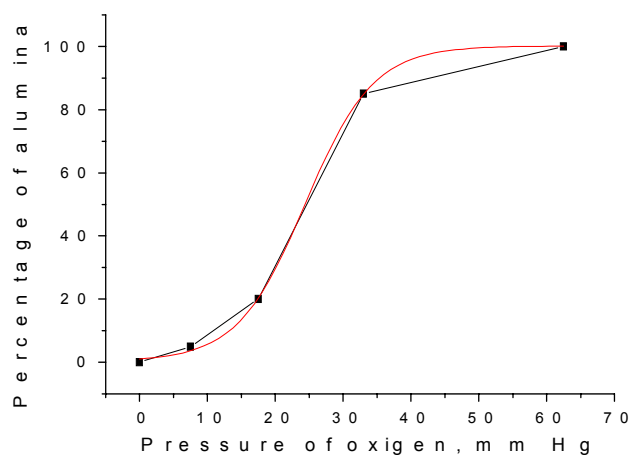


Figure 5: Percentage of Al oxide output versus oxygen pressure within the chamber

Synthesis of Al-AlN compositions with controlled phase ratio

Table 3 shows the composition of Al-AlN powders produced in the low-pressure nitrogen containing gas.

Sample	Gas	Pressure, mm Hg	S, m ² /g	Nitride content, %
N1	N ₂	150	26	1,6
N2	N ₂	350	57	3,7
N27	N ₂ + 10% NH ₃	350	59	57,9

Table 3: Synthesis of powders in nitrogen-containing gas

It is worth noting that aluminum is the metal reacting with nitrogen most easily. Nevertheless, pure aluminum particles coated with AlN can be produced.

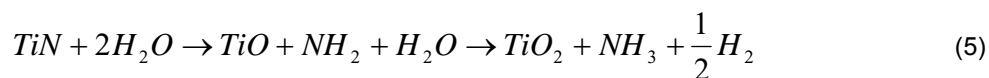
Experiments [6] indicated that molecular nitrogen is chemically inert at lower pressure. Nitrides in the powders of the investigated metals are either absent versus the pressure or found as a trace amount. A quantity of fixed nitrogen was determined via decomposition of the samples in boiling sulfuric acid and in boiling concentrated alkali by the Kjeldal method. Both the chemical and X-ray methods for the analysis confirm this fact. The chemical analyses show that a detectable amount of AlN (more than 2% of mass) is synthesized at pressures exceeding 350 mm Hg. It is necessary to accentuate that Al is the metal readily producing nitride.

The dissociation energy of the nitrogen molecule N₂ (53.7 kJ/mole) is far in excess of the sublimation energy of aluminum (18.8 kJ/mole) that is close to the energy density stored by the electrical circuit. The synthesis of nitride requires an additional activation. Disturbances in the stoichiometric contents of nitrogen in the reaction region at pressure reducing and a short time of the process are also of considerable importance.

A small addition of the ammonia substantially increases the output of nitride (sample 27 in Table 4). Nevertheless, the size of particles practically remains the same. These experiments indicate that a small quantity of nitride prevents the agglomeration of the particles formed. It can be seen from comparison of the specific area S in the Table 3. This fact may be useful in the study of such coating particle behavior in the combustion waves.

X-ray diffraction patterns show that Zr and Ti wires exploded in the low-pressure nitrogen give the steps of ZrN and TiN, correspondingly. X-ray data also show the absence of any iron in the iron powder and copper nitride in the copper powder produced in nitrogen.

The coating of pure Ti particles with TiN is believed to exist. This coating is not stable under the action of water vapors: the decomposition reaction can occur:



Therefore, storage of the powder at moist air leads to formation of TiO and TiO₂ layers.

X-ray diffraction patterns

The phase analysis and determination of the fine crystal structure parameters of the powders have been implemented by means of X-ray diffraction apparatus DRON-UM1 with filtered copper radiation K α . The relative error in the determination of the phase constitution in the powder was under 10%, and in the determination of the parameters it was under 0.1%.

The coherent scattering regions (RCS) for the produced powders were determined on the data of roentgen lines broadening at small angles. Table 4 and Fig. 6 present some results for the aluminum and Al-Al₂O₃ powders.

From Table 4 it is seen that the pure metal has the maximum values of the medium RCS size (in the range of 15-54 nm), the size range for alumina is from 22 to 34 nm, and the metastable oxide phase (γ - Al_2O_3) has the minimum RCS size. The RCS range of metastable Al oxide is 1.5-2 times less than that of the stable α -modification. These results are not conflicted with the results of electron-microscopic analyses and the data of the specific surface area (S) by the BET method according to which the oxide powder fineness is higher than the metal one.

Sample	w/w_s	O_2 mm Hg	Al_2O_3 (γ - Al_2O_3) %	RCS, nm α - Al_2O_3	RCS, nm γ - Al_2O_3	RCS, nm Al	S m^2/g
N5	1.0	0	0	-	-	15	29
N9	0.6	7.5	5 (100)	-	9	20	31
N59	0.6	17.5	15-20 (90)	22	9	28	34
A30	0.6	33	80-85	-	20	54	39
A13	0.6	62.5	100 (70)	-	12	-	49
A11	0.9	62.5	98 (70)	-	12	-	38
A12	0.25	62.5	95 (80)	34	15	45	45

Table 4: The phase constitution and medium size of RCS of powders based on aluminum

Figure 6 shows the identity of X-ray diffraction patterns of the Al samples produced in the low-pressure nitrogen and in rare gas. This analysis means that the aluminum nitride concentration is less than 10%, that is, the sensitivity of method. Kjeldal method gives the AlN concentration of 3,7% (Table 3).

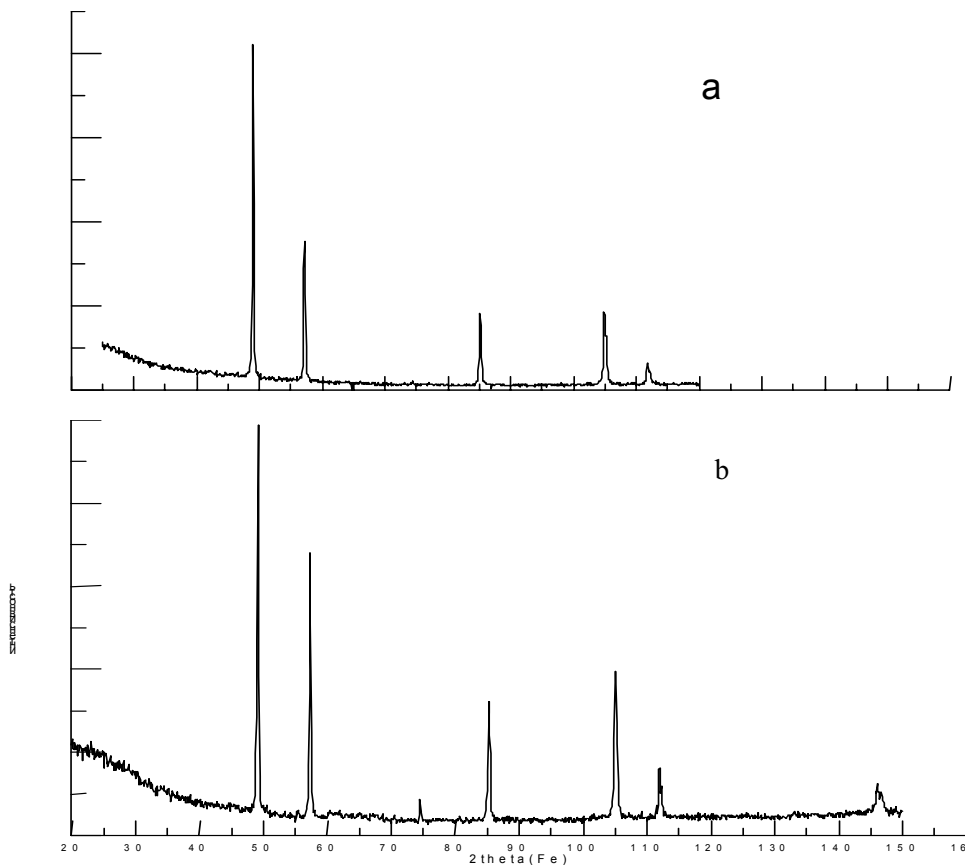


Figure 6: X-ray diffraction patterns of the Al powders [5]: sample (a) produced in low-pressure N_2 , sample (b) produced in $\text{Ar} + \text{He}$

Conclusion

The results of investigation first indicate the importance of the initial microstructure of a wire metal and shed light on the mechanism of the exploding destruction of a metal wire under the influence of fast Joule heating. From the beginning of the current flow, the distribution of heat is not uniform. Joule dissipation is higher at the bounds of the crystallites and at the defects because electrical resistance is higher there. The heterogeneity of heat determines the disintegration of a metal, and the size of the particles depends on the initial size of the microstructure.

Further experiments will study the influence of the initial microstructure (size and size distribution of crystallites) on the property of powders (size distribution of particles, thermal behavior, and so on). It will be possible to develop the computer simulation and to reach full understanding of the process.

Phase composition and phase structure of powders produced under different conditions of heating and environment are overwhelmingly important. The stability of phase constitution of particles as well as the stability of their energetic and other characteristics during storage time and their behavior under external influences are also sufficient.

In conclusion we can say that the exploding wire method is a very promising method of ultra-fine powders production. It is possible to produce ultra-fine powders of a pure metal and compounds with controlled phase compositions. Real future success requires the coordinated joint efforts of a wide circle of researchers and technologists, producers and users.

References

- 1) M. M. Mench, K. K. Kuo, C. L. Yeh, Y. C. Lu, Comparison of thermal behavior of regular and ultra-fine aluminum powders (Alex) made from plasma explosion process, *Combust. Sci. and Tech.*, 135, p. 269-292, 1998
- 2) F. Tepper, L. A. Kaledin, Combustion characteristics of kerosene containing ALEX nano-aluminum, *Lectures of the III International Workshop on Unsteady Combustion and Interior Ballistics*, 2, Saint Petersburg, 2000
- 3) V. N. Simonenko, V. E. Zarko, A. B. Kiskin, V. S. Sedoi, Yu. A. Biryukov, Effect of Alex and boron additives on ignition and combustion of Al-KNO₃ mixture, *Proc. of the 32nd International Annual Conference of ICT*, Karlsruhe, p. 122.1-122.12, 2001
- 4) Yu. A. Kotov, O. M. Samatov, V. S. Sedoi, L. I. Chemezova, A. A. Chertov, Heating of conductors by high-density current, *Megagauss Fields and Pulsed Power Systems* (Eds. V. M. Titov and G. A. Shvetsov), Nova Science Publishers, New York, p. 497-502, 1990
- 5) V. S. Sedoi, V. V. Valevich, Characterization of ultra-fine powders produced by the exploding wire method, *Proc. of the 32nd International Annual Conference of ICT*, Karlsruhe, p. 80.1-80.10, 2001
- 6) V. S. Sedoi and V. V. Valevich, Obtaining of ultra-fine metal powders by the method of exploding wires in the low-pressure nitrogen, *Letters in J. of Tech. Phys.*, 25 (14), p. 81-84, 1999

Material Properties of Gel Propellants

Ulrich Teipel*, **
Ulrich Förter-Barth**

* Georg-Simon-Ohm Fachhochschule Nürnberg
Mechanische Verfahrenstechnik
Partikeltechnologie und Fluidmechanik

** Fraunhofer Institut für Chemische Technologie
(ICT) Dept. Energetische Materialien

Abstract

Gel propellants provide rocket propulsion systems of high specific impulse, low sensitivity and low vulnerability in combination with the capability to control the thrust, i.e., variation of thrust and thrust cut off. The rheological characterization is essential for the development of adequate gel propellant formulations and thus for the design of an applicable propulsion system. In this contribution, the rheological behavior of a gel propellant consisting of nitromethane as fuel and nanoparticles of silicon dioxide as gelling agent was examined. The experiments were conducted under steady state shear flow and oscillatory shear. The nitromethane/silicon dioxide gels exhibit non-Newtonian flow behavior over the whole concentration range examined. Additionally, a yield stress is determined for all the gels. The viscoelastic properties are typically gel-like in that the storage and the loss moduli are both independent of frequency.

Introduction

In recent years, the challenge of achieving high performance while also improving the safety characteristics of rocket propellants has become an important goal within the industry. Gel propellants offer the potential to satisfy such demands because they combine certain advantages of liquid propellants with other attractive properties typical of solid propellants. Gel propellants can be designed as mono or bi-propellants. When used as a bi-propellant, both the fuel and oxidizer can be prepared as gels. The safety of the system is improved by separating the fuel and oxidizer. In general, gel propellants exhibit a specific impulse comparable to liquid propellants, but their performance can be increased even further through the addition of additives such as metal particles. A significant advantage of gel propellants over solid rocket propellants is the ability to control the thrust by controlling the mass flow of propellant into the combustion chamber. The rocket motor can even be turned on and off or pulse driven as required. Furthermore, gel propellants are less sensitive than liquid propellants and can be handled, stored and transported more securely because of their solid-like properties. This is especially important when, for instance, fissures or leakage sites develop within the combustion chamber of a gel propellant driven rocket motor. The viscoelasticity of the gel propellant significantly reduces the risk that the propellant will leak from the motor and inadvertently ignite.

The rheological properties of a gel propellant significantly affect a number of key operational and production requirements, including the propellant material behavior, casting and spraying operations, and combustion within the rocket motor. The characterization of the mechanical properties of the gel provides basic information critical to the production and storage of gel propellants, rocket motor casting as well as the design of the entire rocket motor system.

This study examined the mechanical properties of nitromethane gelled with nanometer sized silicon dioxide. In combination with suitable oxidizers and additives, nitromethane exhibits a specific impulse $I_s > 2400 \text{ Ns}\cdot\text{kg}^{-1}$ and is much less toxic than hydrazine derivatives, thus providing environmental and handling advantages compared to such compounds.

Experimental

Steady state shear flow

The rheological behavior of the gels prepared was examined in steady state and oscillatory shear flow using a UDS 200 rotational rheometer manufactured by Physica Meßtechnik GmbH. Cone and plate measurement fixtures were used.

Under steady state shear flow, the characteristic material function can be described as follows:

$$\tau(\dot{\gamma}) = \eta(\dot{\gamma}) \cdot \dot{\gamma} \quad (1)$$

Here $\eta(\dot{\gamma})$ is a characteristic material function that describes the flow properties when the fluid is subjected to a rheometric flow.

Various models are available in the literature ^[1] to describe the material behavior of fluids in stationary shear flow. Examples of several model functions ^[1, 2] that describe nonlinear flow behavior are presented in this section.

The power law function of Ostwald/de Waele can be used to model shear thinning (pseudoplastic) or shear thickening (dilatant) flow behavior:

$$\tau = K_1 \cdot \dot{\gamma}^n \quad (2)$$

K_1 is termed the consistency coefficient and n is called the flow index. Shear thinning behavior corresponds to $n < 1$, while shear thickening behavior exists when $n > 1$. Ideal viscous (Newtonian) behavior corresponds to $n = 1$.

= 1. This model is unfortunately not effective in describing the flow behavior of many fluids at very small shear rates (near the limiting viscosity at zero shear rate) and at very high shear rates. The viscosity function for such power law fluids is expressed as follows:

$$\eta(\dot{\gamma}) = K_1 \cdot \dot{\gamma}^{n-1} \quad (3)$$

The model presented by Ellis is more suitable for describing flow behavior in the low shear rate region:

$$\eta(\tau) = \eta_0 / (1 + K_2 \cdot \eta_0 \cdot \tau^m) \quad (4)$$

Here, K_2 and m are fitted model parameters.

When the shear stress applied to a fluid must exceed a threshold value (i.e., yield stress) before the onset of irreversible deformation, the material is said to exhibit plastic flow behavior. Below the yield stress the fluid exhibits reversible (elastic) deformation. Highly concentrated disperse systems, in which the solid particulates tend to aggregate, exhibit such viscoplastic material behavior. Materials that exhibit a linear relationship between the shear stress and shear rate at stresses above the yield stress, τ_0 , are known as Bingham fluids.

If the behavior at shear stresses above the yield stress, τ_0 , is nonlinear, the material can be described by the Herschel-Bulkley equation:

$$\tau = \tau_0 + K \cdot \dot{\gamma}^n \quad (5)$$

This power law equation allows one to describe shear thinning or shear thickening fluids that exhibit a yield stress, τ_0 .

Besides shear rate dependence, non-Newtonian behavior can also manifest itself as shear time dependence. For instance, if a material's viscosity decreases with time at a constant shear rate, it is said to exhibit thixotropic behaviour.

Oscillatory shear flow

In oscillatory shear flow, the fluid is subjected to a periodic (e.g., sinusoidal) deformation $\gamma(t)$ with an amplitude $\hat{\gamma}$ at a radial frequency $\omega = 2 \pi f$ [1]:

$$\gamma(t) = \hat{\gamma} \sin(\omega t) \quad (6)$$

At sufficiently small amplitudes—i.e., in the linear viscoelastic range—subjecting the material to an oscillatory (sinusoidal) shear deformation results in a sinusoidal shear stress $\tau(t)$ output. Viscoelastic material behavior is characterized by the existence of a phase shift δ between the shear stress output $\tau(t)$ and the deformation input $\gamma(t)$:

$$\tau(t) = \hat{\tau} \cdot \sin(\omega t + \delta) \quad (7)$$

By definition, the phase shift, δ , of a perfectly elastic solid is zero and that of a purely viscous fluid is $\pi/2$, whereas for viscoelastic fluids $0 \leq \delta \leq \pi/2$.

The shear stress function can be described in terms of the frequency dependent complex shear modulus $G^*(\omega)$,

$$\tau(t) = \hat{\gamma} |G^*(\omega)| \cdot \sin(\omega t + \delta(\omega)) \quad (8)$$

The complex shear modulus can also be expressed as

$$|G^*(\omega)| = \frac{\hat{\tau}(\omega)}{\hat{\gamma}} \quad (9)$$

The complex shear modulus $G^*(\omega)$ of a viscoelastic material is composed of two material functions, a real and an imaginary component, called the storage modulus, $G'(\omega)$, and the loss modulus, $G''(\omega)$, respectively. The storage modulus $G'(\omega)$ is proportional to the deformation energy stored by the material (the elastic component), while the loss modulus $G''(\omega)$ is proportional to the amount of energy dissipated by the material (the viscous component).

$$|G^*(\omega)| = \sqrt{G'(\omega)^2 + G''(\omega)^2} \quad (10)$$

Oscillatory shear experiments must be conducted at deformations within the material's linear viscoelastic range. In this range, at a constant radial frequency ω , the deformation amplitude $\hat{\gamma}$ is proportional to the resulting shear stress amplitude $\hat{\tau}$, i.e., $\hat{\tau} \sim \hat{\gamma}$. This is only the case at sufficiently small oscillatory deformations. Within the linear viscoelastic region, the moduli $G'(\omega)$, $G''(\omega)$ and $G^*(\omega)$ are independent of the oscillatory amplitude in tests conducted at a constant frequency.

Materials

The gel propellants examined consisted of nitromethane as the continuous phase and nanometer sized silicon dioxide particles as the dispersed phase. Nitromethane exhibits Newtonian flow behavior with a dynamic viscosity of $\eta(25^\circ\text{C}) = 0.61 \text{ mPas}$. Its density is $\rho = 1139 \text{ kg/m}^3$. The silicon dioxide particles were obtained from Degussa AG, Frankfurt and had a density $\rho = 1.51 \text{ g/cm}^3$ (determined by gas pycnometry) and a specific surface area $SV = 260 \text{ m}^2/\text{g}$ (determined by gas adsorption). The mean size of the primary particles was $\bar{x} = 7 \text{ nm}$.

Results

Steady state shear flow behavior of the nitromethane/silicon dioxide gels

Prior to the rheological characterization, the nitromethane/silicon dioxide gels were stirred for several hours to deagglomerate the particles and homogenize the gel. The rheological properties were then determined under steady state shear flow. Figure 1 shows the relative viscosity of the gel as a function of shear rate. The concentration of dispersed particles was varied from 4 to 8 vol. %. Figure 1 also shows the viscosity function of pure nitromethane.

The relative viscosity, η_{rel} , is defined as the ratio of the gel viscosity to that of the matrix fluid at a constant shear rate $\dot{\gamma}$.

$$\eta_{rel} = \frac{\eta_{gel}|\dot{\gamma}}{\eta_{nitromethane}} \quad (11)$$

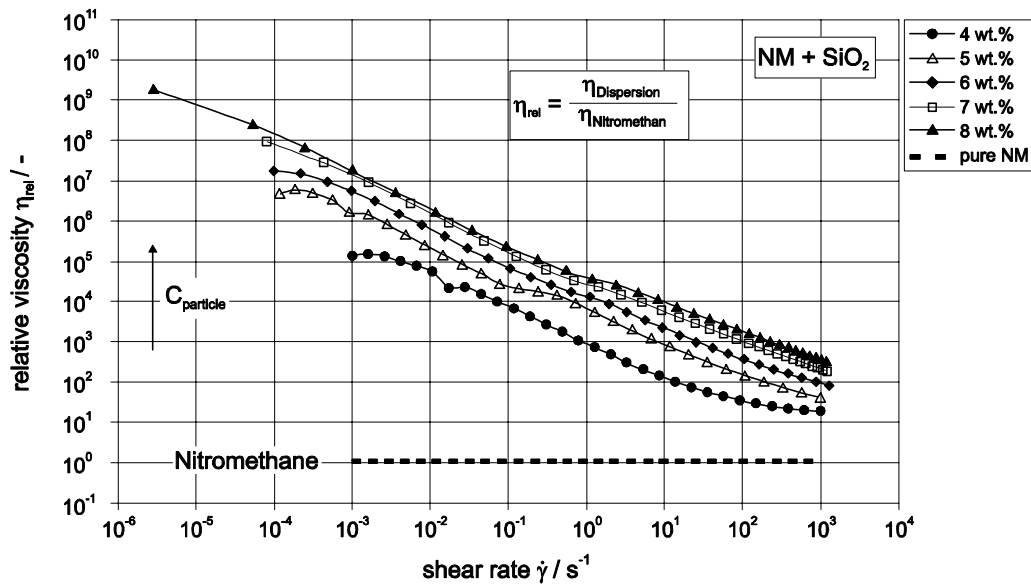


Figure 1: Relative viscosity of the nitromethane/silicon dioxide gels as a function of shear rate

With increasing silicon dioxide concentration, more pronounced shear thinning flow behavior is observed. This nonlinear material behavior of the gel can be attributed to particle-particle interactions as well as the changed hydrodynamics of the multiphase system compared to the single phase fluid. This viscosity increase as a function of concentration is especially pronounced at low shear rates. In this shear rate region the interparticulate interactions dominate compared to the relatively small hydrodynamic forces, so that the rheological properties of the suspension depend very strongly on the solids concentration and structural interactions within the suspension. Increasing the shear rate leads to an increase in the hydrodynamic forces, which in turn results in a shear induced structuring of the nanometer sized particles and a corresponding decrease in the viscosity at a given concentration. The viscosity difference as a function of concentration is therefore much smaller in the high shear rate region than in the low shear rate region, due to the hydrodynamic structuring that occurs in the system at higher shear rates.

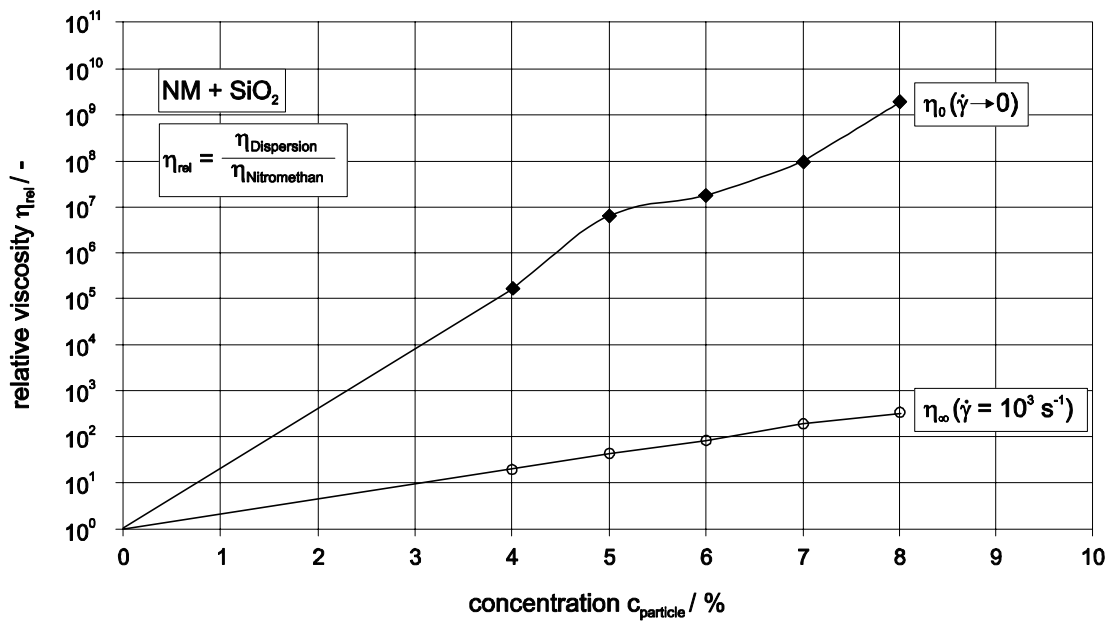


Figure 2: Relative viscosity of the nitromethane/silicon dioxide gels as a function of particle concentration

Figure 2 shows how the viscosity of the gel depends on solids concentration at the limiting viscosity at zero shear rate ($\dot{\gamma} \rightarrow 0$) and at a shear rate $\dot{\gamma} = 1000 \text{ s}^{-1}$.

As the silicon dioxide concentration increases, the inner particulate structure of the system becomes ever more pronounced. This inner quiescent structure in the nitromethane/silicon dioxide gel leads to the limiting viscosity at zero shear rate behavior shown in Figure 2. The viscosity difference between the suspension and the pure fluid is ≈ 106 at a solids concentration $c_{\text{particle}} = 8 \text{ wt.}\%$. In contrast to the behavior of the limiting viscosity at zero shear rate, the slope of the relative viscosity function at the maximum shear rate is much lower. This relatively small increase in the viscosity of the nitromethane/silicon dioxide gel within this shear rate range arises because hydrodynamic effects are dominant and lead to development of a shear induced structure within the silicon dioxide particles. The viscosity difference may also indicate that the gel's inner structure undergoes reversible breakdown at such high shear rates [1].

The flow behavior of the nitromethane/silicone dioxide gel can be described using the following equation for the shear stress:

$$\tau = \tau_0 - \eta_{\infty} \cdot \dot{\gamma} + \eta^* \cdot \dot{\gamma}^{\alpha} \quad (12)$$

Here τ_0 is the yield stress of the gel, η_{∞} is the viscosity at a shear rate $\dot{\gamma} \rightarrow 0$, η^* is the viscosity that characterizes structuring within the disperse system and α is the exponent that characterizes structural changes within the system.

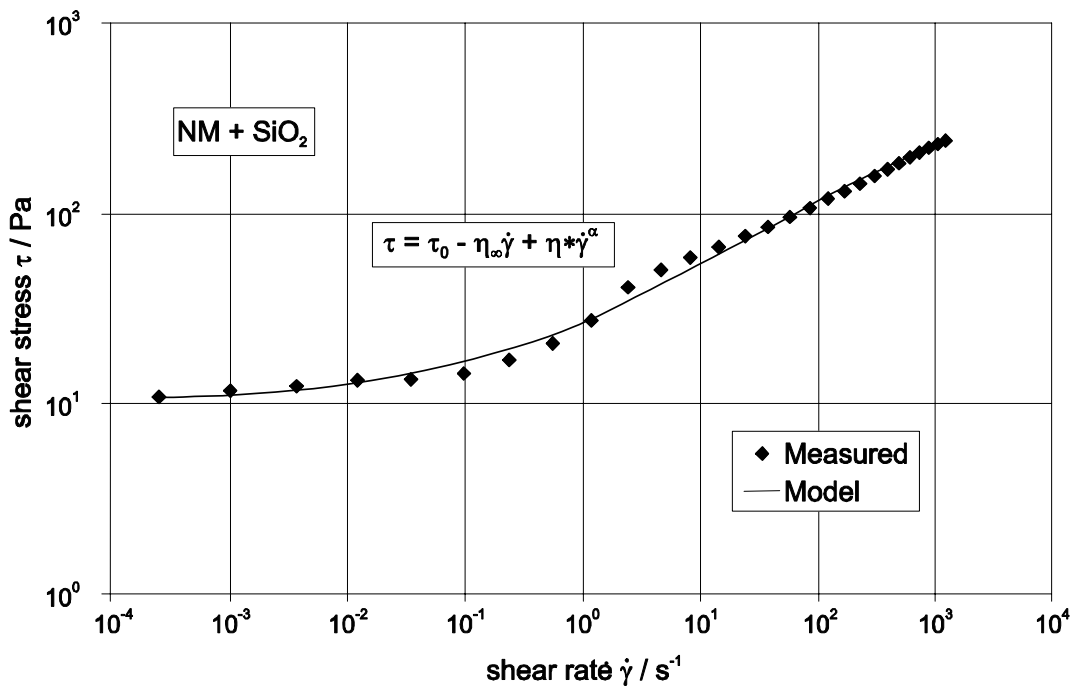


Figure 3: Measured values and model for the shear stress of a nitromethane/silicone dioxide gel

Figure 3 shows the measured shear stress values for the nitromethane/silicone dioxide gel with a concentration $c_{\text{particle}} = 8 \text{ wt.}\%$ compared with the shear stress function calculated from equation (12). There is good agreement between the calculated and measured values.

Viscoelastic properties of the nitromethane/silicon dioxide gels

Viscoelastic properties can be determined via oscillatory shear experiments. The complex shear modulus determined via dynamic experiments in the linear viscoelastic region can be separated into two material functions as shown in equation (10), the storage modulus $G'(\omega)$ and the loss modulus $G''(\omega)$. Figure 4 shows the storage modulus of the nitromethane/silicon dioxide gel at various solids concentrations.

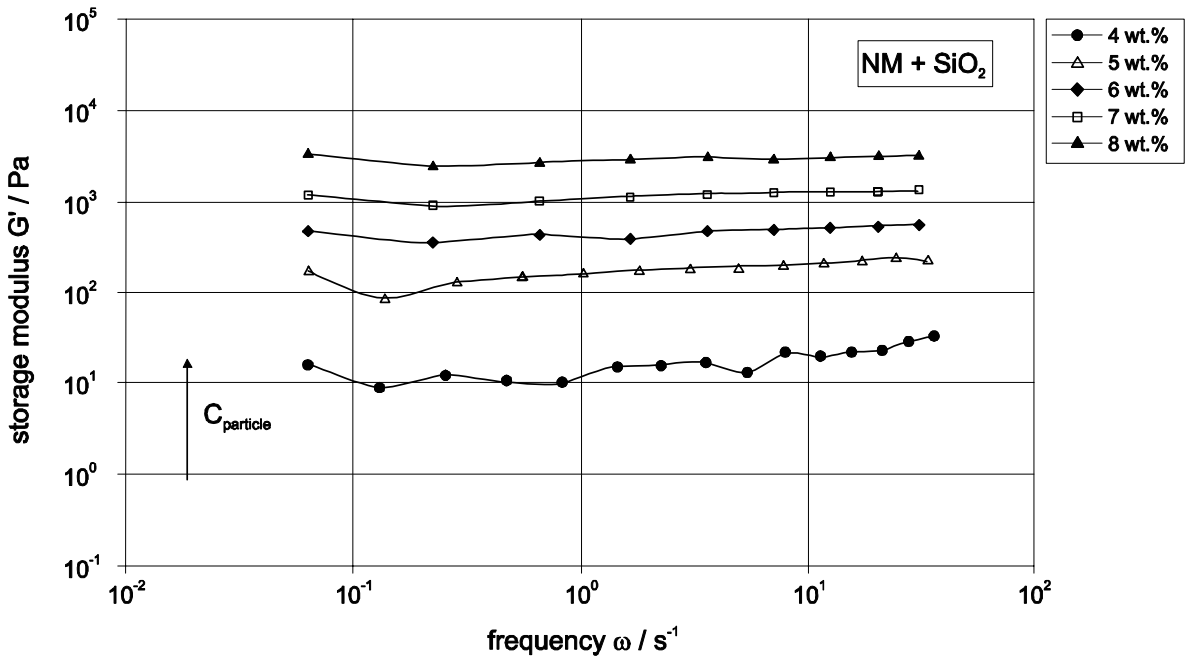


Figure 4: Storage modulus as function of frequency of the nitromethane/silicone dioxide gels

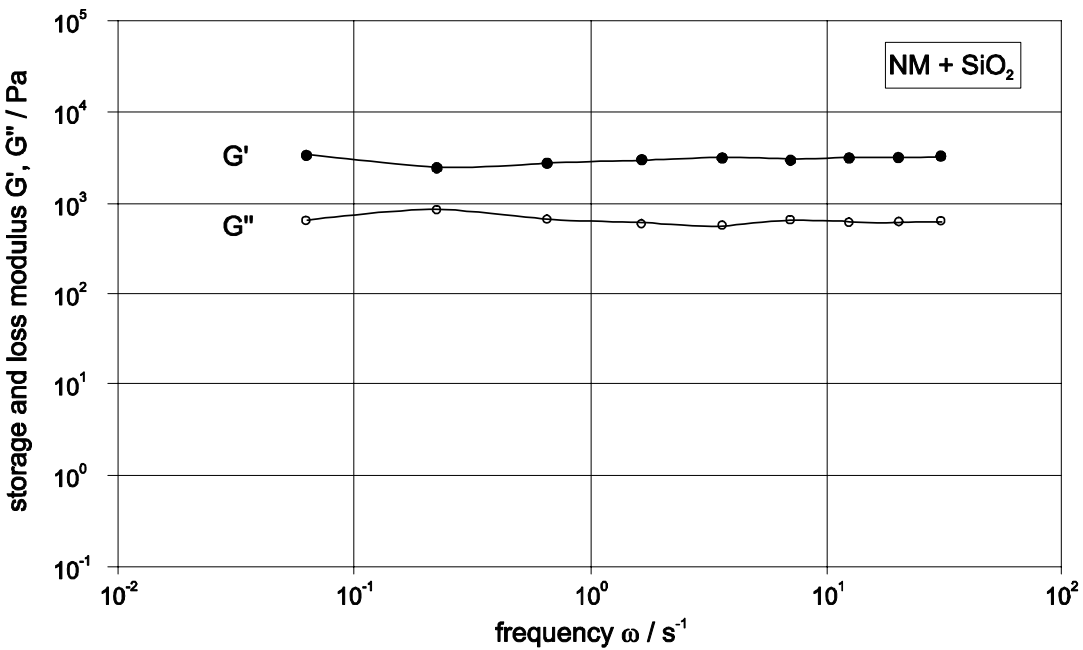


Figure 5: Storage and loss modulus as function of frequency of a nitromethane/silicone dioxide gel ($C_{particle} = 8 \text{ wt.}\%$)

In the concentration region examined, the storage modulus was independent of the radial frequency, indicating the existence of a compact inner structure in the nitromethane/silicone dioxide gel. Figure 5 shows example results of the storage and loss moduli as a function of frequency for the gel with a solids concentration $c_{\text{partic}} = 8 \text{ wt.}\%$. The moduli $G'(\omega)$ and $G''(\omega)$ are independent of frequency, meaning that within this frequency range the nitromethane/silicone dioxide gel exhibits elastic, solid-like behaviour.

From this rheological study the following hypothesis concerning the material behavior of gel propellants are proposed:

- A gel propellant must exhibit shear thinning behavior when subjected to stationary shear flow
- The limiting viscosity at zero shear rate (η_0) of a gel propellant should be as high as possible
- The shear viscosity at high shear rate (η_∞) of a gel propellant should be sufficiently small
- A gel propellant should exhibit a yield stress τ_0 .
- The elastic component of the complex modulus must always be higher than the viscous component
- The moduli $G'(\omega)$ and $G''(\omega)$ should be independent (or nearly independent) of the oscillatory frequency ω

Conclusion

The nitromethane/silicone dioxide gels examined in this study exhibited pronounced shear thinning behavior with a yield stress when subjected to stationary shear flow. This behavior is attributable to the inner structure of the gel, which leads it to exhibit solid-like properties. At high shear rates the hydrodynamic forces exceed the interparticle interaction forces, producing flow induced structuring of the nanometer sized silicon dioxide particles and pronounced nonlinear flow behavior. The shear stress equation introduced in this work accounts for the change in the inner particle structure during stationary shear flow and thus provides a good description of the material behavior of this class of nitromethane gel propellants. The oscillatory shear experiments showed that the storage and loss moduli were independent of frequency in the range examined, meaning that the gel exhibits elastic behavior at low frequencies.

References

- 1) U. Teipel, Rheologisches Verhalten von Emulsionen und Tensidlösungen, PhD-Thesis, University of Bayreuth, Scientific Publication of Fraunhofer ICT, 22, 1999
- 2) C. W. Macosko, Rheology: principles, measurements, and applications, VCH Publishers Inc., New York, 1994

Ignition and Combustion of Propellants containing Aluminum Nanoparticles

V.A. Arkhipov*
A.G. Korotkikh**
V.T. Kuznetsov*
A.B. Vorozhtsov

* Tomsk State University, Russia

** Tomsk Polytechnical University, Russia

Abstract

In this paper presented integrated experimental research on ignition and combustion of model composite solid propellants (SP) and gelled fuels containing nanopowder of aluminum with the mean size of particles less than 0.1 microns, which obtained by electrical explosion of wires in an atmosphere of argon, nitrogen and mixture this gases. As gel was used weigh in kerosene of aluminum nanopowders of various modifications. At manufacturing of SP were used different polymer binders (butyl rubber and HTPB), as an oxidizer the ammonium perchlorate of various dispersivity was applied. As metal fuel the powders of aluminum with the mean size of particles ($10 \div 15$) μ were used, and also ultrafine aluminum of various modifications, which contents varied in range ($5 \div 20$) %.

Introduction

The increase of the propellants energetic characteristics in the last 40 years is connected with use of metal powders (generally aluminum) as one from main components, which weight contents in solid propellants reaches 22 %. Experience of operation, and also the extensive experimental and theoretical researches of such propellants, carried out in Russia, USA, Western Europe and Japan, bring out large disadvantages due metal combustion incompleteness, "two-phase" losses of specific impulse and erosive effect on the nozzle walls.

The creation of a new generation of high-energy materials requires search of the new alternate approaches, as which most perspective represent developments of nonmetal solid propellants with new formulation of oxidizers and binders, and also use of ultrafine aluminum, the sizes of particles in which on the orders are lower, than at authorized propellants. Recently problems of ignition and combustion of SP and gels with ultrafine aluminum are strongly investigated in a series of countries (see, for example, activity [1-4]).

In the present work the outcomes of a integrated experimental research of ignition and combustion of model composite propellants (solid and gels), containing a powder of ultrafine aluminum with the mean size of particles less than 0.1 microns are submitted.

At realization of researches some experimental techniques and experimental setups were used:

- The experimental setup for measurement of gels ignition time;
- The experimental setup for measurement of SP ignition (by the heated surface) time;
- The experimental setup for measurement of SP ignition (at radiant heating) time;
- The experimental setup for measurement of SP burning rate.

The measurement of gels ignition time was conducted on the experimental setup consisting of an injector for pulse gel supply in a quartz pipe, heated up to specific temperature by an electrical spiral. The delay of ignition time registered on the two-radial oscilloscope on a difference of a signal from the pressure transducer (moment of an injection) and photodiode (moment of ignition). The measurements were conducted at atmospheric pressure in range of temperature (573 ÷ 873) K.

The research of SP ignition by the heated up body was conducted on a hot metal plate in air environment at atmospheric pressure in range of temperatures (570 ÷ 715) K. In a plate on depth 0.25 mm from the grinding finish intended for a contact to a researched sample, pressed a thermocouple. The researched sample of diameter 10 mm and height 5 mm fastened to a rod, which freely moved in a vertical direction on a directing handset. The moment of ignition was fixed on appearance of a flame. For period of an induction the period from a moment of a contact of a sample with the heated up plate before appearance of a visible flame registered by the photodiode was received.

For measurement of SP ignition time at radiant heating the experimental setup "Uranum" explicitly submitted in [5] was used. The measurement of SP burning rate was conducted in an air at atmospheric pressure, and also in a bomb of constant pressure filled by argon in a pressure range (1 ÷ 8) MPa. SP samples with diameter 10 mm and height (30 ÷ 40) mm armored on a lateral area were used. The burning rate was measured by a method of burning down delays registered on the oscilloscope.

The experimental researches were conducted for gels and SP. As gel was used weigh in kerosene of ultrafine powders of various modifications. At manufacturing of SP were used different polymer binders (butyl rubber and HTPB), as an oxidizer the ammonium perchlorate of various dispersivity was applied. As metal fuel the powders of aluminum with the mean size of particles (1 ÷ 5) μ were used, and also ultrafine aluminum of various modifications, which contents varied in range (5 ÷ 20) %.

Short Review

The successes in a manufacture technology of ultrafine metal powders have allowed paying attention the researchers to a capability of their use as components of high-energy systems. The new technology of ultrafine metal powders manufacturing by an electroexplosive method in atmosphere of various gases opens broad capabilities for use them as the additions for control of rate of high-temperature oxidation of polymeric materials and compositions on their basis. The addition of a ultrafine powder of aluminum promotes increase of flammability of heterogeneous systems, rate of their burning, reduces agglomeration of particles and enables regulations of a index ν in the law of burning rate from pressure. Having a high specific surface (up to $12 \text{ m}^2/\text{g}$) the ultrafine metal powders can successfully compete to known catalysts and inhibitors of high-energy systems combustion [4, 6]. The high dispersivity of a aluminum powder ($0.05 \div 0.1 \mu$) practically does not influence a level of thermal flux in a condensed phase and temperature of combustion surface, however increases a gradient of temperature at a surface from the direction of a gas phase [7, 8]. Besides it is possible, that at addition 20 % of aluminum the part it can begin to react already in a reactionary layer of condensed phases, as it was noted for other metals [9]. The researches of V. Rogozhnikov with the employee's [10] have shown that the addition of fine aluminum $\sim 1 \mu$ in ammonium perchlorate strongly increases flammability, ability to burning and propensity it to transition to a convective combustion mode. The most probable reason of this influence the authors see in interaction of aluminum with primary products of disintegration of ammonium perchlorate; thus, owing to, large thermal effect of oxidation of aluminum the gases with high temperature will be generated which penetrating in a powder, ignite it particles, than rather cold products of disintegration of the ammonium perchlorate much easier. The data on combustion and explosive characteristics of binary mixtures of an ultrafine powder of aluminum (*Alex*) with NH_4ClO_4 , KClO_4 , KNO_3 , NaNO_3 are submitted in [6]. The results on ignition by a light flux of structures containing *Alex* are adduced in [4] where is shown that the addition to propellant 18 % *Alex* allows twice to reduce energy of steady ignition. The features of ignition and combustion of a ultrafine powder of aluminum in oxidizing environments are investigated in [11, 12]. Was shown, that the ignition of an aerosol at total concentration of oxygen in a flow ($17 \div 41$) % happens in the event that temperature of a flow makes ($473 \div 573$) K that the temperatures of ignition of particles of ordinary aluminum are much lower.

The low temperature limit of ignition, first of all, is connected to activity of an obtained aerosol of aluminum; with minimum width of an oxide layer on particles which are not prohibitive to evolution of heterogeneous reaction and self-heating of particles, at an injection of oxygen in a flow. The combustion of *Alex* in atmosphere of an air happens in two stages. The ignition happens at the temperature of ($623 \div 823$) K then the particle achieves temperature of the first stage 1473 K and after some delay temperature it is sharply increased up to ($2273 \div 2673$) K. In quoted above papers is shown that irrespective of a way of a ultrafine powder of aluminum obtaining (method of evaporation of metal in vacuum or electroexplosive way) the particles are ignited at the temperature which is characteristic one of a combustion surface of high energy materials.

It is known [13] that the condition of a catalyst particle surface plays an essential role in combustion processes. Efficiency of effect of the catalytic additions with a high specific particles surface on processes of ignition and combustion of high energy systems were investigated by many authors [14-17]. Was shown that during combustion the accumulation of metal particles on a surface of combustion and them agglomeration happens. The activity of metal as catalyst is determined by the size of secondary particles. It is agglomerates of initial particles of catalyst and their sizes weakly depend on a specific surface of primary particles [16]. It explains low efficiency of effect of catalyst with a high specific surface of particles on burning rate of known heterogeneous systems [13]. The suppression of particle agglomeration process, for example, at the expense of change of a dispersivity of particles of an oxidizer, increases efficiency of catalysts of combustion [18]. As the ultrafine powder of metals less than ordinary (regular) are subject of agglomeration at combustion there is a capability of their use as effective catalysts.

Experimental study of metallized gels ignition

The development of reliably working controllable rocket engines of small draft for management of flying devices flight is one of urgent problems modern rocket building not decided till now. One of perspective types of controllable rocket motor is the engine on gelled fuel. Alongside with an opportunity of deep regulation of draft, use of metallized gels compositions allows to increase density of fuel and its specific impulse and also safety of functioning of the engine [19]. However results of experimental improvement aluminum gelled fuel have shown that the real efficiency these propellant is much lower predicted ones [1]. One of the possible reasons it is use in structure gelled fuel of regular powders of aluminum dispersivity that makes $(3 \div 30) \mu$. Thus probably incomplete combustion of aluminum and also increase of two-phase losses of a specific pulse. The pinch of efficiency of high-energy materials requires the new approaches one of which is the application in a composition of fuel compositions of ultra disperse powders of aluminum which sizes on the orders are less at reference powders. Recently problems of ignition and combustion of solid and gelled fuel containing UFA is intensively explored [2-4, 20, 21]. For increase of problem gelled fuel it is expedient to use ultra disperse powders of aluminum (average size of particles $\sim 0.1 \mu$) combustion ensuring high completeness of metal and reduction of particles oxide of aluminum in products of combustion.

In the present message the results of experimental study of gelled fuel ignition process consisting from kerosene with particles weighed in it of ultra disperse aluminum are submitted. As a filling compound the powders of aluminum obtained by a method of electrical explosion of wires were used [22].

In the present message the results of experimental study of gelled fuel ignition process consisting from kerosene with particles weighed in it of ultra disperse aluminum are submitted. As a filling compound the powders of aluminum obtained by a method of electrical explosion of wires were used [22].

For experimental research of ignition process of fuel at atmospheric pressure the experimental setup was used which circuit is given in a fig. 1. The experimental setup consists of reactor as quartz tube by diameter 90 mm and length 400 mm set in electrical heater, injection system of fuel and measuring system of ignition delay time. The heater consists from nichrome spiral (diameter of wire 0.7 mm) reeled immediately on quartz tube and located in asbestos insulator. As a radiant of electrical energy the laboratory autoformer ensuring quantity of current $\sim 7 \text{ A}$ was used at the voltage $(150 \div 180) \text{ V}$. The heater ensures temperature range in reactor $(573 \div 973) \text{ K}$. Temperature is checked with help chromel-alumel thermocouple 3 and amplifier.

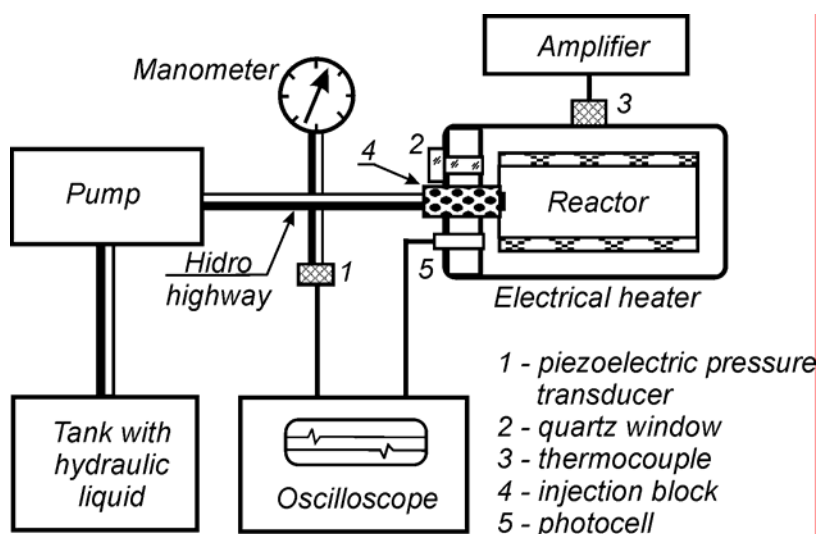


Figure 1: The scheme of experimental setup for measuring of gel ignition delay time

The injection system of fuel consists of the pump, hydrohighway, and tank with hydraulic liquid, injection block and control manometer. For measurement of ignition time delay the system including piezoelectric pressure transducer 1 of type LH-601, photocell of type FD-256, double-beam memory oscilloscope of type S9-8 is used. For visual supervision of process the quartz window 2 is used.

Experimental procedure is realized as follows. In section injection block the portion of particular weight fuel M is located. The reactor is heated up to given temperature and is withstood within several minutes for smoothing temperature field inside tube. With the help of the pump in hydrohighway the pressure up to a threshold of operation a spring injection block (~ 20 MPa) raises then the portion of fuel is injected in reactor where there is ignition and combustion. The injection moment t_1 is fixed by occurrence of pressure peak in hydrohighway measure by the pressure transducer 1 and is registered on the first channel of oscilloscope. The ignition moment of fuel t_2 is registered with the help of the photocell 5 on the second channel of oscilloscope. The ignition time delay (at the given calibration of oscilloscope) is defined as $t_{ign} = t_2 - t_1$. The typical oscillogram of ignition process is submitted in fig. 2.

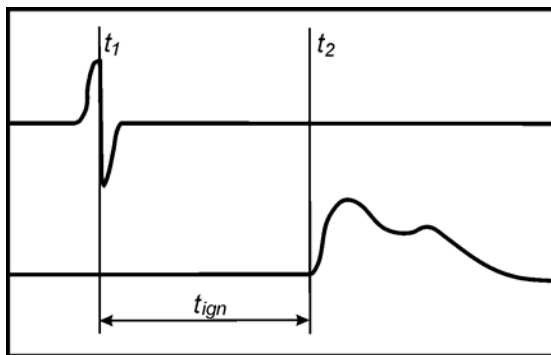


Figure 2: An oscillogram of ignition process

The gelled fuel prepared by dispersion of aluminum particle powder (Al_{ex}) in kerosene. A medial diameter of aluminum particles $\sim 0.1 \mu$. The mass content of aluminum in composition of fuel made $z = 0.3$. In experiments the powders of different modifications obtained by electrical explosion of wires in an atmosphere of different gases – in argon (Al_{ex}), in nitrogen (Al_{ex}^{TM1}), in intermixture 30 % of nitrogen and 70 % of argon (Al_{ex}^{TM2}) and in intermixture 75 % of nitrogen and 25 % of argon (Al_{ex}^{TM3}) were used

The part of experiments was carried out for kerosene not containing powder of aluminum.

For select of fuel injected mass portion the calculations stiohiometric composition of fuel on known procedure were carried out [23] with reference to requirements of experiments.

$$M_{air} = \frac{p_a \cdot V}{R \cdot T} \quad (1)$$

where

p_a – atmospheric pressure of air,

$V = 2.54 \cdot 10^{-3} \text{ m}^3$ – volume of reactor;

$R = 285.7 \text{ J/(kg}\cdot\text{K)}$ – gas constant of air;

T – temperature of air in reactor.

At calculation of fuel mass portion M the following responses were taken into account. For kerosene (mass content of carbon and hydrogen $z_c = 0.856$, $z_{H_2} = 0.144$).



For metallized gel (mass content of carbon, hydrogen and aluminum $z_c = 0.856$, $z_{H_2} = 0.144$; $z_{Al}=0.3$):



It was taken into account also that the mass content of oxygen in air $z_{O_2} = 0.232$.

The results of calculation of fuel mass (under condition of its complete combustion) in dependence's from temperature of air in reactor are submitted in fig. 3. According to calculation results mass of injected fuel portion was chosen in gamut $M = (0.1 \div 0.2)$ g.

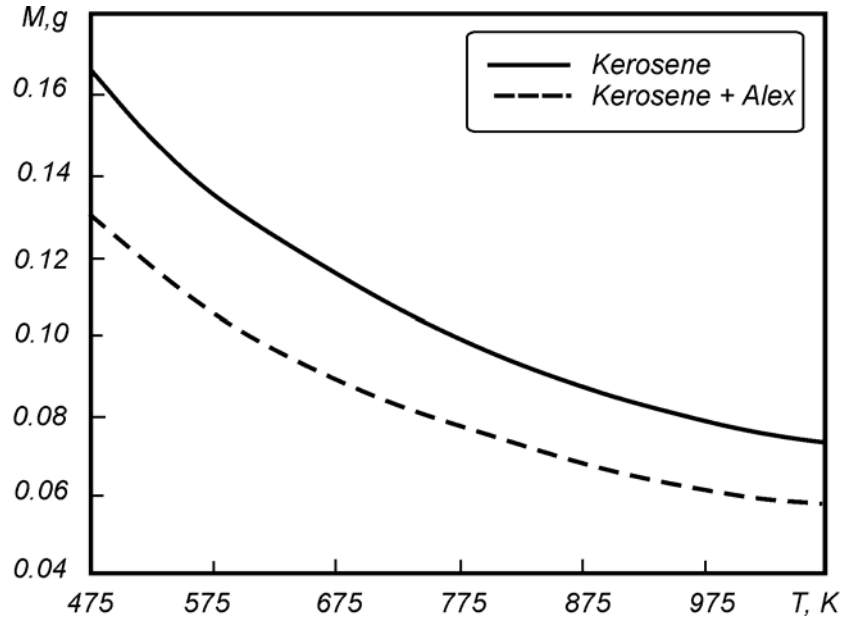


Figure 3: Predicted mass of fuel (under condition of its complete combustion) in dependence from temperature of air in reactor

As result of carried out experiments the dependence of ignition delay time from temperature $t_{ign}(T)$ for surveyed fuel compositions were obtained. Some observed data's particular on five doubling experiences for each value of temperature is submitted in fig. 4. The confidence interval at quantity of confidence probability 95 % did not exceed 26 %.

In all carried out experiments the inconvertible ignition and burning of fuel compositions in gamut of temperatures (573 \div 973) K was observed. The approximation of dependence $t_{ign}(T)$ spent by method of least squares has allowed to receive the following dependence's:

for kerosene	$t_{ign}(T) = 35 \exp(-0.00554 \cdot T)$
for kerosene + Alex	$t_{ign}(T) = 76.4 \cdot \exp(-0.007 \cdot T)$
for kerosene + Alex ^{TM2}	$t_{ign}(T) = 221 \cdot \exp(-0.0081 \cdot T)$

In these dependence's $[t_{ign}] = s$ and $[T] = K$.

From the analysis of the obtained results it is visible that the ignition delay times with growth of temperature from 573 up to 973 K sharply decrease (from 1174 up to 153 ms for kerosene and from 1126 up to 83 ms for gelled fuel). At identical value of temperature the ignition delay time of gelled fuel is less than for pure kerosene thus the difference is increased with growth of temperature from 48 ms at 573 K up to 70 ms at 973 K.

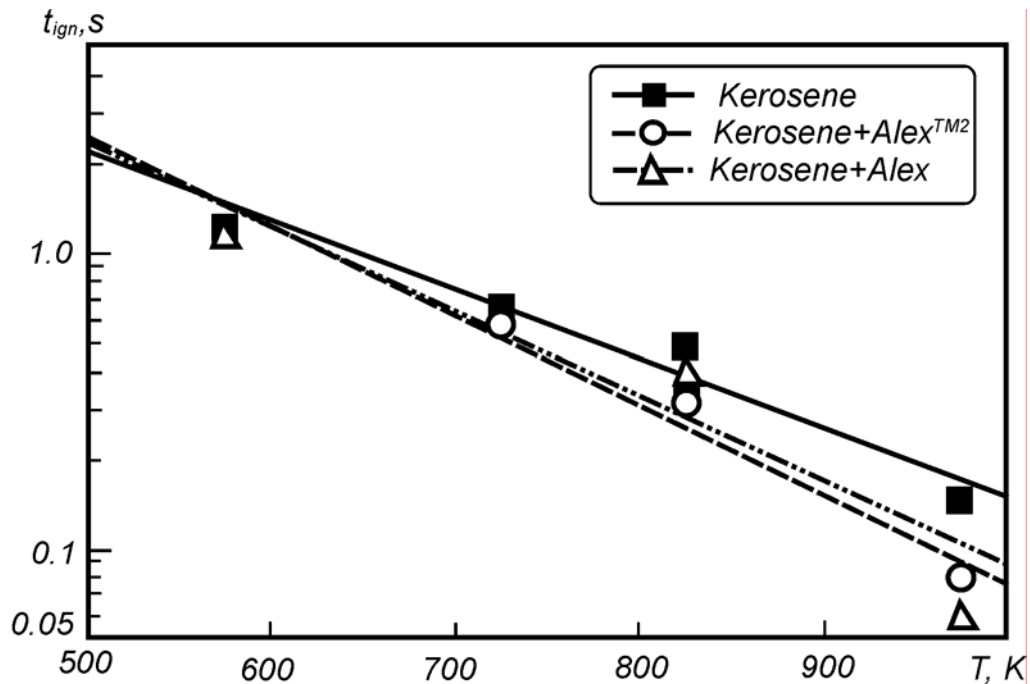


Figure 4: Dependence of ignition delay time of fuel kerosene + Alex from temperature

On the given setup measuring ignition time delay t_{ig} for gelled fuel containing also were carried out weigh of an active powder of aluminum Alex (30 % on weight) in kerosene at temperatures 723, 823 and 973 K. The ignition time delay such fuel is less than for kerosene and gelled fuel kerosene + usual Alex. At what more percentage of organic in mixture of gases is obvious that than at reception of powders Alex the less ignition time delay of gelled fuel. The difference in quantity t_{ign} makes at temperature 973 K:

for kerosene + Alex – 80 ms; for kerosene + Alex^{TM1} – 36 ms;
 for kerosene + Alex^{TM2} – 70 ms; for kerosene + Alex^{TM3} – 64 ms.

The results obtained during experimental study not bad are compounded with the data of operation [21].

Reduction t_{ign} at addition of Alex in structure of fuel ~ 25 %. In view of wide scatter of the skilled data ~ (10 ÷ 20) % would be possible by this fact to neglected and to made by conclusion that the addition of Alex at least does not increase quantity t_{ign} . However smaller meanings t_{ign} for mixture (kerosene + Alex) are received for all carried out series.

To explain physics of reduction t_{ign} at addition of Alex it is unequivocally difficult without the mathematical analysis of a problem. However, it is qualitatively possible to offer the following mechanisms:

- Occurs cutting of an oxide film from Al particles in kerosene vapor to the subsequent development of exothermic reactions of oxidation Al.
- There is a radiating heating of Al particles, which accumulate heat and promote earlier ignition of kerosene vapour.

For specification of mechanisms of reduction t_{ign} at addition of Alex the realization of experiments with powders of aluminum different dispersivity and with other technology of their reception is necessary.

Technique of Preparation of Solid Propellants Compositions

In activity were investigated AP/Al/HTPB (butyl rubber mark BKL) compositions. During SP manufacturing varied the contents and dispersivity of an oxidizer and metal. The ammonium perchlorate was used as monofractional dispersivity less 50μ and $(160 \div 315) \mu$, and consisting from a mixture of these fractions at various ratios last.

For mixing of propellant compositions the mixer with self-cleaning blades was used. The full time of batch depends, how fast stir well propellant weight (is usual 2÷3 hours). Then, the vacuum pump was connected to the mixer and during $(30 \div 40)$ minutes a propellant was vacuumed. The cure of propellant was conducted at $(343 \div 345)$ K during 3 day. The catalysts of iron and soot were added in quantity 1 %. Density of cured samples made 1770 kg/m^3 ; dispersion of its density did not exceed 20 kg/m^3 . The structure of propellant is shown in tab.1. The numbering of propellant compositions is adduced pursuant to the technological logbook. In the table are indicated the contents and dispersivity of ammonium perchlorate and metal, and also quantity of polymer and nature of entered catalyst. In bidispersed ammonium perchlorate a ratio of fractions less 50μ and $(160 \div 315) \mu$ as 60/40. The catalysts were added into systems based on HTPB.

№ sample	HTPB, %	AP with dispersivity less than 50μ , %	Al		
			Al, %	Dispersivity, μ	Features of Alex manufacturing
29	18	62	20	$0.01 \div 0.1$	Alex by explosion in Ar
31	18	62	20	$10 \div 15$	ASD-1
35	18	62	20	$0.01 \div 0.1$	Alex by explosion in N_2
36	18	62	20	$0.01 \div 0.1$	Alex by explosion in Ar UF Fe explosion in Ar
37	18	62	20	$10 \div 15$	ASD-1 UF Fe explosion in Ar
38	18	62	20	$0.01 \div 0.1$	Alex explosion in Ar
39	18	62	20	$0.01 \div 0.1$	Alex explosion in Ar, precipitated in kerosene
40	30	70	–	–	
41	30	70	–	–	UF Fe explosion in Ar
42	30	70	–	–	Regular Fe
43	18	62	20	$10 \div 15$	ASD-1. UF Fe + soot(1:1)
44	18	62	20	$0.01 \div 0.1$	Alex explosion in Ar UF Fe + soot(1:1)

Table 1: Compositions on the base of HTPB

Research of SP Ignition by the Heated Solid

The ignition of model SP was investigated in conditions of conductive heating on the metal unit in environment of an air at atmospheric pressure in an interval of temperature (570 ÷ 715) K. As the heated up surface the polished metal plate from a stainless steel diameter 50 mm and length 5 mm, molded in recess of a massive copper rod diameter 70 mm and length 200 mm was used. The rod was heated up with the help of a nichrome spiral. In a plate on distance (0.2 ÷ 0.3) mm from the grinding finish intended for a contact to a researched sample, molded a thermocouple, which calibrated on the mercury thermometer in range (273 ÷ 873) K with an error no more than one degree. The indications of the thermocouple were fixed with the help of potentiometer *PP-63*. The researched sample as a tablet of diameter 10 mm, altitude 5 mm fastened to a rod, which freely moved in a vertical direction on a directing handset of a rotary bracket. The rod had optimum weight ensuring the best reproducibility of experience (~ 0.35 kg). The moment of ignition was fixed on appearance of a flame; for induction period the interval of time from a moment of a contact of a sample with the heated up plate before appearance of a visible flame was considered. The time of ignition was measured with the help of stopwatch with an error ± 0.2 s dispersion) of the experimental data on hold time in parallel tests (not less than 3) did not exceed 15 %.

The tests were conducted in the following sequence. In the beginning temperature of a plate at which the sample was ignited with hold time no more than 60 seconds was determined. Then a series of tests for a construction of ignition time delay relation from temperature of a plate for each propellant was conducted. The results of researches are shown in tab. 2, 3.

№ sample	Ignition time delay, s				
	563 K	578 K	593 K	608 K	623 K
36	32.8 ± 0.8	17.5 ± 0.6	11.2 ± 0.4	5.3 ± 0.2	2.0 ± 0.2
37	34.0 ± 1.2	18.2 ± 0.8	11.5 ± 0.6	5.5 ± 0.4	2.1 ± 0.2
41	27.6 ± 1.0	16.0 ± 0.8	7.5 ± 0.5	5.0 ± 0.3	2.0 ± 0.2
42	42.4 ± 1.2	28.4 ± 0.8	16.2 ± 0.6	8.0 ± 0.5	3.2 ± 0.2

Table.2: Ignition time delay of propellants containing 1 % of iron powder

№ sample	Ignition time delay, s				
	623 K	633 K	643 K	653 K	670 K
29	37.0 ± 2.0	25.2 ± 1.6	15.0 ± 0.6	9.4 ± 0.4	4.0 ± 0.4
31	37.0 ± 2.0	27.0 ± 2.0	14.6 ± 0.6	9.2 ± 0.5	4.4 ± 0.4
35	36.0 ± 3.0	23.5 ± 3.0	15.0 ± 1.0	8.4 ± 1.5	4.0 ± 0.5
38	34.0 ± 2.0	18.6 ± 2.0	11.0 ± 1.0	5.1 ± 0.6	2.6 ± 0.2
39	34.0 ± 2.0	20.4 ± 1.0	11.4 ± 0.5	6.2 ± 0.4	3.3 ± 0.2
40	65.0 ± 5.0	33.0 ± 2.0	16.0 ± 1.2	9.0 ± 0.8	–

Table 3: Ignition of propellants AP/HTPB

The analysis of experimental results of SP ignition on the heated up surface (tab. 2, 3) shows:

- The addition of 1 % of ultrafine *Fe* essentially reduces ignition delay time (for nonmetal SP this effect is more expressed).
- For SP without *Fe* the ignition delay time for SP containing UFA is lower than for SP containing regular *Al*.
- With increase of surface temperature in all cases ignition time delay decreases.

On samples with heat-resistant binder (butyl rubber) and UFA if there is a small-sized fraction AP (less 50 μ) the mode of explosive ignition is detected. In a mode of explosive ignition the appearance of a flame is accompanied by sharp sound effect, fragmentation and combustion with high speed of a warm up layer of a sample with consequent extinguishing. Further, after heating of the rest of a sample the explosive character of ignition was repeated. The detected mode of explosive ignition, evidently, is provoked by intensive oxidation and combustion UFA in a warm up layer of propellant.

It is known [11, 12] that with increase of a dispersivity of an aluminum powder temperature of a beginning of its oxidation is reduced and at the sizes of particle (0.08 \div 0.2) μ it makes of the order 570 K. Further temperature of a particle can amount to 1500 K and after some delay is sharply increased up to (2300 \div 2700) K. Availability in propellant of ammonium perchlorate of a small-sized fraction and rather high temperature of a surface promote evolution of the given process in a warm up layer of propellant. If in propellant to reduce the contents of ammonium perchlorate of a small-sized fraction (up to 10 %), the explosive ignition is not observed. Lowering of a temperature interval of ignition similarly acts also that was achieved by replacement heat-resistant butyl rubber on less heat-resistant and more active binder HTPB. However addition in a structure of propellant 1 % UF *Fe* has lowered temperature of ignition on (50 \div 90) K, but the mode of ignition (sample № 36) has not changed. It is necessary to note that of a direct correlation between a mode of ignition and burning rate of the given propellant at atmospheric pressure is not determined.

The addition of a iron powder into propellant results in lowering ignition time delay (tab. 2) and, the less size of particles, the more effective it influence (samples № 41, 42). UF *Fe* has lowered temperature of ignition of a propellant with butyl rubber on (80 \div 90) K, and propellant with HTPB on (40 \div 50) K..

It is known [19] that the efficiency of catalyst effect drops with increase of SP burning rate. Therefore represents certain interest of realization of researches on an evaluation of efficiency of UF *Fe* effect on process of ignition in conditions of intensive heat supply, for example, at heating by a light flux in range (50 \div 300) W/sm² (fig. 5). Such rate of heating can be realized on the set up of a radiation heating "Uranum" [5]. The techniques of ignition by a light flux can be useful and to determination of a place of catalyst effect during SP combustion.

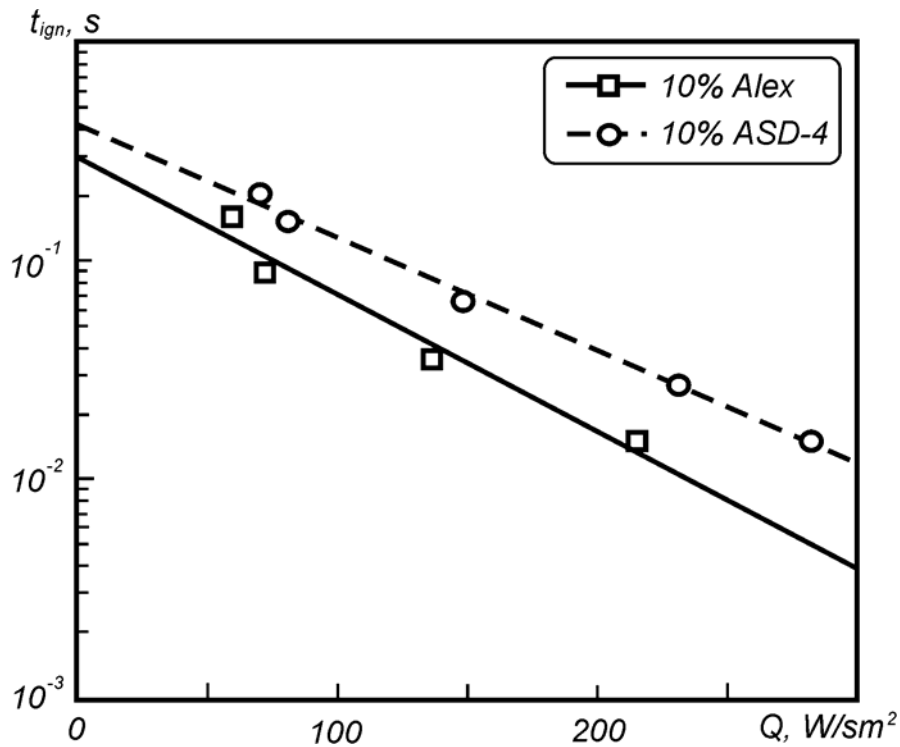


Figure 5: Dependence of ignition delay time of SP based on AP/BKL from radiation heating

From the analysis of the received results it is visible that ignition time delay with growth of radiation heating intensity from 69 up to 280 W/sm^2 decrease from 0.20 up to 0.015 s with for sample containing aluminum powder of mark ASD-4 and from 0.16 up to 0.015 s with for sample containing UF aluminum of mark Alex in a range of intensity of radiation (58 ÷ 214) W/sm^2 . At identical value of radiation heating intensity the ignition time delay of SP containing UFA is less than for SP containing aluminum powder of mark ASD-4 thus the difference increases with growth of radiation heating intensity.

Some reasons of reduction of ignition time delay are supposed at radiation heating connected with increase in thermal stream at surfaces of ignition propellants at addition UF of metals in structure SP. The first effect is connected to the greater specific area of particles surface UF of metals in comparison with regular powders of metals which increases activity of particles with connections in gas phase. The second – the small weight of UF particles conducts to reduction of time heating and ignition of particles in comparison with larger particles. The third – the temperature of ignition of UF metals particles is lower than at regular powders.

SP Burning Rate

Technique of SP burning rate determination

SP burning rate at increased pressure (1 ÷ 8) MPa determined in a bomb of constant pressure in atmosphere of argon on samples diameter 10 mm and length (30 ÷ 40) mm armored on a lateral area by PVC tape. The burning rate at atmospheric pressure was determined on an air. Were used either cured samples or molded from of uncured weight and made in the sleeve from two layers of a tracing paper. The burning rate was measured by a method of blow out of wires, error of measurement of rate is 10 %.

Influence of aluminum characterized in efficiency ratio K , i.e. relation of metallized SP burning rate to nonmetal SP burning rate with other things being equal. By the same method determined efficiency of replacement of aluminum with dispersivity (10 ÷ 15) μ (brand ASD-1) on fine aluminum (0.01 ÷ 0.1) μ (Alex). For cured samples the exponent ν in the burning rate law was determined.

Combustion of SP at atmospheric pressure

For finding – out of the mechanism of influence of aluminium with the size of particle ($0.01 \div 0.1$) μ the part of tests is conducted at atmospheric pressure. Efficiency of addition of metal considered in relation to combustion of nonmetal SP. In tab. 4 the relations of influence of a dispersivity of aluminum and quantity of added metal are adduced. Considered combustion of SP with a factor of extra oxidizer coefficient 0.40.

Dispersivity of Al, μ	Value K at the various weight contents Al			
	5 %	10 %	15 %	20 %
50 \div 100	1.0	1.0	0.8	0.7
10 \div 15	1.0	1.0	0.9	0.9
0.01 \div 0.1	1.2	1.4	–	1.8

Table 4: Influence of a dispersivity and quantity of added metal on value K

From the adduced data follows that the addition of large particles of metal results in lowering burning rate the stronger than higher is the contents of aluminum in a considered system. A/α increases burning rate and the efficiency it grows in accordance with increase of the contents of metal in SP.

In tab. 5 the efficiency of effect of aluminum on value K for systems with various extra oxidizer coefficient α is shown. Into SP added 20 % of metals.

Dispersivity of Al, μ	Value K		
	$\alpha = 0.4$	$\alpha = 0.54$	$\alpha = 0.61$
50 \div 100	0.7	1.0	1.0
10 \div 15	0.9	1.0	1.0
1 \div 2	1.2	1.2	1.5
0.01 \div 0.1	1.8	2.0	2.2

Table 5: Influence of a dispersivity of aluminum to value K

That is at normal conditions on burning rate render influence only ultra dispersed particles of aluminum. In tab. 6 the data on combustion of SP are adduced at $\alpha = 0.54$, containing 20 % of aluminum distinguished by a dispersivity of ammonium perchlorate. Here the values of efficiency A/α in relation to metal with dispersivity (10 \div 15) μ are adduced.

Dispersivity of Al, μ	Burning rate, mm/s			
	AP < 1 μ	AP < 50 μ	AP (160 \div 315) μ	AP (300 \div 400) μ
10 \div 15	2.0	1.8	1.6	1.3
0.01 \div 0.1	no burning	no burning	2.0	2.2
Ratio	–	–	1.25	1.69

Table 6: Influence of a dispersivity of an oxidizer and dispersivity of aluminum on SP burning rate

From the data of tab. 6 it is visible, that the SP containing small-sized oxidizer and metal, at atmospheric pressure do not support combustion. The increase of the sizes of particles of ammonium perchlorate in systems containing particles of aluminum with size $(0.01 \div 0.1) \mu$ results in noticeable increase of burning rate. It is necessary to note anomalous character of relations of burning rates of SP containing aluminum of various dispersivity. If in case of the size of metal particles $(10 \div 15) \mu$ the burning rate of compositions decreases in accordance with increase of the contents of particles of an oxidizer, at addition of a fine oxidizer grows. In tab.7 the data on influence of conditions of manufacturing and storage Alex on burning rate of SP with a factor of extra oxidizer coefficient 0.40 containing 10 % of metal are adduced. Efficiency of effect evaluated in comparison with a SP containing 10 % of metal particles with the size $(10 \div 15) \mu$ the burning rate of which at atmospheric pressure is equal 0.9 mm/s.

Atmosphere for Alex manufacturing	Burning rate, mm/s	$K_{(10 \div 15)\mu}$	$K_{(Alex)}$
Argon	1.3	1.4	1.0
Argon	1.4	1.5	1.0
Nitrogen-argon (1 : 3)	1.3	1.4	1.0
Nitrogen-argon (1 : 1)	1.7	1.9	1.36
Argon, storage in air 6 months	1.6	1.8	1.28

Table 7: Influence to burning rate and value K of various consignments of Alex

Therefore the contact of aluminum particles with certain volume of nitrogen at the moment of manufacturing or at long duration storage on an air result in noticeable increase of efficiency of ultra dispersed aluminum during combustion of SP based on AP. In tab. 8 the experimental data on influence of catalysts of soot and powder iron on burning rate of SP based on HTPB, as nonmetal, and with 20 % of aluminum with dispersivity $(10 \div 15) \mu$ and $(0.01 \div 0.1) \mu$ are adduced. Quantity of the added components did not exceed 1 %. As the components used soot of a brand MP-75 and metal iron of two kinds, large particles GOST 13610-79 and ultra dispersed iron with the size of particles $(0.01 \div 0.1) \mu$. A factor of extra oxidizer coefficient of considered systems is 0.40. In tab. 9 the efficiency of addition of the components of catalysts in various SP is shown.

SP	Burning rate, mm/s				
	Initial	Soot	Fe GOST 13610-79	UF Fe	Soot + UF Fe (1 : 1)
Without Al	1.23	1.60	1.84	2.74	2.90
20 % Al $(10 \div 15) \mu$	1.67	–	–	–	2.90
20 % UFA	3.54	–	–	5.40	3.50

Table 8: Influence of catalysts on burning rate of SP based on HTPB

SP	Value <i>K</i>			
	Soot	<i>Fe</i> GOST 13610-79	UF <i>Fe</i>	Soot + UF <i>Fe</i> (1 : 1)
without <i>Al</i>	1.30	1.49	2.22	2.36
20 % <i>Al</i> (10÷15) μ	–	–	–	1.74
20 % UFA	3.54	–	1.52	1.52

Table 9: Efficiency of catalysts effect on various SP

From the adduced data follows that, most effectively to add the components in non-metal SP. The presence of metal reduces influence of the components the stronger than less sizes of particles of the latter. So the addition of soot increasing burning rate of nonmetal SP in 1.3 times practically does not influence compositions containing 20 % UFA. The efficiency of addition UF *Fe* as decreases from 2.2 times for nonmetal SP, till 1.52 for SP containing UFA. The noted relation is traced and at addition of the mixed component (soot and UF *Fe*).

Combustion of SP at increased pressure

Experimental researches were carried out using SP with bidispersed ammonium perchlorate with a particles size of fine fraction less than 50 μ and large fraction - (160 ÷ 315) μ . A ratio of fractions was 40/60. BKL butyl rubber cured by quinol ether was used as a combustible-binder. The metal fuel (aluminum) content was varied in the range (5 ÷ 20) %. Besides, additives of catalysts (powder of iron with a diameter of particles ~ 100 μ and ultrafine powders of iron, copper and nickel) were entered into the structure of metallized solid propellants. An additive of catalyst in quantity up to 4 % was entered into the structure of compositions due to reduction of aluminum content. A meaning of oxidizer excess coefficient was varied in the range $\alpha = (0.40 \div 0.54)$. Compositions of studied samples are shown in Tab. 10.

Sample	α	BKL, %	AP, %	<i>Al</i>		
				Content, %	Mark	Dispersion, μ
1	0.40	18	62	20	ASD-4	5 ÷ 10
2	0.40	22	68	10	ASD-4	5 ÷ 10
3	0.54	16	74	10	ASD-4	5 ÷ 10
4	0.40	18	62	20	Alex	0.01 ÷ 0.1
5	0.40	22	68	10	Alex	0.01 ÷ 0.1
6	0.54	16	74	10	Alex	0.01 ÷ 0.1
7	0.43	25	70	5	Alex	0.01 ÷ 0.1

Table 10: Structures of solid propellants containing aluminum powders

Measuring the burning rate of solid propellants was carried out in a constant pressure bomb (CPB) filled with argon in the range of pressure (1 ÷ 8) MPa. The burning rate was determined by a time of passage of burning wave front through a certain site of a charge (method of burning wires). Several duplicating experiences were carried out for each experimental point.

Results of measuring the SP burning rate ($\alpha = 0.40$) obtained in the CPB at an increased pressure, are given in Fig. 6. When increasing the pressure, the increase of studied SP burning rate depends on the aluminum content and its dispersivity. For SP containing 5 % of Al UFP (sample 7) the burning rate increases from 3.4 to 6.6 mm/s, at the content of 10 % Al UFP (sample 5) – from 3.8 to 9.5 mm/s in the range of pressure (1.0 ÷ 6.3) MPa. When the content is 20 % of Al UFP (sample 4) burning rate increases from 6 to 21.5 mm/s in the range of pressure (1.0 ÷ 8.0) MPa. With increasing Al UFP percentage the burning rate of SP grows at identical meanings of pressure. For SP containing 10 % of ASD-4 aluminum powder (sample 2), the burning rate increases from 2.8 to 5.6 mm/s, for 20 % of ASD-4 (sample 1) - from 3.0 to 4.9 mm/s.

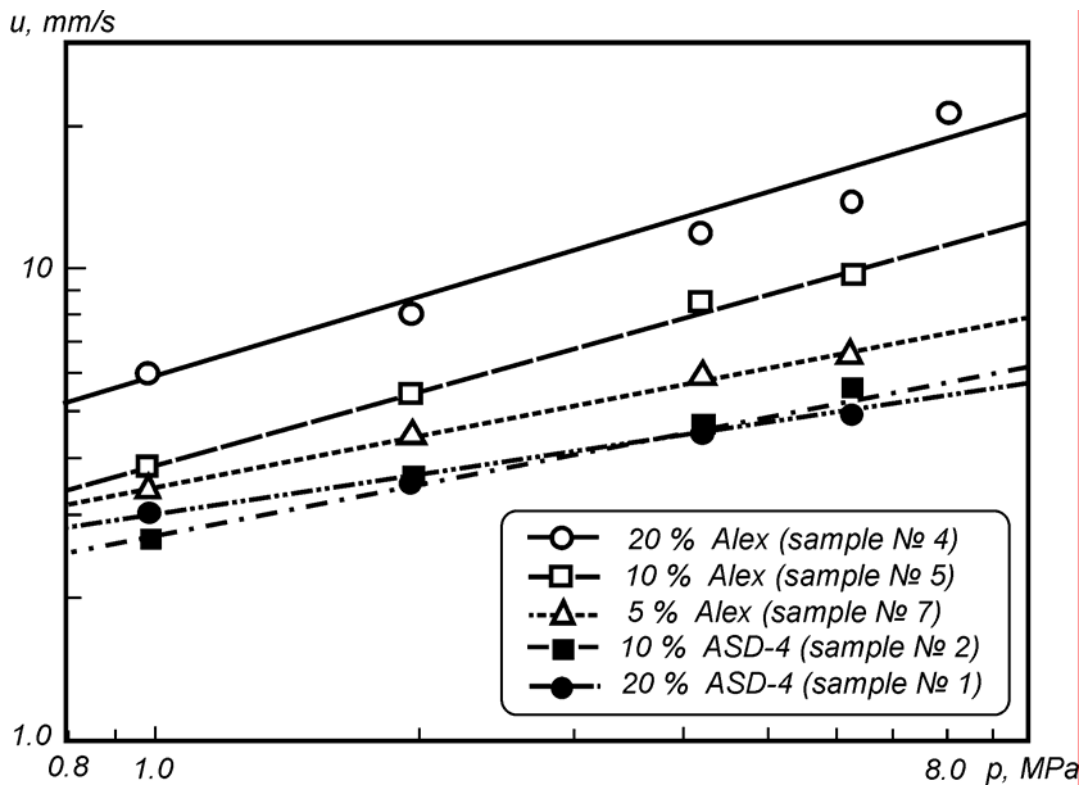


Figure 6: Dependence of burning rate SP ($\alpha = 0.40$) from pressure

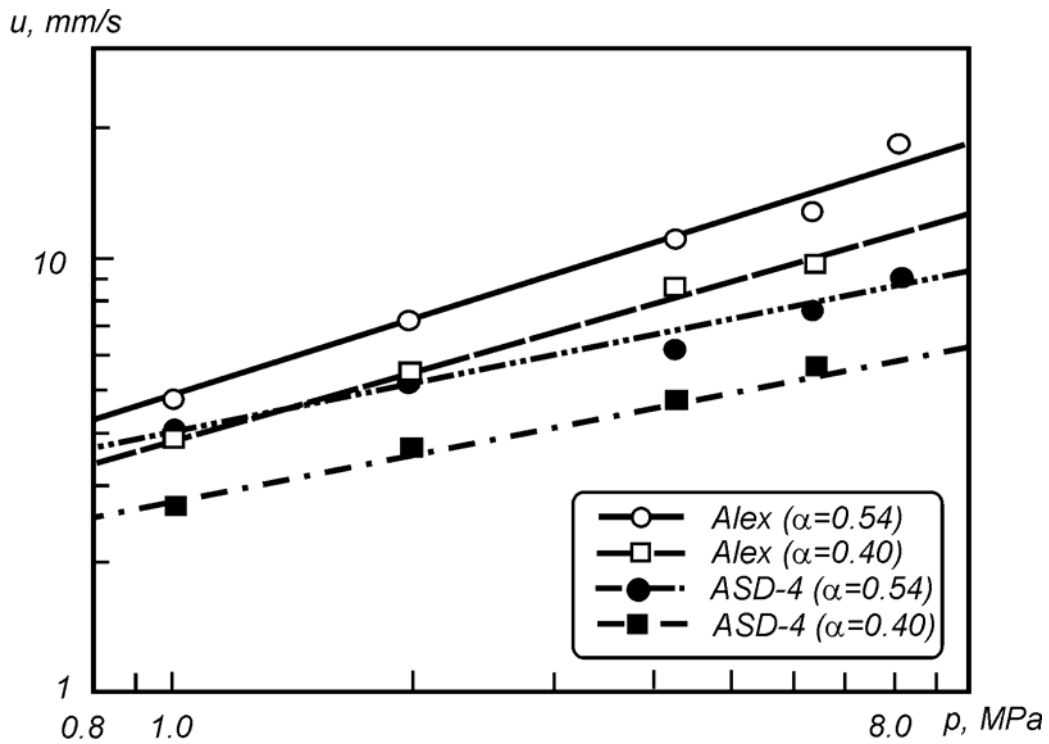


Figure 7: Dependence of burning rate SP containing 10 % aluminum powder from pressure

Let's note an increase of value for SP containing aluminum UFP (Alex) in comparison with composition containing ASD-4 aluminum powder (Tab. 11).

Mark of aluminum	ν value at mass content of aluminum		
	5 %	10 %	20 %
ASD-4	–	0.37	0.28
Alex	0.36	0.52	0.56

Table 11: Values of exponent in the burning rate power law for SP containing aluminum powders of different dispersivity in the range of pressure (1 ÷ 8) MPa

An influence of metals UFP additive as a catalyst in the SP composition was estimated by an effectiveness coefficient K (ratio between the burning rate of metallized composition with additive of catalyst and the burning rate composition without additive of catalyst under other the equal conditions). Results of the study are given in Tab. 12. The studies were carried out in air at atmospheric pressure. Regular aluminum powder ASD-4 was used as a metal fuel. Its content was made 10 %. When additives of metal catalysts, the burning rate of mixture compositions increases by a factor (1.1 ÷ 1.47).

Catalyst content	1 % Fe UFP	1 % Cu UFP	1 % Ni UFP	1 % Fe UFP	1 % Fe
K	1.15	1.47	1.10	1.24	1.11

Table 12: Efficiency of catalyst influence on the SP burning rate

Properties of ultrafine powders of metals with sizes of particles less than 0.1μ differ significantly from those of usual powders. Extreme obtaining conditions (powerful high-voltage nanosecond electrical pulse, temperature about 104 K, shock wave, superfast quenching of products of the wires electrical explosion with rates of 107 K/s) provide special properties of electroexplosive powders. One of the factors influencing on the SP burning rate is the release of stored energy of UFP produced by the wires electrical explosion. However, results of the differential thermal analysis [1] have found out absence of the given effect for SP containing aluminum UFP (Alex) with a different term of storage.

In such a way, the above mentioned theoretical dependences for the burning rate of SP containing aluminum powder require essential correction and can not be used for comparison of quantitative characteristics. However, they accord quantitatively with our experimental data and allow explaining process physics and mechanism of influence of aluminum particles dispersivity on the SP burning rate:

- The heat input to the SP surface is spent for warming up a reactionary layer (condensed phase) up to certain temperature and mainly for the evaporation of components of oxidizer and fuel. The combustion can arise only in the formed vapors. Their heating should result in development of reaction. The heat released during this combustion (in the gas phase) will be spent on the heating vapors and evaporating new portions of condensed phase. When additive UFP of metals into the SP composition, the heat release at the expense of combustion metals occurs in an area closely approximating to the combustion surface. It results in an increase of total heat flux to the propellant and, accordingly, in an increase of SP burning rate.
- Ultrafine particles of metal are ignited rapidly and burn down nearby the SP surface. That results in increasing a heat release rate due to heterogeneous reactions on the surface of particles and in increasing the SP burning rate according to Zel'dovich's model. When additives of metals UFP, the increasing the SP burning rate is connected not only to the additional heat release due to combustion particles, but also to the increasing gas phase reactions rate because of the total increase of temperature in the combustion zone.

Discussion

Research of uncured samples, containing the aluminum of a various dispersivity in a quantity from 5 % up to 20 % (tab. 4) confirmed earlier obtained outcomes for SP containing UFA and have shown that at addition more than 10 % of large aluminum is observed noticeable lowering of burning rate of researched SP (up to 30 %). One from the possible reasons of observable effect can be the incomplete combustion of metal and outflow of heat from a zone of combustion by the not burnt down particles of aluminum.

UFA, agrees [5] is ignited on distance ~ 5 mm near to a surface of combustion, i.e. is ignited and burns down at once as soon as occurs on a combustion surface. This effect, evidently, and the increase of SP burning rate is explained at addition of UFA. Besides the catalytic influence of UF particles to high-temperature oxidation (combustion) of polymeric combustible, this influence the stronger is possible than the metal particles [24] are more small-sized. The noted effect does not depend on a factor of excess of an oxidizer of a considered system (see tab. 5). It is necessary to note, that the steady combustion at normal conditions is characteristic only for SP weights containing a rather large oxidizer, not less $(160 \div 315) \mu$ (tab. 6). Probably in this case main role-plays formation of a warm up layer in a sample. In case of a small-sized oxidizer the warm up layer is wider but temperature it is insufficient for decomposition heat-resistant butyl rubber, as does not allow to realize process of steady combustion. However it is not enough of obtained experimental data for correct conclusions and the further researches in this direction are necessary.

In accordance with [6] properties of UF metals properly depend on conditions of manufacturing and storage. Therefore in activity the research of influence of conditions of manufacturing and storage on SP burning rate (see tab. 7) is conducted. The obtained experimental data show, that presence of nitrogen in environment of manufacturing or the long duration storage of a powder on an air results in sharper increase of burning rate, in comparison with green one in atmosphere of argon.

The outcomes on influence of catalysts of combustion of the investigated systems (tab. 8, 9) have shown that the greatest effect is observed at addition of catalysts in nonmetal SP. At addition into SP UFA the efficiency of

catalysts of iron and soot drops. Probably, it is connected that the structures containing UFA burns with the greater rate and at higher temperatures. However for the description of catalysis even at a qualitative level the realization of additional experiments, extension of a circle of catalysts is necessary.

The analysis of experimental data adduced in tab.10-14, shows that the efficiency separately of taken fraction of aluminum practically does not depend on a factor of extra oxidizer coefficient of system and is increased in accordance with decreasing the sizes of metal particles. So at transition from the sizes of particles of aluminum with dispersivity $(10 \div 15) \mu$ to $(0.01 \div 0.1) \mu$ the burning rate is increased in $(1.4 \div 2.0)$ times. The greatest increase is observed at reduced pressure of the order 1 MPa. The efficiency of UFA is increased in accordance with increase of the contents of the latter in SP. Simultaneously use of UFA results in increase of an exponent in the burning rate law. It is necessary to note, that the aluminum with dispersivity $(10 \div 15) \mu$ practically does not influence on the burning rate law. The obtained outcomes do not contradict the data adduced in [6].

Conclusion

- Ignition time delay of metallized gels on the based kerosene and UFA is exponential decrease with growth of temperature and have a little less value than for pure kerosene.
- The influence UFA, UF *Fe* and soot on high-temperature oxidation of butyl rubber and HTPB in combustion and ignition regimes is considered.
- Is shown that the addition of UFA results in increase of burning rate both at atmospheric pressure, and in an interval $(1 \div 8)$ MPa. The detected effect practically does not depend on a factor of extra oxidizer coefficient of composition and is increased in accordance with growth of the contents of UFA in SP.
- The relation of steady combustion of SP on mixed combustible polymer + metal from a dispersivity of an oxidizer is detected. For development of effective systems the additional researches are required.
- Is obtained that the availability of nitrogen on particles of UFA promotes increase of activity of metal during combustion and ignition.
- The consideration of influence of catalysts of iron and soot on investigated processes has shown that the UF catalysts are most effective for nonmetal systems. The efficiency of catalysts is reduced at addition of UFA into system. The mechanism of a phenomenon is not clear and requires further research.
- Is obtained the structures of SP for which the mode of explosive ignition is characteristic. The mechanism of a phenomenon is not clear and requires further research.

Acknowledgement

This study was partly supported by the Russian Foundation for Basic Research (Grants No. 05-03-32729, 05-08-18237).

References

- 1) Mench M.M., Yen C.L., and Kuo K.K. Propellant burning rate enhancement and thermal behavior of ultrafine aluminum powders (Alex) // "Energetic Materials: Production, Processing and Characterization" of the 29th International Annual Conference of ICT. – Karlsruhe, Germany, 1998. P. 30–1-15.
- 2) Tepper F., and Kaledin L.A. Combustion characteristics of kerosene containing Alex nano-aluminum // Lectures of the 3rd International. Workshop "Unsteady Combustion and Interior Ballistics". – Saint Petersburg, 2000. V. 2. P. 320-325.
- 3) Arkhipov V.A., Korotkikh A.G., and Kuznetsov. Study of ignition and burning processes of solid propellants containing of metal nanopowder // News of Russian Academy of Rocket and Artillery Sciences. 2005. Rev. 1(42). P. 18-25.
- 4) Simonenko V.N., and Zarko V.E. Comparative studying the combustion behavior of fine aluminum // "Energetic Materials": 30th International Annual Conference of ICT. – Karlsruhe, Germany, June 29 – July 2, 1999. P. 21–1-14.
- 5) Kuznetsov V.T., Marusin V.P., and Skorik A.I. On a mechanism of ignition in heterogeneous systems // Combustion, Explosion and Shock Waves. 1974. V. 10, No. 4. P. 526-529.
- 6) Ivanov G.V. Combustion and explosion of pyrotechnic mixtures based on ultrafine Al powder / International Workshop on Chemical Gasdynamics and Combustion of Energetic Materials. Book Abstracts. – Tomsk, 1995. P. 10.
- 7) Zenin A.A., Glazkova A.P., Leipunsky O.J., and Bobolev V.K. Effect of aluminum on defloration of ammonium perchlorate with polyphormaldehyde // Combustion, Explosion and Shock Waves. 1968. V. 4, No. 3. P. 299-304.
- 8) Zenin A.A., Glazkova A.P., Bobolev V.K., and Leipunsky O.J. About a role of radiation of a flame at combustion of metallized mixtures // The reports of an Academy of Sciences. 1968. V. 181, No. 3. P. 637-643.
- 9) Pokhil P.F., and Romadanova L.D. About combustion of structures based on oxidizer of a potassium perchlorate of and metal fuels in vacuum // Journal of FCh. 1965. V. 39, No. 11. P. 2757-2759.
- 10) Andreev K.K., Rogozhnikov V.M. About combustion of powder ARS and its mixtures with aluminum at increasing pressure // "The theory of explosive substances", MchTI. Vol. 53. 1967. P. 176-181.
- 11) Gen M.Ya., Frolov Yu.V., and Storozhev V.B. On combustion of particles of subdispersed aluminum // Combustion, Explosion and Shock Waves. 1978. V. 14, No. 5. P. 153-155.
- 12) Ilyin A.P., and Proskurovskaya L.T. Two stage combustion of ultradispersed aluminum powder in air // Combustion, Explosion and Shock Waves. 1990. V. 26, No. 2. P. 71-72.
- 13) Boldyreva A.V., Bezrukov B.N., and Karnaukhov A.P. The catalyst specific surface influence on the burning velocity of fashionable composite fuels // Combustion, Explosion and Shock Waves. 1966. V. 2, No. 4. P. 146-147.
- 14) Bobolev V.K., Gen M.Ja., Mal'tsev V.M., Melesov G.P., Pokhil P.F., Seleznev V.A., Sissenko A.N., and Chuiiko S.V. Mechanism of the ironcontent catalytic additives effect on defloration of composite systems // Combustion, Explosion and Shock Waves. 1971. V. 7, No. 3. P. 366-375.
- 15) Korobeinichev O.P., Victorenko A.M., Tereschenko A.O., and Kolomeichuk N.N. Mechanism of catalyzed influence on combustion systems burning // Combustion, Explosion and Shock Waves. 1972. V. 8, No. 4. P. 511–517.
- 16) Demenkova L.J., Kundo N.N., and Kadochnikova N.F. Effect of specific surface and catalyze disperses on a burning of model mixtures with PHA // Combustion, Explosion and Shock Waves. 1974. V. 10, No. 1. P. 41-44.
- 17) Korobeinichev O.P., Victorenko A.M., Tereschenko A.O., and Kolomeichuk N.N. Study on a structure of catalyzed PNA-PMMA mixture surface // Combustion, Explosion and Shock Waves. 1974. V. 10, No. 3. P. 345-353.
- 18) Nikiforov V.S., and Bakhman N.N. Oxidizer dispersity influence on efficiency of catalyzes of burning // Combustion, Explosion and Shock Waves. 1972. V. 8, No. 4. P. 505-511.
- 19) Palaszewski B., and Zakany J.S. Metallized gelled propellants: oxygen/RP-1/aluminum rocket combustion experiments // AIAA Paper. 1995. No. 95–2435.
- 20) Turns S.R., Wong S.C., and Ryba E. Combustion of aluminum – based slurry agglomerates // Combustion Science and Technology. 1987. V. 54. P. 299-318.
- 21) Arkhipov V.A., Korotkikh A.G., Kuznetsov V.T., and Savel'eva L.A. Ignition of gels fuels containing ultrafine aluminum // Chemical Physic. 2003. Vol. 22, No 8. P. 30-33.

- 22) Ivanov G.V., and Surkov V.G. Electro explosion met stable powders with stored energy for self-propagation high temperature synthesis // 5th International Symposium on Self-Propagation High Temperature Synthesis (SHS-99): Book of Abstracts. – Moscow, 1999. P. 91-96.
- 23) Knorre G.F., Arefyev K.M., Blokh A.G. at al. Theory of burning processes. – M.-L.: Energy. 1966. – 491 p.
- 24) Kanqyng Deng, Guangtion Zang, and Quiban Zang. The characteristics and mechanism for superfine aluminum powder combustion. // Theory and Practice of Chenergetic Materies Beiging Funstitute of Technology Bers. Oct, 1996. P. 312-321.
- 25) Olsen S.E., and Becstead M.W. Burn time measurements of single aluminum particles in steam and carbon dioxide mixtures // Prepared for Presentation at the International Seminar on Intra – Chamber Processes, Combustion and Gas Dynamics of Dispersed Systems. – St. Petersburg, Russia, June, 1995. P. 11.

Nomenclature

M – mass of fuel, g;

p_a – atmospheric pressure of air, Pa;

R – gas constant;

t_{ig} – ignition time delay, s;

ν – burning rate pressure sensitivity;

BR – butyl rubber;

SP – solid propellant;

M_{air} – mass of air, kg;

V – volume of reactor, m³;

T – temperature of air in reactor, K;

α – extra oxidizer coefficient;

AP – ammonium perchlorate;

HTPB – polybutadiene, hydroxyl terminated;

UFA – ultrafine powder of aluminum.

